Title

Thermal Reservoir Networks for Modularly Expandable Thermal Microgrids

Authors

Wetter, Michael
Dee, Virak
Fu, Hongxiang
et al.

Publication Date

2026-01-26

FINAL REPORT

Thermal Reservoir Networks for Modularly Expandable Thermal Microgrids

Michael Wetter[1]
Virak Dee[4]
Hongxiang Fu[3]
Jianjun Hu[1]
Eric Nyenhuis[2]
Rémi Patureau[3]
Matthias Sulzer[1]
Andrew Tech[2]

[1]*Lawrence Berkeley National Laboratory*
[2]*Southland Industries*

January 2026

[3] Work done while the author was with Lawrence Berkeley National Laboratory.
[4] Work done while the author was with Southland Industries.

ESTCP Project EW23-7686

REPORT DOCUMENTATION PAGE

Form Approved
OMB No. 0704-0188

1. REPORT DATE
1/26/2026

2. REPORT TYPE
Final Report

3. DATES COVERED *(From - To)*

4. TITLE AND SUBTITLE
Thermal Reservoir Networks for Modularly Expandable Thermal Microgrids

5a. CONTRACT NUMBER

5b. GRANT NUMBER

5c. PROGRAM ELEMENT NUMBER

5d. PROJECT NUMBER EW23-7686

5e. TASK NUMBER

5f. WORK UNIT NUMBER

6. AUTHOR(S)
Michael Wetter, Jianjun Hu, Hongxiang (Casper) Fu, Remi Patureau and Matthias Sulzer
Lawrence Berkeley National Laboratory

Eric Nyenhuis
Southland Industries

7. PERFORMING ORGANIZATION NAME(S) AND ADDRESS(ES)
U.S. Department of Energy for performance at Lawrence Berkeley National Laboratory
Building Technology & Urban Systems Division (BTUS)
1 Cyclotron Road
Berkeley, CA 94720

8. PERFORMING ORGANIZATION REPORT NUMBER
EW23-7686

9. SPONSORING/MONITORING AGENCY NAME(S) AND ADDRESS(ES)
Office of the Deputy Assistant Secretary of Defense (Energy Resilience & Optimization)
3500 Defense Pentagon, RM 5C646
Washington, DC 20301-3500

10. SPONSOR/MONITOR'S ACRONYM(S)
ESTCP

11. SPONSOR/MONITOR'S REPORT NUMBER(S)
EW23-7686

12. DISTRIBUTION/AVAILABILITY STATEMENT
DISTRIBUTION STATEMENT A. Approved for public release: distribution unlimited.

13. SUPPLEMENTARY NOTES

14. ABSTRACT
The technical objectives of this project were to provide the DoD with modular thermal energy network solutions that enable staged retrofits, significantly reducing lifecycle costs and peak electrical demand, while enhancing energy efficiency, resilience, robustness and adaptability to technological advancements, while improving overall energy supply security for mission-critical operations.

15. SUBJECT TERMS
energy & water, energy efficiency, HVAC, heat pump

16. SECURITY CLASSIFICATION OF:			**17. LIMITATION OF ABSTRACT**	**18. NUMBER OF PAGES**	**19a. NAME OF RESPONSIBLE PERSON**
a. REPORT	**b. ABSTRACT**	**c. THIS PAGE**			Michael Wetter
UNCLASS	UNCLASS	UNCLASS	UU	160	**19b. TELEPHONE NUMBER** *(Include area code)* 510-486-6990

Standard Form 298 (Rev. 8/98)
Prescribed by ANSI Std. Z39.18

FINAL REPORT

PROJECT: EW23-7686

TABLE OF CONTENTS

Page

TABLE OF CONTENTS (Continued)

TABLE OF CONTENTS (Continued)

TABLE OF CONTENTS (Continued)

LIST OF FIGURES

Page

LIST OF FIGURES

Page

LIST OF TABLES

Page

ACRONYMS AND ABBREVIATIONS

ALCC	Annualized life cycle costs.
AW HP	Air-to-water heat pump.
CHW	Chilled water.
COP	Coefficient of performance of a heat pump or chiller.
DHC	District heating and cooling.
DHC	Domestic hot water.
DoD	Department of Defense.
ECM	Energy conservation meausure.
ESTCP	Environmental Security Technology Certification Program.
ETS	Energy transfer station.
fTMY	Future typical meteorological year.
HP	Heat pump.
HVAC	Heating, ventilation and air-conditioning.
JBA	Joint Base Andrews.
LCC	Life cycle costs.
MILP	Mixed Integer Linear Programming.
O&M	Operation and maintenance.
PBD	Platform-Based Design.
PI	Proportional-integral controller.
PJM	Pennsylvania-New Jersey-Maryland electrical interconnection.
PV	Photovoltaic.
SC	Space cooling.
SH	Space heating.
TMY3	Typical meteorological year, version 3.
WW HP	Water-to-water heat pump.

ACKNOWLEDGEMENTS

This research was supported by the Environmental Security Technology Certification Program (ESTCP) of the U.S. Department of Defense (DoD), under Contract No. EW23-BB-7686.

We thank Keith Welch and Tim Tetreault from ESTCP, and Lucas Tufano, and McKinley Siegle from Noblis for their guidance.

We thank Sergio Corona from Southland Industries for completing the building energy conservation measure and load assessment.

We thank the DoD team at Joint Base Andrews, including Krist Zimmerman, Patrick Adamson, Anthony Lizza, Lt Col Graham Auten, Stephanie Frizzo, Maj Cory McCart, Wayne Gagnon, 1 Lt Caleb Boone, Mohammad Alikahani, Joshua Miller, David Jordan, Ahmed Abdullah, Mazibur Khan, Jennifer Valentine, Michael Delea, David Kramer, Joseph Thornberry, Joseph Osborne, and Greg Spells for their important project support.

We thank the Navy Geothermal Office and the RESPEC team, including Andrew Sabin, Dan Hoyer, Danny Rauchenstein, Kevin Kitz, Matthew Minnick, Haiyan Zhou, Randy Williams, and Saundra Anderson for their collaboration, for their specification of soil data and borefield geometry, and for providing the FEFLOW results for the validation of the new zoned borefield model presented in Appendix K.

We thank Massimo Cimmino from Polytechnique Montréal, Canada, for the implementation of the new zoned borefield model presented in Appendix K.

ABSTRACT

The Department of Defense (DoD) faces the substantial challenge of cost-effectively retrofitting one to two installations per month, each comprising approximately 1,000 buildings, to improve resilience, reduce energy consumption, and enhance energy supply security. Achieving these objectives requires optimal system selection and effective risk mitigation during system integration. To address this need, we introduce Platform-Based Design (PBD), a structured, hierarchical methodology adapted from other industrial sectors to the domain of energy system retrofits. We demonstrate the effectiveness of PBD through a techno-economic feasibility study comparing geothermal-coupled thermal energy networks (TENs) with conventional energy systems for heating, cooling, and powering 17 buildings at Joint Base Andrews (JBA) in Maryland.

Our analysis illustrates that the PBD approach enables rigorous, data-driven, sequential decision-making, resulting in a family of Pareto-optimal systems, among which the TEN emerged as the most promising solution. The selected TEN design integrates geothermal borefields, heat recovery heat pumps, photovoltaic (PV) arrays, and battery storage. Compared to the baseline system – gas heating combined with air-source chillers – the proposed TEN reduces annual imported energy by 74% and peak electricity demand by 45%, achieves a levelized cost of energy of $0.210/kWh, and substantially enhances resilience. Life-cycle costs increase by approximately 6%, and initial investment costs are about 2.5 times higher than the baseline. However, if central plant infrastructure, district loops, and utility-scale PV and battery systems are privately funded and operated, the initial investment would fall below the baseline system cost.

Critical to achieving these significant performance improvements were detailed nonlinear dynamic simulations coupling geothermal heat transfer, energy system operation, and realistic feedback control logic. These simulations identified essential design modifications and control strategy refinements that substantially reduced energy use, peak demand, and compressor short-cycling, thereby improving durability and reliability—issues that would have been significantly more expensive to resolve during operation. Additionally, the verification step highlighted sensitivities to key design parameters that could reduce initial investment by approximately $2 million and reduce annual life-cycle costs more than $300,000.

We recommend adopting the PBD methodology for future feasibility studies and TEN pilot projects to gain valuable operational experience. Furthermore, we recommend that DoD invest in transferring and scaling the PBD methodology to other installations. This entails developing standardized computational frameworks and component libraries as well as training industry in conducting PBD. Such investments would enable rapid, robust, reliable, and cost-effective retrofits, supporting DoD's ambitious energy system modernization goals.

EXECUTIVE SUMMARY

PURPOSE

This feasibility study examines the techno-economic viability of integrated energy systems, focusing specifically on TENs for retrofitting heating, cooling, and power systems at Department of Defense (DoD) facilities. Joint Base Andrews (JBA) in Maryland serves as the subject of the case study. This study introduces Platform-Based Design (PBD) as a structured methodology for analyzing energy system retrofits. PBD has successfully delivered transformative results in various industries by enabling data-driven decision-making for complex systems. Here, we examine its potential to systematically compare alternative retrofit solutions and reduce risk in selecting optimal energy system configurations. Adopting PBD is critical for realizing reliable, cost-effective, and scalable retrofits at the pace required to meet the energy modernization goals of DoD installations.

The DoD portfolio comprises approximately 300,000 buildings distributed across 500 installations, representing roughly 33% of its total energy consumption. Many of these buildings have deferred necessary energy system retrofits, resulting in reduced operational reliability and diminished resilience. Given a typical retrofit cycle of 25 years, the DoD faces the substantial challenge of retrofitting one to two installations per month, each containing an average of 1,000 buildings. These retrofits need to be cost-effective, ensure operational reliability and enhance resilience. Furthermore, these retrofits must support phased deployment approaches that can adapt to varying levels of capital availability at individual installations, whether funding is provided directly through DoD appropriations or partial privatization of the energy infrastructure assets.

> A fundamental paradigm shift in energy system design, construction, and operation is urgently needed to accelerate the reliable deployment of integrated thermal and electrical storage, thermal energy grids, electrical microgrids, heat pumps, and similar technologies. Currently, energy systems planning is typically conducted in isolated work streams following a sequential waterfall approach, where verification takes place only after construction is completed. This fragmented method results in inefficiencies, costly modifications, and unreliable operation. To overcome these challenges, two critical paradigm shifts are necessary:
>
> 1. **From isolated to integrated planning:** Replacing traditional waterfall approaches with a holistic, Platform-Based Design enables integrated, data-driven decision-making across disciplines and domains at appropriate abstraction levels. This structured, digital, and tool-agnostic framework improves interdisciplinary collaboration, manages complexity, and reduces errors.
> 2. **From physical to virtual testing:** Replace costly late-stage physical testing with early-stage digital simulations. Virtual models serve as precise, reusable system specifications for quality assurance and optimization. Early virtual verification reduces expensive post-construction modifications and ensures reliable system operation from the start.
>
> These paradigm shifts invest more effort upfront in the design phase, greatly reducing total project costs, construction delays, and operational risks. The outcome is faster, more reliable, and cost-effective deployment of advanced energy solutions.

Therefore the study's central objective is twofold: First, it aims to rigorously evaluate the techno-economic viability of integrated energy systems designs, with a particular emphasis on TENs, in comparison to conventional energy systems. Second, it seeks to demonstrate that the application of the PBD process - novel at this scale and complexity for building energy system retrofits - enables data-driven, sequential decision-making for energy system design. The significance of this second objective lies in the considerable potential of PBD for transferability to future demonstrations and, ultimately, for scaled deployment of techno-economically optimized energy system retrofits across DoD installations as the PBD process reduces cost, improves performance, and de-risks design and operation.

METHODOLOGY

Based on site visits and interviews conducted with facility personnel at JBA and with DoD/ESTCP management, we developed a sequential design and decision-making process centered around the following core steps:

1. Assess retrofit needs to make building systems ready for heat pumps or TEN.
2. Identify Energy Conservation Measures (ECMs) as "no-regret" actions that should be implemented independently of the selected energy system retrofit solution.
3. Derive Pareto-optimal energy system configurations based on projected future energy demands (post-ECM implementation), balancing minimal lifecycle cost and minimal imported energy requirements.
4. Select the most suitable solutions aligned with JBA-specific objectives.
5. Conduct detailed, realistic (near-world) modeling of the selected solutions, coupling geother-mal heat flow, irradiance, energy system operation and feedback control, to evaluate their robustness, operational reliability, sensitivities and resilience against extreme weather conditions (e.g., cold snaps and heat waves), and to ensure compliance with DoD objectives and requirements, thereby reducing risks associated with the implementation and operation of the selected system design.
6. Document the detailed solutions comprehensively, providing the necessary information to facilitate drafting tender documents.

This structured and traceable design approach leverages the PBD workflow as its underlying principle. By integrating state-of-the-art optimization and simulation tools within a fully digital PBD workflow, the method enables informed, data-driven decision-making that explicitly considers overall system dynamics at each stage of the design process.

JBA CASE STUDY

In collaboration with site personnel, we identified 17 buildings at JBA as well as potential areas suitable for installing photovoltaic (PV) arrays and a geothermal borefield. Each proposed energy system must reliably meet the heating, cooling, domestic hot water, and electricity demands of these selected buildings.

To establish a baseline for comparison, we defined a conventional energy solution characterized by the lowest initial investment and life-cycle costs. This baseline solution assumes prior implementation of ECMs at each building. Specifically, the baseline comprises gas-fired heating systems combined with air-source chillers in each building, without incorporating PV or battery storage.

In agreement with site personnel, we defined the solution space to encompass four distinct system options, each permitting various configurations regarding component selection and sizing:

1. Gas-fired heating systems paired with air-source chillers installed individually in each building.
2. Reversible air-to-water heat pumps installed individually in each building.
3. Reversible water-to-water heat pumps installed individually in each building, integrated with a building-site geothermal borefield and dry coolers.
4. A thermal energy network (TEN) that interconnects all buildings through a district thermal loop. This network incorporates a central energy plant equipped with a geothermal borefield and a reversible heat pump system coupled to a dry cooler, which can also provide free-cooling or heating. The geothermal borefield in this scenario includes two independently operated sections, designed separately for short-term and seasonal thermal energy storage.

For all options, PV arrays and battery storage systems can be integrated into the system configuration. Their maximum capacities have been determined in coordination with site personnel, based upon rooftop suitability and available space.

As performance targets for evaluating the proposed energy system designs, we identified the following quantitative and qualitative objectives:
Quantitative Performance Objectives:

- Imported energy reduced by at least 50% compared to baseline.
- Imported peak energy reduced by at least 40% compared to baseline.
- Life-cycle cost no more than 120% of the baseline.
- Investment cost no more than 200% of baseline.
- Levelized cost of energy for heating and cooling no more than 0.25 USD/kWh.

Qualitative Performance Objectives:

- System complexity: Rated medium-high (expert judgment, based on feedback from mechanical design firm).
- Compatibility with industry installation capabilities: Rated medium-high (expert judgment).
- Alignment with site operational capabilities: Rated medium (expert judgment).
- Robust operation: Verified stability demonstrated through dynamic simulations that couple geothermal borefields, energy systems and controls.

All four energy system options were evaluated through techno-economic optimization, addressing steps 1 to 6 of the outlined PBD design methodology. Specifically, step 3 involves deriving Pareto-optimal configurations based on projected future energy demands (post-ECM implementation), minimizing both life-cycle costs and imported energy. Step 4 subsequently involves selecting the most suitable solutions in alignment with Joint Base Andrews' defined objectives. Based on this analysis, the solution best matching the defined performance objectives was identified as configuration 4, the thermal energy network with a geothermal borefield, photovoltaics (PV), and battery storage.

The techno-economic optimization described above assumed perfect foresight of weather conditions, building loads, and utility prices, and employed simplified physical models - particularly for geothermal heat transfer and heat pump performance - and it used idealized perfect control, as is common practice in large-scale optimization analyses. Recognizing the limitations inherent in these assumptions and the need to mitigate risks associated with future construction and operation, we applied steps 5 and 6 of the outlined method.

Step 5 involved high-fidelity, dynamic simulation modeling of the selected candidate solution representing the detailed design of the geothermal borefield, the mechanical and control systems. These detailed models incorporate realistic feedback control logic, providing validated digital specifications of the energy system. Such a modeling approach enables rigorous verification of the system's robustness, operational reliability, and resilience, and facilitates further refinements.

Step 6 entailed comprehensive documentation of the detailed solutions through digital specifications, which can directly inform the preparation of tender documents. Additionally, the control logic was specified in accordance with the proposed ASHRAE Standard 231P "Control Description Language," enabling digital deployment and verification of control strategies - a novel contribution of this project. Furthermore, the modular structure of the developed design supports a staged build-out of the installation, facilitates the transfer of key energy and control components to other projects and sites, and allows cost-effective replication as well as successive improvements or replacements with emerging technologies.

This enhanced level of modeling detail represents a significant advancement beyond traditional building energy modeling approaches, which typically idealize controls and merely estimate energy use: Our models implement realistic feedback control mechanisms, analogous to established practices in other engineering domains such as automotive and aerospace industries. Ultimately, this methodology not only reduces risks associated with system implementation but also paves the way for broader adoption of digital twins throughout the construction and operational phases of building energy systems.

After applying the Platform-Based Design (PBD) methodology, the selected energy and control system for Joint Base Andrews - a thermal energy network incorporating a geothermal borefield, heat recovery heat pumps installed at each building, photovoltaic systems (PV), and battery storage for daily peak shaving - successfully meets the defined performance objectives.

Specifically, the achieved quantitative performance objectives are as follows:

- Imported energy: 74% reduction compared to baseline.
- Peak electricity import: 45% reduction compared to baseline.
- Life-cycle cost (LCC, USD): 106% of the baseline.
- Initial investment cost (USD): 244% of the baseline. However, if the central plant, the district loop and PVs and batteries are privatized, then investment costs is below the baseline.
- Levelized cost of energy for heating and cooling: 0.210 USD/kWh.

Additionally, qualitative performance objectives - including system complexity, industry installation capabilities, site operational capabilities, and robust operation - have been fulfilled according to expert judgment provided by the industry partner, Southland.

KEY FINDINGS

We first discuss the key findings of the techno-economic analysis, followed by the insights gained from the application of the BD process.

Energy system

The Pareto-optimal analysis reveals that adding photovoltaics (PV) and battery storage to the baseline gas heating system with air-source chillers increases life-cycle costs by more than 30%. While the addition of PV and batteries enhances resilience and energy independence, the air-source chillers render the system vulnerable to heat waves. Similarly, reversible air-source heat pumps (Option 2) exhibit comparable disadvantages, becoming vulnerable during winter cold snaps. Consequently, we consider Option 2 unsuitable due to its similar life-cycle costs, higher imported energy demands, and greater sensitivity to extreme outdoor temperatures relative to other available system options 3 and 4.

The distributed geothermal heat pump solution (Option 3) and the thermal energy network (Option 4) both demonstrate similar techno-economic performance. However, the thermal energy network solution is particularly advantageous and is therefore recommended. Specifically, the thermal energy network achieves comparable life-cycle costs while significantly reducing imported energy and peak demand. This improved performance results from its central geothermal borefield, which effectively mitigates sensitivity to extreme outdoor temperature fluctuations through short-term and seasonal thermal storage. Additionally, the reduced energy and peak demand offered by the thermal energy network design enables considerable cost savings for emergency power generation and utility benefits which could create opportunities for capacity-based incentives. These additional benefits are not reflected in the presented life-cycle cost calculations.

Although the initial investment in the thermal energy network system is more than two times higher compared to the conventional Gas solution, it offers notable strategic benefits. The modular structure of the thermal energy network facilitates staged implementation, transferability of key energy and control components to other sites, and cost-effective replication. Furthermore, the centralized plant provides opportunities for utility-scale grid services, potentially generating additional revenue streams. Although grid service revenues were not explicitly included in this study, existing operational plants demonstrate the feasibility and economic viability of such services, highlighting their potential value in future design phases.

The techno-economic performance of the thermal energy network system is sensitive to appropriate equipment sizing and optimized operational control strategies. Detailed simulations reveal rare potential electricity demand spikes caused by the simultaneous dispatch of multiple heat pumps. These findings indicate that implementing advanced predictive control strategies could further enhance system performance. Moreover, predictive control that diurnally and seasonally optimizes energy storage based on predicted weather, loads and energy prices can optimize operational efficiency, reduce peak electricity demand, and improve system resilience. Additionally, predictive control would facilitate optimal utilization of thermal storage, potentially lowering investment and operational costs and enabling active participation in utility-scale grid balancing markets.

Finally, evaluations conducted across various future energy rate scenarios, based on data from the U.S. Energy Information Administration's Energy Outlook 2023, indicate that the proposed thermal energy network solution is robust against fluctuations in energy prices.

Platform-Based Design Process

The Platform-Based Design (PBD) process proved instrumental in enabling a holistic and structured analysis of competing energy system architectures. Specifically, it facilitated data-driven system selection and sizing, detailed verification, and subsequent refinement of the preferred solution. The PBD approach integrated multi-objective techno-economic optimization with realistic, nonlinear dynamic simulations to validate and improve system design. Had we relied exclusively on techno-economic MILP optimization, we would have significantly overestimated the geothermal borefield capacity - by approximately a factor of two - resulting in inappropriate equipment specification and undersized system components. Conversely, had we conducted only detailed nonlinear system simulations without prior optimization, we would have lacked clear guidance on optimal configuration, insight for developing control strategies and performance targets.

Perhaps most importantly for future designs, the verification step using detailed nonlinear simulations of the coupled geothermal, district energy, and control systems revealed several critical insights:

1. The initial central plant design, despite being reviewed by experienced design professionals, proved insufficient to meet the required dynamic performance specifications. This shortcoming became apparent only through detailed dynamic simulation with realistic feedback controls. The verification process thus led to significant hydraulic design adjustments.
2. The detailed simulation identified previously unnoticed shortcomings in the initial control specifications. Specifically, initial control sequences did not adequately address dynamic operational needs, resulting in insufficient system capacity and performance. These issues were revealed only through dynamic simulation incorporating realistic feedback control loops, enabling subsequent optimization of control strategies.
3. By explicitly modeling the full dynamics of the system and its context, we identified that certain components commonly used in milder regions - such as dry coolers for free cooling/heating (i.e., without use of chillers or heat pumps) in central European installations - were unsuitable for JBA due to local weather conditions.

Additionally, the detailed simulations highlighted sensitivities related to heat pump sizing, district loop dimensions, and control sequences. If these parameters are not carefully managed, they could significantly impact the system's techno-economic performance and operational effectiveness.

This verification step is critically important as such oversights can result in costly design revisions, construction change orders, and stranded assets.

The PBD methodology also supports modularity and standardization, enabling staged deployment, transferability of key energy and control components to other projects and installations for cost-effective replication. Reusable components can be further refined as part of detailed design and implementation specifications. Although the current study did not exhaustively evaluate all potential technology alternatives, the established framework readily allows systematic testing and comparison of alternative components, such as different heat pump technologies or emerging thermal storage solutions.

In conclusion, adopting a digitalized workflow formalized through PBD offers significant potential to enhance the reliability, resilience, and cost-effectiveness of energy systems for DoD installations. By adapting proven methodologies from other industrial sectors to the energy domain, this approach facilitates informed decision-making, optimized system design, and scalable deployment across DoD facilities.

CONCLUSION AND RECOMMENDATIONS

For JBA, we recommend proceeding with the selected thermal energy network configuration, comprising a central geothermal borefield, heat recovery heat pumps at each building, rooftop PV, and batteries for daily peak shaving. This solution meets all defined quantitative and qualitative performance objectives.

TENs integrate proven equipment in new ways. Key risks are how they are designed and operated together as a system. PBD addresses this risk. For future projects at JBA and other installations, we therefore recommend applying the PBD methodology to ensure a structured, holistic comparison of design alternatives and subsequent risk mitigation through detailed verification.

For ESTCP, we recommend further developing and refining the PBD methodology into a standardized, modular, and reusable workflow. Such a standardized workflow will enable cost-effective, scalable, and accelerated retrofits, directly addressing the DoD's ambitious retrofit targets. Specifically, ESTCP should invest in establishing a modular framework of reusable template components and standardized control logic specifications, aligned with emerging standards such as ASHRAE Standard 231P (Control Description Language). This approach will enable the development of an DoD library of verified components, ready for application within the PBD framework.

Additionally, our findings highlight the critical importance of detailed nonlinear simulation and verification as integral components of future feasibility studies. By explicitly modeling realistic system dynamics and feedback control interactions, potential operational and sizing issues - otherwise only detected late during commissioning or operation - can be identified and corrected cost-effectively during the design phase. This verification using a coupled energy system, subsurface and control system model that is part of the PBD methodology is critically important to reduce the risk of costly design revisions, construction change orders, and stranded assets.

In summary, further investment in refining and deploying the PBD methodology is essential to achieving reliable, resilient, and cost-effective energy system retrofits at scale across DoD installations.

1.0 INTRODUCTION

The DoD portfolio includes approximately 300,000 buildings across 500 installations, accounting for about 33% of its total energy consumption. Many of these buildings have deferred necessary energy system retrofits, leading to reduced operational reliability and resilience. With a typical retrofit cycle of 25 years, the DoD faces the challenge of retrofitting around one to two installations per month, each containing an average of 1,000 buildings. These retrofits must be cost-effective, ensure operational reliability, and enhance resilience, while supporting phased deployment approaches as capital becomes available at the individual installations.

In support of this need, this feasibility study investigates the techno-economic feasibility of a thermal energy network (TEN) for retrofitting energy systems that provide heating, cooling, and power to DoD facilities, using Joint Base Andrews (JBA) in Maryland as a case study. The TEN is contrasted to conventional, building-level solutions with respect to their energy use, peak power demand, resilience, life cycle costs and investments.

To conduct the feasibility study using an approach that promises to allow a scaled retrofit across DoD installations, the feasibility study introduces Platform-Based Design (PBD) for energy system retrofits of DoD sites, as PBD was transformative in various industries (Alberto Sangiovanni-Vincentelli, 2007). Using PBD, this feasibility study conducts data-driven, sequential decision-making for these systems that are inherently complex as they integrate thermal and electrical systems with storage to achieve techno-economic performance that significantly surpasses conventional solutions. Besides enabling holistic comparisons among alternative energy systems, PBD also allows systematically reducing risks for the most promising solution. These steps are crucial for achieving cost-effective and scalable retrofits that meet the energy modernization goals of DoD installations.

The study's central objectives are twofold: First, to rigorously evaluate the techno-economic viability of integrated energy system designs, particularly of a TEN, compared to conventional energy systems. Second, to demonstrate that the application of the PBD process, novel at this scale and complexity for building energy system retrofits, enables data-driven, sequential decision-making for energy system design. The significance of this second objective lies in PBD's considerable potential for transferability to future demonstrations and scaled deployment of techno-economically optimized energy system retrofits across DoD installations.

2.0 SUMMARY OF HYPOTHESES

In this section, we will provide the motivation for the feasibility study and describe the key objectives that the analysis and discussions in the subsequent sections will validate.

2.1 BACKGROUND

The DoD owns nearly 300,000 buildings across its 500 installations, accounting for nearly 33% of the DoD's total energy use. Many of the buildings have installations that have deferred retrofits. This leads to inefficient operation, higher maintenance costs, and can impede resilience and operational reliability. There is an opportunity to retrofit installations through TENs for improved energy efficiency, reduced peak electrical demand and improved energy supply security. These attributes increase resilience and system reliability. They also free up electrical capacity to allow growth of other electrified consumers on the installation, such as data centers. Through system integrations, we show that such retrofits can be done in a way that is cost-effective from a life cycle point of view, improves energy efficiency and energy supply security. Moreover, a TEN allows privatizing the thermal energy distribution system, much like electrical microgrids can be privatized, thereby avoiding higher investment costs to DoD.

2.2 OBJECTIVE OF THE DEMONSTRATION

To cost-effectively retrofit DoD installations, to improve energy efficiency, reduce peak electrical demand, improve resilience, robustness, reliability and energy supply security, we have identified several key objectives. The key objectives that pertain to the energy system are:

- **TENs are a cost-effective, resilient, robust solution to retrofit sites without increase in life cycle costs:** Implementing solutions for groups of buildings rather than individual ones allows the DoD to realize benefits through system design that are optimized for networked thermal loads. This approach reduces life cycle costs through system integration and economies of scale, enables greater resilience by electrifying building and heating systems. Thermal grids enhance resilience by providing a more reliable and flexible energy infrastructure that can better withstand severe weather events and operational disruptions. Additionally, they offer robustness against technological changes, ensuring that the system can adapt to new advancements without significant overhauls.
- **TENs increase energy supply security:** The high efficiency and low peak demand of TEN, together with using electricity as the only energy input, allows for high energy supply security. Their high efficiency leads to a reduced energy import to the base, reducing requirements for emergency energy storage. Their low peak electrical demand, as compared for example to air-source chillers or heat pumps, allows for reduced emergency power supply capacity. Their modular design allows operating only part of the system to provide services to mission critical loads. As they only require electricity and no other energy carrier, their emergency energy supply can be provided by the same technology as is used by the base for other electrical emergency supply. These aspects all improve reliability, reduce costs and simplify the supply of emergency energy.

- **Staged investments make transformation financially viable without compromising resilience:** The modular design process enables staged investments and high customization to different sites, reducing initial capital expenditures. This approach allows for incremental retrofit as additional capital becomes available, ensuring continuous improvement of the system. Importantly, staged investments do not compromise system performance or resilience; instead, they enhance robustness by allowing the system to evolve and integrate new technologies over time, thereby maintaining operational integrity and adaptability.

Achieving the above objectives requires a holistic design across many design experts. This requires decision making for complex systems across a multi-disciplinary team. Moreover, the system performance depends on its dynamic operation, necessitating dynamic analysis of its operation as part of the design. Success will also require requirements that are specific and measurable. These requirements need to be verified along every step of the design-build-operate process, ensuring requirement satisfaction even in view of a fragmented supply chain. In order to reliably achieve these objectives in a way that allows scaling the deployment of TENs, we also add the following key process objectives:

- **Model-based engineering enhances data-driven decision-making and system robustness:** Utilizing linear and nonlinear dynamic models in the design and analysis of thermal networks significantly improves decision-making by providing data-driven, more accurate and comprehensive system analyses compared to conventional ad-hoc workflows. This method enhances the robustness of the system by identifying optimal design configurations, optimal sizing and operational strategies, and predicting system behavior under various scenarios, including extreme conditions. It enables the development of systems that are not only efficient but also capable of maintaining performance under adverse circumstances.
- **PBD eases complex system integration, reduces costs, and improves resilience:** Implementing a PBD approach simplifies the development process of complex energy systems. It enables more efficient integration of diverse technologies such as geothermal sources, low-temperature thermal networks, distributed energy resources (DERs) and advanced controls. By allowing a comprehensive system-level optimization, PBD enables life cycle cost reduction. Its layered design approach, starting with a high-level abstraction that enables holistic optimization, and successive refinement of the selected candidate system using pre-configured reusable components, enables a cost-effective, robust, flexible design that is capable of adapting to technological advancements and changing energy markets.
- **Digitalized workflow scales retrofit measures while enhancing resilience and robustness:** Adopting a digitalized workflow with formal performance verification at each stage of the design-build-operate workflow facilitates the scalable implementation of retrofit measures in existing DoD sites. This workflow includes the reuse of validated models, data-driven model parameterization, and the use of advanced control sequences. It ensures that the design intent is realized and that the system operates as expected. By leveraging digital tools, the workflow enhances resilience by allowing for rapid adjustments to operational strategies in response to real-time data or unexpected events. It also contributes to the robustness of the system by enabling continuous monitoring and optimization, ensuring long-term reliability and performance.

3.0 TECHNOLOGY DESCRIPTION

In this section, we will describe three main items: (i) the energy technology that we analyzed, (ii) the design process that was used to select cost-effective energy systems and de-risk their design and operation, and (iii) the modeling frameworks that were used. We will close with describing advantages and limitations of each of these three items.

This section therefore gives the key technical and process background for the analysis of the later sections.

3.1 THERMAL ENERGY NETWORKS

We selected TENs as a key candidate solution, besides several decentralized, building-only energy systems, to reduce life cycle costs, increase energy efficiency, reduce peak electrical demand and improve energy supply security through the integration of DERs. Combined, these measures improve energy efficiency, grid stability and resilience.

TENs are also known as district energy systems. They distribute thermal energy for heating and cooling from one or multiple sources and storage devices to multiple buildings within a site. Under appropriate site conditions, TENs are a cost-effective means to improve energy efficiency and reduce peak electrical demand, and thus help with electrical grid reliability, increase resilience to heat wave, cold snaps and technology changes. Through their integration of storage and DER, they also improve energy security. As TENs can avoid use of cooling towers or air-source heat pumps in the buildings, and instead offer an opportunity to centralize such maintenance intensive devices, in particular if wet cooling towers are used, they can also reduce maintenance burden.

A key innovation in modern TENs is the concept of reservoir networks. Based on the work of Sommer et al. (2020), reservoir networks utilize a modular approach where thermal reservoirs act as hubs for storing and distributing thermal energy. Two key properties of reservoir networks is that additional loads can be added to a reservoir network, and that reservoir networks can be meshed together to form a reservoir mesh as explained in Wetter and Hu (2019). This modularity allows for:

- **Scalability**: TENs can be expanded incrementally as funding becomes available or demand grows in two ways: Within a thermal grid, additional buildings, storage and plants can be modularly added. Moreover, within a campus, additional loops can be built and interconnected with existing loops to share excess waste heat or cold across the base.
- **Design Flexibility**: Different thermal energy sources, including low-temperature waste heat such as from data centers and various types of storage systems, can be integrated seamlessly.
- **Operational Flexibility** Large TENs provide an opportunity for cost-effective storage integration, thereby providing utility-scale opportunities for bidding load flexibility into an electricity market.
- **Optimized Energy Use**: Thermal loads are balanced across the network, reducing peak demand and improving overall efficiency as excess waste heat and waste cold can be shared across buildings and supplemented with storage or centralized plants as needed.

The design contract for these reservoir networks involves defining clear interfaces, agreed upon operating envelopes and functionalities provided by the modules, ensuring compatibility and interoperability between different components and technologies. This standardized approach simplifies the integration of various DERs and facilitates maintenance and upgrades.

Implementing TENs with reservoir networks requires a comprehensive, model-based design process that can select the most cost effective technology options and robustly design their integration, taking into account the dynamics of integrating multiple energy sources, storage options, and building types. The outcome of such a holistic data-driven design process will be cost-effective solutions that reduce peak electricity, increase grid reliability, improve resilience and energy security, and provide robust operation.

3.2 PLATFORM-BASED DESIGN PROCESS

Designing and deploying TENs in complex conditions like a DoD site necessitates a robust design process supported by the Platform-Based Design (PBD) process. PBD is a systematic approach that streamlines the planning and deployment of complex system designs by using common platforms at different levels of abstraction into which various systems and technologies (e.g., components) can be integrated. Appendix B explains in more detail the main principles of PBD.

In the context of TENs, PBD offers several advantages (Sulzer et al., 2023):

Modularity: PBD enables the use of interchangeable components, facilitating a standardized design process through DoD sites. Modularity also facilitates upgrades and expansion.

Regularity and structure: PBD uses standardized components across a system, assembled through clear design rules. This allows for high reusability, fast development time and simplified maintenance compared to bespoke design. This restriction in design space achieves lower costs, reduced integration risk, and more successful first design attempts.

Small design iterations: The layered structure, starting at a high level of abstraction and followed by a formal refinement that increases design resolution, allows for short iteration cycles when selected architectures miss performance targets.

Reduced risk: The successive refinement that occurs during the design process in which design progresses from holistic system optimization to detailed component design and simulation-based verification reduces integration risks as designs are continuously tested for requirement satisfaction at every stage of the design process.

Reduced design and planning time: Standardized platforms reduce the time needed for system design, planning, and testing.

Cost Efficiency: Leveraging common platforms reduces duplication of efforts and resources.

By integrating advanced modeling techniques within the PBD process, in our analysis MILP and Modelica, we can enhance the design process to address the complexity and scalability required for TENs.

The outcome is a well-structured PBD process that incorporates models at different levels of abstraction, e.g., fit-for-purpose, thereby enabling designers to tackle complex system integration tasks effectively, ensuring sound investment decisions and robust system performance.

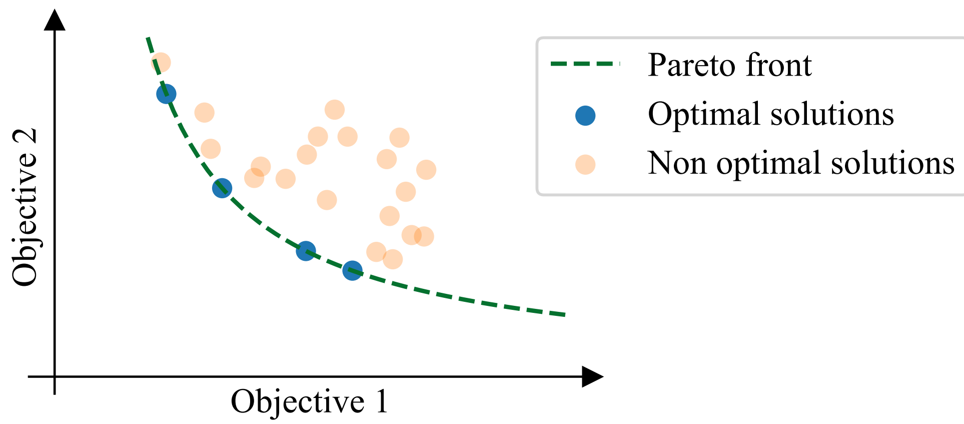

Figure 1. Pareto front. The blue points minimize *Objective 1* and *Objective 2*.

3.3 MODELING FRAMEWORK

Exploring design options, optimizing system performance, and verifying that the thermal microgrid operates as intended requires an integrated model framework. This framework comprises models at different levels of abstraction, integrated through the PBD process. The modeling framework utilizes Mixed-Integer Linear Programming (MILP) and nonlinear dynamic system modeling using the Modelica equation-based language. MILP is used for system architecture selection including component sizing, while nonlinear system models are used for detailed design and verification. The nonlinear dynamic system models represent the performance and dynamic interaction of the equipment, piping networks and controls. The next section explain the modeling framework in more detail.

3.3.1 Mixed-Integer Linear Programming (MILP) Models

Mixed-Integer Linear Programming (MILP) is a mathematical optimization technique that handles decision variables that are both continuous and discrete (integer-valued). In the context of TENs, MILP models are integral to the early stages of the design process, particularly for system architecture exploration and multi-objective optimization (Bollinger, Marquant, and Sulzer, 2019).

Within the PBD framework, MILP models are used for the following.

- **System Configuration Optimization**: Determine the optimal mix of technologies (e.g., gas boilers, heat pumps, thermal and electrical storage) and their capacities to meet the thermal demands of the network.
- **Operational Strategy Development**: Optimize control strategies for the operation of the thermal and electrical system, including scheduling of equipment and energy flow management.
- **Multi-Objective Trade-Off Analysis**: Evaluate trade-offs between competing objectives such as life cycle costs vs imported energy, the latter as a measure for increasing energy supply security.

The MILP optimization computes a Pareto front that corresponds to the optimal solutions for given objectives, as shown in Fig. 1

By incorporating MILP models into the PBD process, designers can perform high-level optimization that informs the overall system architecture. This integration ensures that the system design aligns with strategic objectives and provides a solid foundation for subsequent detailed design.

3.3.2 Modelica Models

Modelica is an object-oriented, equation-based language designed for modeling and simulating of complex multi-domain physical systems (Mattsson and Elmqvist, 1997). It is used extensively in various industry sectors for design and control of components and systems. In the design of TENs, Modelica models are crucial for detailed system analysis, refinement, and verification.

Within the PBD framework, Modelica models from the Modelica Buildings Library (Wetter, Zuo, et al., 2014) are utilized for the following.

- **Detailed System Design**: Modelica is used for the detailed sizing and to verify the sizes suggested by the simplified models used by the MILP optimization.

  For example, the Modelica Buildings Library has detailed models for geothermal borefields that are coupled to energy systems in order to verify or improve the sizing, taking actual system-level operation into account.

- **Detailed Dynamic Simulation**: The models represent the dynamic behavior of HVAC equipment, storage technologies, ground coupled heat exchange in borefields, in the TEN distribution and in its service lines. They also model supervisory and local loop feedback control, including equipment dispatch and lock-out, setpoint resets and proportional-integral control for temperature tracking. The models compute pressure at each point of the piping network based on equipment sizes, piping dimensions, and control valve positions and pump control signals, and through this, dynamically compute the resulting mass and energy flow rates. Due to these capabilities, the models are used to detecting potential problematic system designs and verify controls as described below.

  For example, Wetter and Hu (2019) shows a problematic system design that is prone to control instability. It also shows how models were used to reproduce the problem in simulation and to develop alternative hydronic and control configurations.

- **Reusable Component Modeling**: Models are modular and reusable, allowing the performance assessment of components such as heat pumps, geothermal borefields, and control algorithms, or of large composite components such as an energy transfer station (ETS) that internally contain heat pumps, storage and controls. This capability facilitates reuse of components, leading to repeatability and standardization of design.

  For example, the ETS described in Section 6.2.4 is based on a design that was used in earlier work (Gautier, Wetter, and Sulzer, 2022; Wetter and Hu, 2019) and expanded in this project to further improve its performance.

- **Control Development, Verification and Potential Integration with Digitalized Workflows in Subsequent Construction**: The MILP optimization uses perfect control, in which control actions are the result of an optimization that has perfect knowledge of the energy system, load and weather, including future loads and weather. Hence, the control is not causal and therefore not implementable. In contrast, in the Modelica development and verification step, actual control logic is modeled as is typically used in a real installation, from supervisory control to local loop control with all scheduling, equipment interlocks, time delays and proportional-integral controllers. These control models are coupled to HVAC system models to verify the correct control operation, to improve the control logic, and to contrast different control strategies. The control models then become the specification for how to implement actual controls (Wetter and Sulzer, 2024). The models can then also be used in a potential phase II to deploy control logic to building automation systems using the emerging ASHRAE Standards 231P and 223P.

  For example, a fully digitalized design-build-deploy workflow based on the proposed ASHRAE Standard 231P has been shown in Wetter, Ehrlich, et al. (2022). Contrasting the control performance has been shown in Zhang et al. (2022) and Milica Grahovac and Wetter (2023). The benefits of a digital control deliver process are discussed in (Pritoni et al., 2024; Wetter, Ehrlich, et al., 2022; Zhang et al., 2022).

- **System Verification**: The MILP optimization uses simplified linear models. It has perfect knowledge of the system and perfect forecast of future loads, weather and energy prices. The Modelica models are used to verify whether the technology selection recommended by the MILP optimization meets the performance specifications and complies with operational constraints.

  For example, Sulzer et al. (2023) show the process of verifying the performance between MILP optimization and detailed Modelica simulations, and Wetter and Sulzer (2024) explains why such a verification is needed.

By integrating Modelica models into the PBD process, designers can refine the system architecture proposed by the MILP optimization and verify its performance through detailed dynamic simulations. This verification step is essential for de-risking the design before implementation.

3.3.3 Integration of MILP and Modelica Models in PBD

The sequential integration of MILP and Modelica models within the PBD process allows a comprehensive exploration of different configurations, the selection of a Pareto-optimal configuration including proposed component sizing, and the subsequent detailed design and performance verification and validation of the selected configuration.

The design process follows a sequential approach:

1. **System Architecture Exploration with MILP**: At this stage, a high-level multi-objective optimization is conducted to determine the Pareto-optimal configurations and their operational strategies. The optimization can be done to minimize strategic objectives such as life cycle costs and energy imported to the site, while meeting constraints such as maximum borefield or PV areas. The outcome is a family of Pareto-optimal configurations, including the capacities of assets such as heat pumps, borefields and batteries.
2. **Selection of Candidate Solutions**: Based on the metrics of the above steps, which also includes auxiliary data such as peak electricity consumption, a particular system architecture

is selected from the family of Pareto-optimal candidate solutions. This selection is done with key stakeholders, and can take into account auxiliary metrics such as investment costs and peak electrical demand reduction to defer potential grid updates. The outcome is a specific configuration that will be used for detailed design.

3. **Detailed Design and Modeling with Modelica**: At this step, the specific configuration is used and its components, hydronic network and control sequence are configured. For example, MILP proposes a certain borefield capacity and heat transfer rate, and at this step, the location and depth of the boreholes are designed. Moreover, archetype systems, for example for an ETS, are selected and their components such as actual heat pumps, energy storage tanks, pumps and control valve sizes are configured. These subsystems are then connected to a complete system model that dynamically computes all heat flow rates, mass flow rates, pressure distributions and control action. The outcome is a dynamic model that can be used in the verification and validation step below.

4. **Verification and Validation**: Using the dynamic model of the above step, the proper operation of the system is tested. Verification tests whether the equipment is operating within prescribed operation envelopes, whether feedback control loops are stable and whether set point temperatures and pressures are maintained. Validation tests whether user requirements such as annual energy use, peak power demand and annual energy costs are met. Validation can also tests the resilience of the system, such as how it operates during a heat wave or how it reacts if a component fails. The outcome is a design that satisfies the specified requirements. The model now becomes a specification for how to build and operate the system.

5. **Iterative Feedback**: At each of the above steps, there may be an iterative feedback. For example, MILP assumes perfect knowledge of the system, perfect knowledge of the future and perfect control, and it simplifies components for computational tractability. If the verification and validation step determines that the required performance cannot be met, an iteration is done and assumptions for MILP may be refined. For example, insight into actual heat pump coefficient of performance (COPs) from Step 3 may be used to refine the COP assumption in MILP. A major benefit of this approach is that iteration loops are small, and missed performance can be corrected early in design before the system is built and operating.

The integration of MILP and Modelica models within the PBD process provides a powerful framework for designing, optimizing, and verifying dynamic systems. This approach addresses the inherent complexity of such systems and supports scalable, robust deployment.

3.4 ADVANTAGES AND LIMITATIONS OF THE TECHNOLOGY

Understanding the strengths and weaknesses of TENs, the design process, and the modeling framework is crucial for informed decision-making. This section describes the advantages, challenges and limitations of these three aspects.

3.4.1 Thermal Energy Networks

TENs offer the following advantages compared to individually heated and cooled buildings.

- **Energy Efficiency**: They increase energy efficiency as buildings can share waste heat and cool among each other. Low temperature waste heat such as from data centers or sewage plants can readily be integrated into 5th generation TENs, further increasing their efficiency.
- **Cost Savings**: They have an economy of scale that allows investment in operational optimization that leads to lower energy and life cycle costs. Their sizes can allow optimal equipment scheduling combined with energy storage to participate in dynamic energy markets.
- **Resilience and Robustness**: Centralized control and modularity enhance the system's ability to respond to disruptions and to adapt to technological changes.
- **Energy supply security**: They are effective means to reduce the amount and the peak of energy that need to be imported to a site to serve building loads. This reduction allows downsizing emergency energy storage and capacity, thereby increasing energy supply security.

The main limitations include the following:

- **Initial Investment**: High upfront costs can be a barrier to implementation.
- **Infrastructure Complexity**: Retrofitting existing buildings and integrating diverse energy sources and storage require careful planning. Due to their dynamic operation and use of energy storage technologies, a PBD approach is strongly recommended to optimize costs, manage design and operational decision complexity, and verify and validate their dynamic performance.
- **Coordination Requirements**: Effective implementation and operation depends on collaboration among various stakeholders. Controls can significantly affect operational energy use (Sommer et al., 2020) and therefore a co-design of the mechanical system and the control is strongly recommended.

3.4.2 Platform-Based Design Process

The PBD process offers the following advantages:

- **Comprehensive Design Coverage**: The layered design approach that is inherent in PBD allows combining strategic optimization with detailed analysis, covering both macro and micro aspects of the system in a formal framework.
- **Risk Reduction**: Early identification of potential issues reduces the risk of costly redesigns late during implementation or during operation.
- **Enhanced Collaboration**: Shared models and standardized formal processes facilitate communication among stakeholders and disciplines. The formal specification at every level of detail also sets clear accountability for the involved designers.

The main challenges include the following:

- **Model Alignment**: Ensuring consistency between the MILP and Modelica models requires careful coordination. Developing reusable components that ensure consistency across the abstraction levels of the different platform layer requires upfront design investments.

- **Data Consistency**: Maintaining accurate and consistent data across different modeling platforms is essential. Using the above reusable components facilitates consistent representation of data that matches the required model details. At the end of this process, these component models represent formal design specifications.
- **Process Management**: Coordinating the iterative design process necessitates robust project management practices and training of project leaders in PBD principles.

3.4.3 Modeling Framework

MILP offer the following advantages:

- **Enhanced Decision-Making**: MILP models provide quantitative data that support informed decision-making regarding technology selection, equipment sizing, investments and operational costs.
- **Efficiency**: MILP allows the exploration of a large solution space that would be intractable with detailed nonlinear models. This enables identifying optimal configurations that would not be possible using manual calculations such as in spreadsheets.
- **Flexibility**: It can incorporate various constraints and objectives, making the models adaptable to different scenarios and requirements.

The main limitations of MILP include the following:

- **Model Simplifications**: MILP requires considerable model simplifications to keep the problem computationally tractable. Important system dynamics, physical and operational constraints may not be part of the model. For example, an important limitation of MILP is that it considerably simplifies the heat exchange and storage in the borefield as MILP does not compute the temperature distribution in the subsurface. Thereby a verification and validation step with nonlinear dynamic system simulation is needed to de-risk design and operational decisions.
- **Data Intensive**: Accurate optimization relies on high-quality input data. The quality of the data impacts the uncertainty of the optimal design decisions.
- **Computational Complexity**: Large-scale MILP problems can be computationally demanding, requiring significant processing power and time.

Using dynamic modeling with Modelica offers the following advantages:

- **Accuracy**: Modelica enables high-fidelity simulations that capture complex dynamic interactions within the system.
- **Reusability**: Its modular approach allows for the creation of libraries of component and subsystems that can be reused in different projects. Such components can be structured to allow easy configuration by users through high-level design specifications (Gautier, Wetter, Hu, et al., 2023).
- **Cross-Domain Modeling**: It is capable of simulating interactions across multiple physical or operations domains (e.g., heat flow, mass flow, pressure distributions, control), providing a

comprehensive system view. It also allows modeling actual control sequences at the level of detail that is used in real installations, thereby enabling a digitalized controls design and delivery process based on open ASHRAE Standards 231P and 223P (Pritoni et al., 2024; Wetter, Ehrlich, et al., 2022).

The main limitations include the following:

- **Complexity**: Developing detailed models that are not already available in a library can be time-consuming and requires expertise in specifying HVAC systems and control logic. To master large system models, training in how to structure system models, and how to effectively use the Modelica language is essential, in addition to domain expertise in energy systems and/or controls.
- **Computational Resources**: High-fidelity simulations can be time-consuming, and the computational efficiency can highly depend on how models are formulated.
- **Data Requirements**: Accurate simulations depend on high-quality component parameters and control logic implementation.

In summary, proper application of PBD workflow requires training in the workflow and the underlying computational tools. However, doing so enables holistic design space exploration and de-risking system integration, leading to cost-effective reliable energy systems. The application of this process will be demonstrated in the subsequent sections.

4.0 PERFORMANCE OBJECTIVES

In this section, we will describe the performance objectives of the study. The performance objectives have been developed in consultation with DoD, and they are categorized into quantitative and qualitative metrics, each with specific data requirements and success criteria. They are designed to assess economic feasibility, energy efficiency and supply security, resilience and operational maintainability. Also considered are practical implementation aspects of the proposed technologies.

Having a set of clear performance metrics is critical to ensure successful feasibility analysis, design and implementation of the TEN. In the subsequent sections, these performance objectives will be used, as needed in a more refined way, to verify whether the design meets the requirements.

4.1 QUANTITATIVE PERFORMANCE OBJECTIVES

The quantitative performance objectives focus on measurable outcomes related to energy supply security, life cycle costs, and investments. Many metrics compare against a baseline, which is a conventional system with gas heating and air-source chiller, without any PVs or batteries, but with building retrofits applied as for all other considered design options. This conventional system is described in Section 6.2.1 and its optimal equipment sizing and operational schedule is determined in Section 7.0.

The following metrics have been identified:

4.1.1 Energy Import

Performance Objective: Significantly reduce the amount of imported energy for the buildings to increase the energy security of the site.
Data Requirements:

- Total energy import data for electricity and gas for the site. (The site has no thermal energy import.)

Success Criteria:

- Imported energy reduced by at least 50% compared to baseline.
- Total energy import is reduced in alignment with DoD's targets.

4.1.2 Life Cycle Cost (LCC)

Performance Objective: Ensure the life cycle cost of the new system remains financially viable.
Data Requirements:

- Detailed cost estimates for capital expenditure (CapEx, investments) and operational expenditure (OpEx, energy and maintenance costs).
- Estimates of equipment lifetime in years.
- Discount rates and inflation factors for financial analysis.

Success Criteria:

- Life-cycle cost no more than 120% of the baseline.
- Levelized cost of energy for heating and cooling no more than 0.25 USD/kWh.

4.1.3 Investments

Performance Objective: Manage initial investment costs effectively.
Data Requirements:

- Capital cost estimates for equipment, installation, and commissioning.
- Comparison of investment costs between the proposed system and the current system.
- Financing options and available budget allocations.

Success Criteria:

- Investment cost no more than 200% of baseline.
- Investment cost no more than 110% of baseline if central plant infrastructure, district loops, and utility-scale PV and battery systems are privatized.
- Identification of what high investment assets can be privatized to reduce DoD investments.
- Identification of phased investment opportunities to spread investments over time.
- Securing funding without compromising other essential DoD operations.

4.2 QUALITATIVE PERFORMANCE OBJECTIVES

Qualitative performance objectives address practical and operational aspects of implementing the new technologies. They are assessed using expert judgment provided by the industry partner Southland and focus on factors such as system complexity and capabilities.

4.2.1 System Complexity

Performance Objective: Maintain an acceptable level of system complexity.
Data Requirements:

- Modularity of the design and control.
- Dynamic analysis of the system, including the dynamic interactions of its components.
- Evaluation of control strategies applied to dynamic model of the energy system.
- Assessment of potential operational challenges such as possible control instability due to coupling of control loops with similar dynamics or large transport delays in piping networks.

Success Criteria:

- System complexity is rated by industry partner Southland as medium-high.
- System is modular to allow staged build-out, to replace or add new components.
- Control of overall system, including the ETS and central plant, is modular and stable, and coupling of control loops, or of resulting control actions, between the various distributed ETSs is minimized by design to reduce risk of oscillatory control.

- Complexity is justified by the benefits (e.g., efficiency, resilience) without posing operational complexities that risk effective operation.
- Comprehensive testing and documentation to ensure control performance and manage complexity.

4.2.2 Industry Installation Capabilities

Performance Objective: Ensure that the required technologies can be installed by the industry using existing capabilities.
Data Requirements:

- Evaluation of industry expertise and experience with similar installations.
- Availability of contractors and suppliers with the necessary skills and certifications.
- Analysis of supply chain constraints and logistical considerations.

Success Criteria:

- No unique installation capabilities are needed.
- Confirmation that the industry can meet installation requirements within the typical project timelines.
- Establishment of partnerships with experienced industry players to mitigate risks.

4.2.3 Site Operation Capabilities

While this section lists operational capabilities, some items such as development of training materials would need to be subject of a phase II that focuses on detailed design, construction and operation.

Performance Objective: Align the new system with the operational capabilities of the site personnel.
Data Requirements:

- Assessment of current staff skills and training levels.
- Identification of additional training needs and resources required.
- Evaluation of operation and maintenance (O&M) procedures for the new system.

Success Criteria:

- Site operation capabilities are rated as medium.
- Site personnel can operate and maintain the new system with reasonable training.
- Development of training programs and support materials to enhance staff proficiency.

4.2.4 Operational Resilience during Equipment Failure

Performance Objective: Ensure resilient operation during equipment failure.
Data Requirements:

- Bill of material of large equipment such as chillers and heat pumps that may be time consuming to replace due to supply chain issues.

Success Criteria:

- Design that relies on standard, off-the shelve equipment that can readily be replaced.
- Design that uses standardized and repeatable installations across buildings to reduce training of maintenance people and to allow sharing of replacement parts across buildings.

4.2.5 Operational Resilience during Heat Wave or Cold Snap

Performance Objective: Ensure resilient operation during heat wave or cold snap failure.[1]
Data Requirements:

- Operational envelopes of heat pump evaporators and chiller condensers.
- Dynamic model of energy and control system that can be used to analyze operation during heat wave and cold snap.

Success Criteria:

- Building retrofit that reduces building loads during extreme weather such as through envelop retrofits.
- Cooling and heating generation that is not sensitive to heat waves or cold snaps, such as geothermal coupled chiller, heat pumps and TEN.
- Model-based testing of system operation during a heat wave and a cold snap.

4.3 SUMMARY OF PERFORMANCE OBJECTIVES

Table 1 summarizes the main performance objectives that have been developed with DoD.

4.4 ALIGNMENT WITH DOD GOALS

These performance objectives were established to ensure that the proposed technologies ensure cost-effective, robust and resilient operation and have high energy supply security. By setting clear quantitative targets and qualitative assessments, we aim to:

- **Enhanced Energy Resilience**: Demonstrate that the proposed systems achieve a high degree of energy resilience through energy generation and storage resources sited on military installations.
- **Enhanced Robustness**: Implement systems that are adaptable to technological changes and can withstand operational challenges.

[1] Assumptions for a heat wave and cold snap are described in Section 8.2.

Performance objective	Data requirements	Success criteria
Quantitative performance objectives		
Imported energy	GWh	50% reduction compared to baseline
Peak energy import	MW	40% reduction compared to baseline
LCC	USD	Less than 120% of baseline
Total investments	USD	Less than 200% of baseline
Investment without assets that are suitable for privatization	USD	Less than 110% of baseline
Levelized costs of energy for heating and cooling	USD/kWh	Less than 0.25 $/kWh
Qualitative performance objectives		
System complexity	Expert judgment	Medium-high
Industry installation capabilities	Expert judgment	Medium-high
Site operational capabilities	Expert judgment	Medium
All control loops show stable operation	Dynamic annual simulation	Verified that all control loops are stable during an annual simulation

Table 1. Summary of performance objectives. By baseline system, we mean a conventional system with gas heating and air-source chiller, without any PVs and batteries.

- **Ensure Economic Viability**: Maintain or improve financial performance over the system's life cycle, making the investment justifiable.
- **Facilitate Practical Implementation**: Utilize existing industry capabilities and align with the operational capacity of site personnel to ensure successful deployment.
- **Ensure energy supply security**: Achieve a high degree of energy supply security by reducing site energy import from the grid and reducing peak power demand, thereby extending the time for which essential services can be provided in case of an energy supply disruption and reducing investments needed for backup power generation.

4.5 CONTINUOUS IMPROVEMENT AND MONITORING

Achieving these performance objectives requires ongoing monitoring and adaptation. We recommended the following:

- **Implement Monitoring Systems**: Use data analytics and digital twins to track performance metrics in real-time and proactively react to extraordinary operating conditions.
- **Conduct Regular Reviews**: Periodically assess performance against objectives and make necessary adjustments.
- **Engage Stakeholders**: Involve site personnel, industry partners, and policymakers in the evaluation process to gather diverse insights.

- **Update Objectives**: Adjust performance objectives as necessary to reflect changing circumstances, technological advancements, or updated DoD goals.

4.6 CONCLUSION

For the successful design and operation of TENs, it is crucial to set clear performance objectives, follow a process that links system selection, design, deployment and operation with measurable performance metrics that are verified along each stage of the process.

By focusing on both quantitative and qualitative metrics, the DoD can ensure that the proposed solutions are cost-effective, robust, resilient and energy secure. The objectives provide a goal post for measuring success and guiding decision-making throughout the project life cycle.

Note, however, that as we progress from architecture selection to system design, new performance objectives and resulting requirements will be added as appropriate for the respective design step (Sulzer et al., 2023).

5.0 SITE DESCRIPTION

In this section, we will describe the site characteristics, the building characteristics, the used typical weather and energy rates. These are key data and assumptions on which the subsequent analysis is based on.

5.1 SITE LOCATION AND HISTORY

Joint Base Andrews (JBA) is located in Prince George's County, Maryland, and named after Lieutenant General Frank Maxwell Andrews (1884-1943), former Commanding General of United States Armed Forces in the European Theater of Operations during World War II. Established in 2009 after merging Andrews Air Force Base and Naval Air Facility Washington, the base is under the jurisdiction of United States Air Force (USAF) 316th Wing, Air Force District of Washington (AFDW). The base is known for being the home base of aircraft which have the call sign Air Force One while the President of the United States is on board.

5.2 SELECTED BUILDINGS

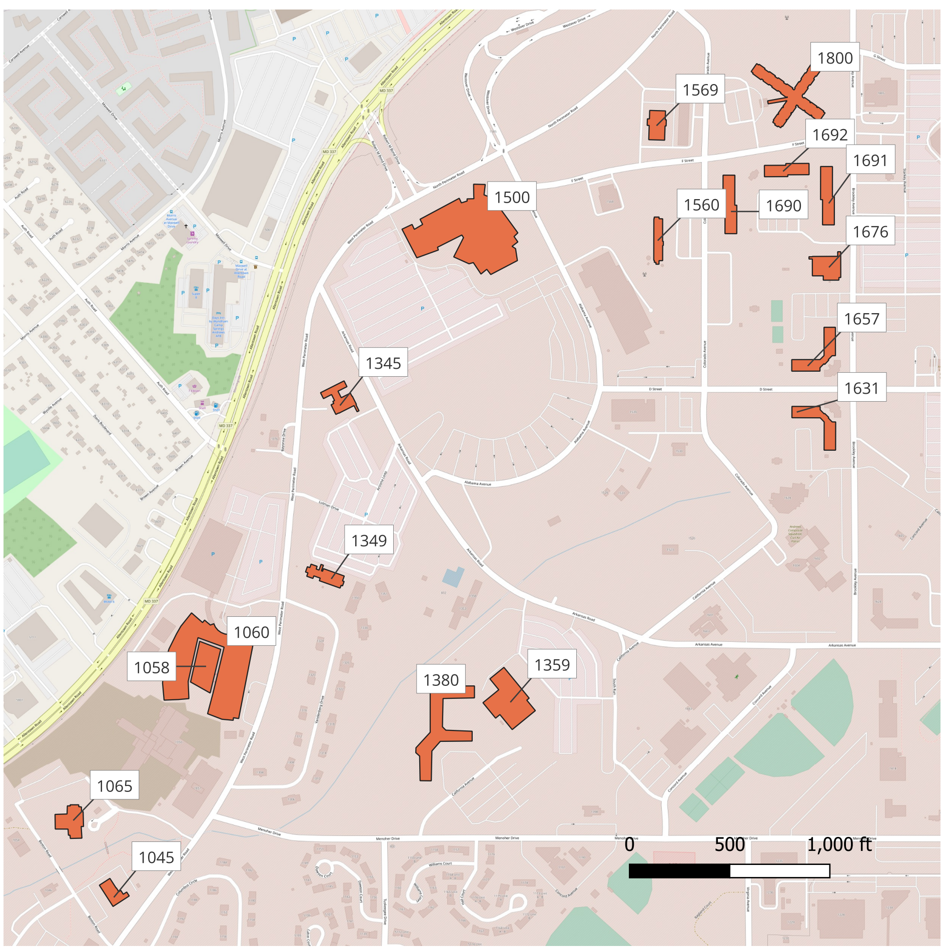

Figure 2. Site map with the different buildings considered.

Number	Name	Gross Area	
		sq. ft.	m^2
1045	Aerospace Physiology Facility	8,230	765
1058&1060	Malcolm Grow Medical	265,117	24,630
1065	Dental Clinic	28,120	2,612
1345	Base Chapel	13,840	1,286
1349	316th Contracting Squadron	18,415	1,711
1359	General Smart Conf Center	45,747	4,250
1380	Presidential Inn	143,000	13,285
1500	Jones Building	330,000	30,658
1560	Navy Communications	25,336	2,354
1569	AAFES Shopette	10,792	1,003
1631	Dorm	45,449	4,222
1657	Dorm	46,000	4,274
1676	Thrift Shop	15,395	1,430
1690	Dorms	53,126	4,936
1691	Dorms	50,532	4,695
1692	Dorms	36,609	3,401
1800	Transient Lodging Facility	69,799	6,485
Total		1,205,507	111,997

Table 2. In-scope buildings on the JBA site

Fig. 2 shows the location of the buildings considered in this study. Table 2 provides a summary of the floor area for each of these buildings.

The selected buildings have a variety of heating and cooling systems. The majority of the buildings are served by central plant systems equipped with either air-cooled or water-cooled chillers and central boiler plants. Cooling is provided primarily by air-cooled chiller systems serving variable air volume (VAV) or fan coil air-side systems. Several smaller, stand-alone service buildings are served by packaged direct expansion (DX) units with gas furnaces for heating. Table 3 shows the existing heating and cooling system in each building.

5.3 CONSUMPTION

This section explains the data and process used to compute the hourly energy consumptions to be served by the analyzed energy systems.

5.3.1 Energy Models for Hourly Load Profiles

To compute the hourly energy consumption, we calibrated whole building energy simulation to measured data, and then applied building and HVAC retrofit measures to the energy models. This was done using the eQuest building energy simulation program, which computes annual hourly time series for heating, cooling and electricity consumption of the buildings.

Many of the JBA buildings had complete and consistent monthly electric and natural gas utility

Building Number	Bldg Description	Airside Type	Cooling Source	Heating Source
1045	Aerospace Physiology Fac	Packaged Single Zone	DX	Furnace
1051	Bandolzer	VAV	Air Cooled Chiller	HHW Boiler
1058/1060	Malcom Grow Medical	VAV	Water Cooled Chiller	HHW Boiler
1065	Dental Clinic	VAV	Air Cooled Chiller	HHW Boiler
1345	Base Chapel	Single Zone	Air Cooled Chiller	HHW Boiler
1349	316 Contracting Squadron	Fan Coil	Air Cooled Chiller	HHW Boiler
1359	General Smart Conf Center	VAV	Air Cooled Chiller	HHW Boiler
1380	Presidential Inn	Fan Coil	Air Cooled Chiller	HHW Boiler
1500	Jones Building	VAV	Water Cooled Chiller	HHW Boiler
1539	Air Force Communications	Packaged Single Zone	DX	Furnace
1560	Navy Communications	Fan Coil	Air Cooled Chiller	HHW Boiler
1569	AAFES Shopette	Packaged Single Zone	DX	Furnace
1631	Dorm	Fan Coil	Air Cooled Chiller	HHW Boiler
1657	Dorm	Fan Coil	Air Cooled Chiller	HHW Boiler
1676	Thrift Shop	Single Zone	Air Cooled Chiller	HHW Boiler
1690	Dorms	Fan Coil	Air Cooled Chiller	HHW Boiler
1691	Dorms	Fan Coil	Air Cooled Chiller	HHW Boiler
1692	Dorms	Fan Coil	Air Cooled Chiller	HHW Boiler
1800	Transient Lodging Facility	Fan Coil	Air Cooled Chiller	HHW Boiler
3500	ANG Readiness Center (N)	VAV	Air Cooled Chiller	HHW Boiler
3501	ANG Readiness Center (S)	VAV	Air Cooled Chiller	HHW Boiler

Table 3. Existing heating and cooling system in each building.

data, which is on par with what is typically encountered for similar DoD facilities. The Malcolm Grow Medical Center (Building 1058/1060) had partial or missing utility data, gaps in billing records, or usage patterns that reflected atypical or intermittent operation. This was primarily due to the fact that the medical facilities were not served by the base wide EMCS system but rather had a separate, dedicated system that had not been configured to gather building meter data.

As a result of the feasibility study, Siemens, the EMCS contractor, was paid to gather meter data producing more than two years of monthly and 15-minute interval data that is now available to support further development. The contracting and subsequent data collection process for this additional meter data took roughly 6-12 months to complete which meant that the data was not available when the energy models were built and calibrated.

The models were calibrated against the utility data of the site using weather data from the Typical Meteorological Year version 3 (TMY3) (Wilcox, 2008) for the Andrews Air Force Base[2].

For the space heating and cooling loads, the energy consumption profiles represent the air handler heating or cooling coil loads, as these are the loads that need to be served by the modeled energy system. For domestic hot water (DHW), they represent the energy provided to the DHW distribution system, as generation and storage losses will be modeled by the system model.

The 20 energy models were calibrated using generally accepted industry practices. Where adequate utility data were available, modeled energy use was compared to measured building utility data on a monthly and annual basis. In most cases, the models were calibrated to achieve approximately ±20% agreement at the monthly level and ±10% agreement on an annual basis.

For buildings in which electrical and/or natural gas utility data were incomplete, unavailable, or showed irregular operating patterns, calibration was limited by the quality of the available data and required reasonable assumptions related to building operation, including periods of erratic use or currently low energy consumption. As a result, strict adherence to standard calibration targets was not possible for all models.

Each model was calibrated as closely as practicable to the available data using professional judgment and consistent application of accepted modeling practices.

The models were based on the following temperature assumptions which were collected during a site visit. The same assumptions were used for both the pre-retrofit and post-retrofit calibration models to generate energy consumption profiles. As we will analyze heat pump systems, and the performance of heat pumps is sensitive to operating temperatures, we will adjust in the subsequent MILP and Modelica models some of these set points while serving the same energy to the loads.

5.3.2 Chilled Water

In the eQuest model, the chilled water supply temperature is 6.7 °C (44 °F) at 5.6 °C (10 °F) design temperature difference.

5.3.3 Heating Hot Water

In the eQuest model, newer buildings with condensing boilers and variable air volume reheat (VAVRH) systems (buildings 1058-1060, 1065, 1359, and 1500) use a heating hot water supply

[2]See Andrews AFB TMY3 (74590).

temperature of 60 °C (140 °F) in the models, while other buildings use 82 °C (180 °F), both at 22 °C (40 °F) design ΔT. Building 1045 uses furnaces with a set point of 49 °C (120 °F).

5.3.4 Domestic Hot Water

The supply temperature to the DHW distribution system is 57 °C (135 °F) for all buildings.

5.3.5 Room Temperature Set Points

The occupied room temperature set points are 21 °C (70 °F) for heating and 24 °C (76 °F) for cooling, with a setback of 18 °C (64 °F) and 28 °C (82 °F), respectively.

5.3.6 Buildings Lacking Measurement Data

Where data were incomplete or inconsistent, reasonable assumptions were required regarding building schedules, operating conditions, and current levels of use. These assumptions were informed by available documentation, discussions with site representatives, and comparison to similar building types. In some cases, buildings were operating at unusually low or irregular loads, which limited the ability to achieve tighter monthly calibration. Table 4 lists buildings with missing or incomplete utility data.

Building Number	Missing Electric	Missing Natural Gas	Notes
1051	Y	Y	
1058/1060	Y	N	Calibrated only to gas data, building modeled based on footprint and levels for 1058/1060.
1065	Y	N	Electric data unavailable, calibrated gas data to DHW baseload.
1657	N	N	Building condemned, model assumes normal use, modeled similar to 1800 TLF.
1690	N	Y	
1691	N	Y	

Table 4. Buildings with missing or incomplete utility data.

For the dorm buildings, the medical center and the dental clinic, additional assumptions had to be done as not all required measurement data were available at the time of the load generation.

The dorm buildings (1631, 1657, 1690, 1691, and 1692) were not under regular operation, as they were either closed, at a low level of usage or had non-functional systems. Therefore, their consumption data were not directly used. Rather, they were modeled under the same assumptions as building 1800 Transient Lodging Facility, using its level of water use based on floor area, water temperature, and occupancy patterns. Building 1800 is a long-term lodging facility for families and we have high confidence with its calibrated model.

Electricity data were not available for Buildings 1058 and 1060 (Malcolm Grow Medical Center) and Building 1065 (Dental Clinic) at the time the calibration models were completed. Therefore, these two medical buildings were calibrated only against natural gas data. To better account for summer base loads, the natural gas data were separated into space heating and DHW consumption. Other process natural gas loads, such as those from autoclaves and sterilizers, were not considered separately as no submetering was available. We calibrated the heating energy mainly by adjusting zonal and outside air flows. This also resulted in a more representative estimation of the cooling energy consumption. By applying typical assumptions regarding occupancy, equipment schedules, air flow, and power densities for hospital building spaces, the estimated electricity consumption, including cooling and other end uses, reflected levels corresponding to the modeled natural gas consumption.

5.3.7 Energy Conservation Measures

After the pre-ECM energy consumption calculation, selected energy conservation measures (ECM) where applied to the model to reduce loads and system temperatures. This system temperature reduction also facilitates the retrofit with heat pumps. We considered retrofit measures in the following categories:

1. Envelope enhancements, including adding insulation, reducing infiltration, and retrofitting windows.
2. Improve control schedules and economizer sequence of operation.
3. Seal ducts.
4. Improve lighting efficiency.
5. Reduce simultaneous heating and cooling.

A detailed ECM matrix is shown in Appendix D. These ECM measures were then applied to the pre-ECM energy models to compute new load data. The post-ECM energy consumption profiles of the buildings are shown in Fig. C.1 through Fig. C.17 and Fig. C.18 shows the energy consumption profile of all in-scope buildings combined.

Table 5 shows the difference of energy consumption between the pre-ECM models and post-ECM models for all considered buildings. Annual electricity consumption was substantially reduced by 31.0%. This decrease of internal load lead to a 10.7% increase of space heating use and 10.0% decrease of cooling load. The difference in cooling and heating consumption is moderate because plant efficiency retrofits are out of scope of these ECMs and will be investigated in the following sections. Despite the increase in annual space heating consumption, the peak demand decreased. Led by a substantial electric peak demand decrease of 21.9%, cooling and space heating peak demands decreased by 4.4% and 2.5%, respectively. We will discuss the future weather conditions shown in Table 5 in section 5.3.8.

5.3.8 Future Weather

As the base expressed its concerned that the TMY3 weather profile may not reflect the future weather conditions under which our proposed system will operate, we also projected the post-ECM energy consumption of in-scope buildings to a future weather file. The file is from the future

	End use					Demand				
Electricity		[MWh]	[kBTU/sf]	[kWh/m^2]			[kW]	[W/sf]	[W/m^2]	
Pre-ECM		12,699	10.5	113.4			4,023	3.3	35.9	
Post-ECM		8,757	7.3	78.2	*-31.0%*		3,141	2.6	28.0	*-21.9%*
Future		8,854	7.3	79.1	*+1.1%*		3,596	3.0	32.1	*+14.5%*
Cooling	[MMBTU]	[MWh]	[kBTU/sf]	[kWh/m^2]		[kBTU/h]	[kW]	[BTU/h/sf]	[W/m^2]	
Pre-ECM	54,566	15,992	45.3	142.8		35,410	10,357	29.3	92.5	
Post-ECM	49,118	14,395	40.7	128.5	*-10.0%*	33,783	9,901	28.0	88.4	*-4.4%*
Future	57,693	16,908	47.9	151.0	*+17.5%*	35,989	10,547	30.0	94.2	*6.5%*
Space Heating	[MMBTU]	[MWh]	[kBTU/sf]	[kWh/m^2]		[kBTU/h]	[kW]	[BTU/h/sf]	[W/m^2]	
Pre-ECM	34,744	10,182	28.8	90.9		24,203	7,093	20.1	63.3	
Post-ECM	38,477	11,277	31.9	100.7	*+10.7%*	23,593	6,914	19.6	61.7	*-2.5%*
Future	34,396	10,081	28.5	90.0	*-10.6%*	20,846	6,109	17.3	54.5	*-11.6%*
DHW	[MMBTU]	[MWh]	[kBTU/sf]	[kWh/m^2]		[kBTU/h]	[kW]	[BTU/h/sf]	[W/m^2]	
Pre-ECM	16,852	4,939	14.0	44.1		2,951	865	2.4	7.7	
Post-ECM	16,851	4,939	14.0	44.1	*0.0%*	2,948	864	2.4	7.7	*0.0%*
Future	16,204	4,749	13.4	42.4	*-3.8%*	2,877	843	2.4	7.5	*-2.4%*

Table 5. Energy consumption computed from models under the pre-ECM, post-ECM, and future conditions for all in-scope buildings. *Electricity* refers non-compressor electric loads such as lighting, plug loads, and terminal fan power, but not consumption of distribution pumps or cooling tower fans that are part of the plant; *Cooling* and *Space heating* both refer to end-use coil loads; *DHW* refers to the load provided to the distribution system.

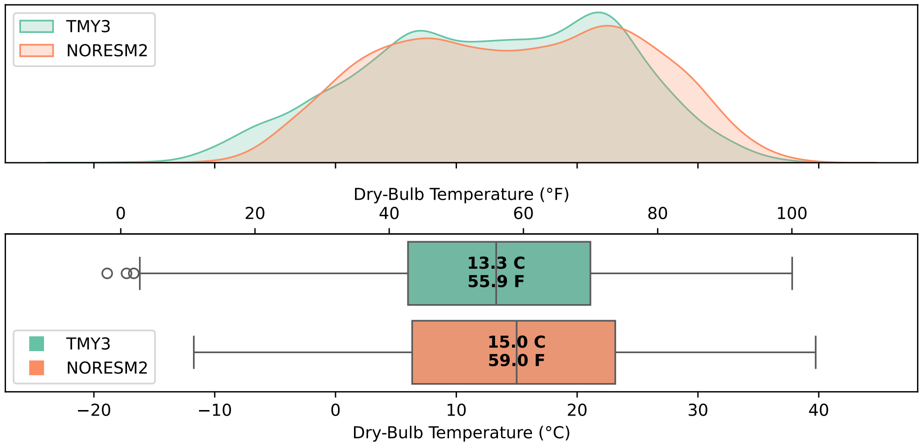

Figure 3. Comparison of temperature distributions of the TMY3 weather file and the fTMY weather files using NorSEM2. The median temperatures are marked in the box-whisker plots.

typical meteorological year (fTMY) dataset (Chowdhury et al., 2023) using the NorSEM2 method developed by the Norwegian Meteorological Institute (Seland et al., 2020).

Fig. 4 shows how the temperature distributions between TMY3 and fTMY. As shown in Table 5, compared to the post-ECM consumption using the TMY3 weather file, the post-ECM models under the fTMY weather file saw a significant increase in cooling consumption of 17.5% and a decrease in space heating consumption of 10.6%. Fig. C.1 through Fig. C.18 show the energy consumption profiles of each individual building as well as all buildings combined for these two weather files. The combined profile in Fig. C.18 shows that the combined load shifted from being slightly heating dominated to slightly cooling dominated.

5.4 SUPPLY

We will now describe the energy rate structure and the available surface area on which PVs may be installed.

5.4.1 Energy Import Rates

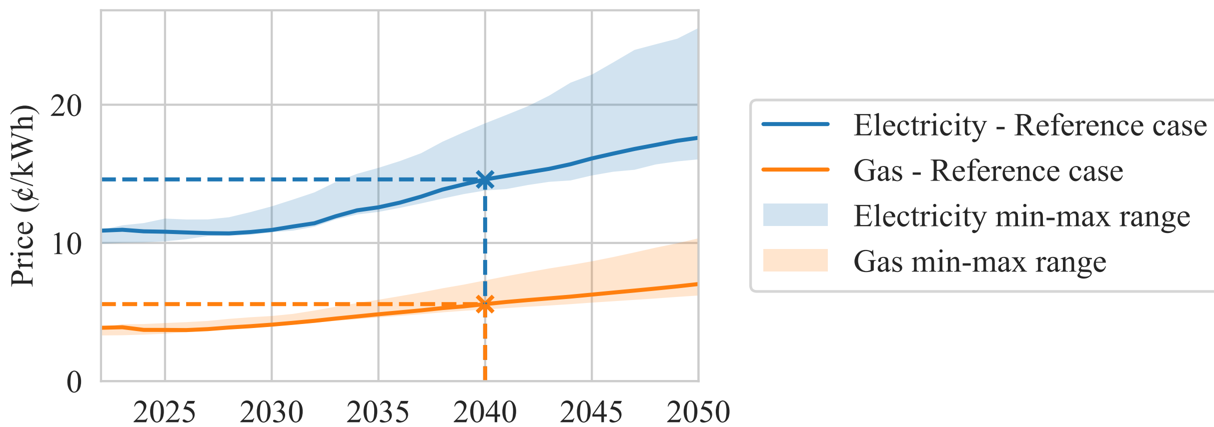

Figure 4. Projected energy price evolution in the South Atlantic region (EIA, 2023a).

The Energy Outlook of the Energy Information Administration (EIA) contains projected future energy rates based on scenarios and factors such as economic growth, future oil prices, the size of domestic energy resources, and technology changes (EIA, 2023b). Fig. 4 shows the energy rates for both electricity and gas, for the reference case scenario called *ref2023* for the South Atlantic region which contains Joint Base Andrews (see J for the region). The projected future energy rates also contain a minimum and maximum bound (EIA, 2023a).

For our analysis, we used the projected future energy rates of the reference case *ref2023* of the year 2040, which lists an average electricity rate of 14.6 ¢/kWh and a gas rate of 5.6 ¢/kWh for gas.

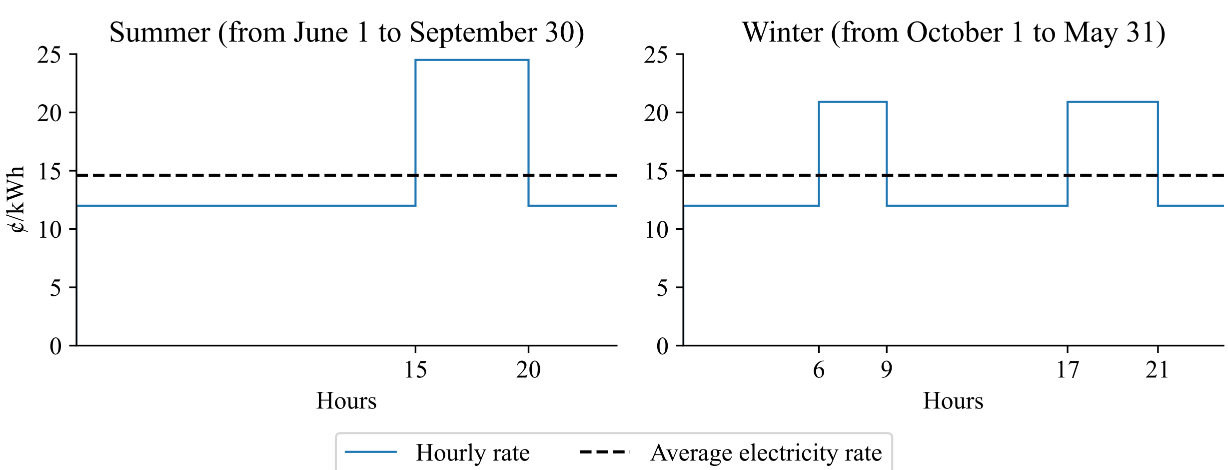

Figure 5. Summer and winter electricity rates.

As many utilities move towards variable rates, and because the spread in rates affects controls for demand shifting, sizing of storage and equipment, we added a spread between normal and high rate of around a factor of two, while keeping the average daily electricity rate at 14.6 ¢/kWh. This leads to the following electricity rate profile, which is also shown in Fig. 5:

- Summer rates are June to September. Low rates are 20:00 to 15:00 at 12.0 ¢/kWh and otherwise it is high rates at 24.5 ¢/kWh.
- Winter rates are October to May. Low rates are 00:00 to 6:00, 9:00 to 17:00, and 21:00 to 24:00 at 12.0 ¢/kWh, and otherwise it is high rates at 20.9 ¢/kWh.

For gas, we use a flat rate.

5.4.2 Electricity Export Rates

As we will discuss below, all candidate solutions have the option to have PV and batteries. The MILP system optimization will size these equipment and compute optimal operation schedules. Should excess electricity be exported, then we assume an export rate of 3 ¢/kWh, which is the annual average Power Purchase Agreement (PPA) price in the PJM Interconnection Region, which includes Joint Base Andrews, in 2019 and 2020 (Bolinger et al., 2023).

5.4.3 Available PV Surfaces

Fig. 6 shows the rooftop and parking lot areas on which PV panels can potentially be installed. After consulting with the base, we assume that for buildings, the default area allocated for PV panels is 80% of the building's footprint. This allocation is reduced to 50% if part of the rooftop cannot be covered, and to 0% if no panel can be installed.

In summary, a total area of 509,000 ft^2 on rooftops and 390,000 ft^2 on parking lots are found to be suitable for PV panel installation. The PV area per building is available in Appendix I.

5.5 FINANCIAL ASSUMPTIONS

We assume a project duration of $D = 20$ years for the capital budgeting analysis and the corresponding life-cycle cost analysis.

Based on the Consumer Price Index for All Urban Consumers (US Bureau of Labor Statistics, 2024), we assume an expected inflation rate of $g = 3$ %, which is close to the average inflation rate in the U.S. of 2.88 % between October 2014 and October 2024.

We also assume a nominal interest rate of $i = 5$ % based on (NYU Stern School of Business, 2024), reflecting the financial risks on energy system investments.

Hence, the real discount rate is calculated as

$$r = \frac{i - g}{1 + g} = 1.94\%. \tag{1}$$

The real discount rate is the rate used to discount future cash flows to their present value.

We use a Capital Recovery Factor of

$$CRF = \frac{r(1+r)^D}{(1+r)^D - 1} = 6.08\%. \tag{2}$$

It allows to convert a present value into a series of equal annual payments over the duration of the project, accounting for the time value of money.

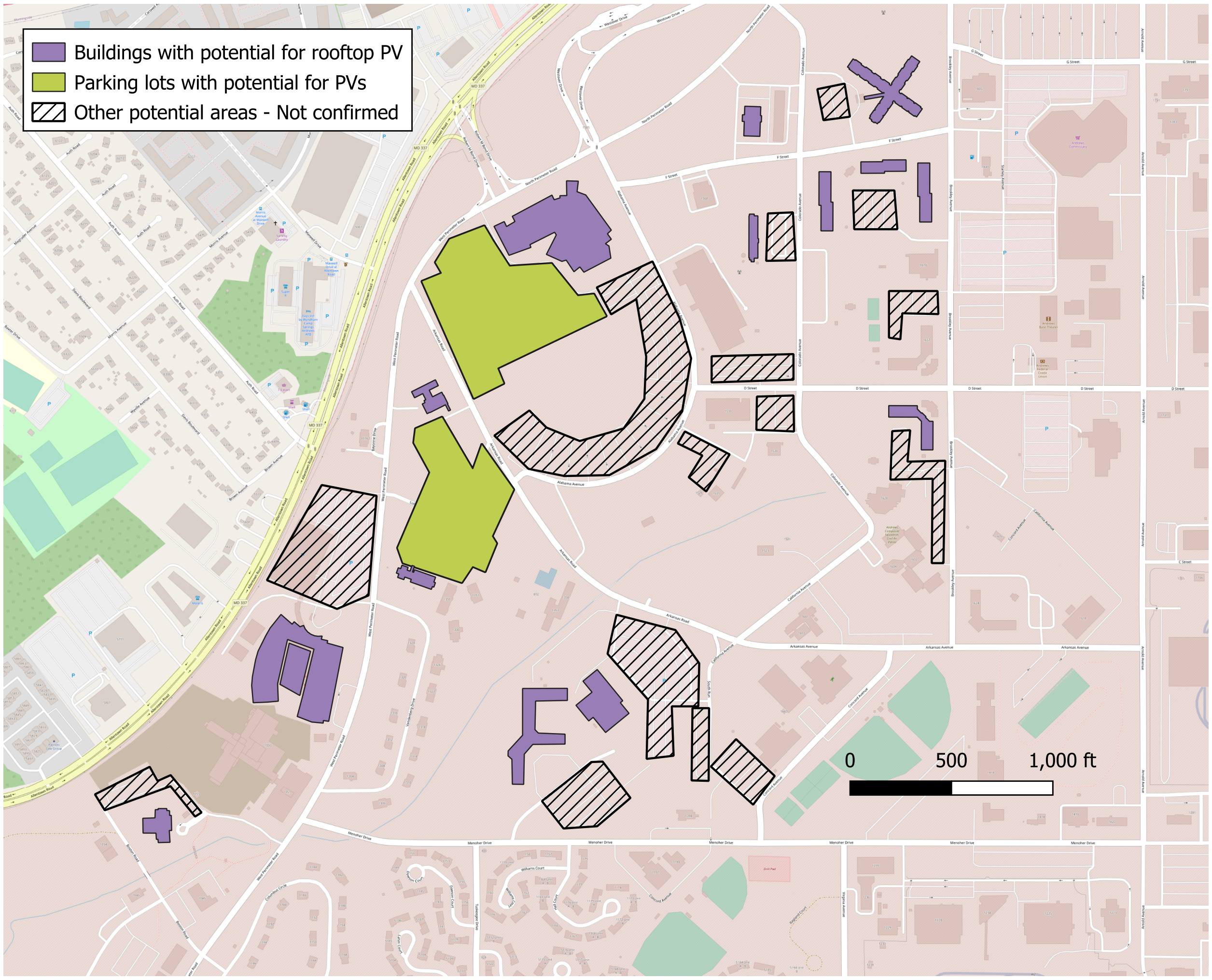

Figure 6. Potential areas for PV panel installation.

5.5.1 Equipment Related Equations

We calculate the investment costs for each equipment as

$$IC_e = IC_{f,e} + IC_{v,e}\, C_e, \tag{3}$$

where e is the equipment considered, $IC_{f,e}$, the initial cost, is the fixed part of its investment cost, and $IC_{v,e}$ is the variable part of the investment cost that depends on its capacity C_e. IC_e are costs related to the acquisition of a equipment in year 0.

Replacement costs are related to the replacement of a equipment. The present value of replacement cost is calculated for each equipment with a lifetime inferior to the project duration as

$$RC_e = \sum_{\substack{t=1 \\ t\, l_e < D}} \frac{IC_e}{(1+r)^{t\, l_e}}, \tag{4}$$

where l_e is the lifetime of the equipment and $t\, l_e$ is the period when the equipment is to be purchased again. The lifetime of each equipment is available in Table 6.

The present value of salvage revenue, which is the estimated value of a equipment at the end of the project duration, is calculated as

$$SR_e = \frac{IC_e(\frac{l_{r,e}}{l_e})}{(1+r)^D}, \tag{5}$$

where $l_{r,e}$ is the remaining lifetime of the equipment at the end of the project.

The present value of operation and maintenance costs for each equipment are calculated as

$$OM_e = \sum_{t=1}^{D} \frac{\alpha_e\, IC_e}{(1+r)^t}, \tag{6}$$

where α_e represents the estimated annual percentage of the investment cost associated with operation and maintenance expenses for the different equipment. The percentage is available in Table 6.

The life-cycle cost, which is the total cost of the equipment over the project duration, is calculated as

$$LCC_e = IC_e + RC_e - SR_e + OM_e. \tag{7}$$

The annualized life-cycle cost, which is the yearly equivalent of the life-cycle cost, is calculated for each equipment as

$$ALCC_e = LCC_e\, CRF. \tag{8}$$

5.5.2 Energy Related Equations

The annualized life-cycle cost for each energy import is calculated as

$$ALCC_{ene} = \sum_{h=1}^{y} EI_{ene,h}\, PP_{ene,h} - \sum_{h=1}^{y} EE_{ene,h}\, SP_{ene,h}, \tag{9}$$

where $y = 8760$ is the number of hours in a year, $EI_{ene,h}$ is the amount of energy imported during one hour h for the energy carrier ene considered (in our case study, the two potential energy carriers are gas and electricity), $PP_{ene,h}$ is the (real) purchase price of this energy carrier during the hour considered, $EE_{ene,h}$ is the amount of energy exported and $SP_{ene,h}$ is its selling price (see Section 5.4.1).

The life-cycle cost is calculated for each energy carrier as

$$LCC_{ene} = \frac{ALCC_{ene}}{CRF}. \tag{10}$$

5.5.3 Total Costs

The total life-cycle cost of the project is calculated as

$$LCC = \sum_{e} LCC_e + \sum_{ene} LCC_{ene}, \tag{11}$$

and considers the life-cycle of each equipment and of each energy carrier.

The total annualized life-cycle cost is

$$ALCC = \sum_{e} ALCC_e + \sum_{ene} ALCC_{ene}. \tag{12}$$

The levelized cost of energy for heating and cooling, $LCOE$, is calculated from the total annualized life-cycle cost $ALCC$ and the expected, average electricity purchase price $\overline{PP_{ele,h}}$ as

$$LCOE = \frac{ALCC - Q_{ele,oth,a}\,\overline{PP_{ele,h}}}{Q_{hea,a} + Q_{coo,a} + Q_{DHW,a}}, \tag{13}$$

where $Q_{ele,oth,a}$ the total annual electricity consumption for building fans in rooms and non-HVAC appliances, $Q_{hea,a}$ the total annual heating consumption, $Q_{coo,a}$ the total annual cooling consumption, and $Q_{DHW,a}$ the total annual DHW consumption.

5.6 SITE GEOLOGY

For the borefield, the Navy Geothermal Office team provided soil properties. The upper 10% of the bores are in northkey/brandywine sands with a thermal conductivity of $k = 1.1\,\mathrm{W/(m \cdot K)}$ and specific volumetric heat capacity of $C = 1.4\,\mathrm{MJ/(m^3 \cdot K)}$. The lower 90% are calvert clay with a thermal conductivity of $k = 1.6\,\mathrm{W/(m \cdot K)}$ and specific volumetric heat capacity of $C = 0.9\,\mathrm{MJ/(m^3 \cdot K)}$.

As the Modelica model requires uniform soil properties, we average these values and use a thermal conductivity of $k = 1.55\,\mathrm{W/(m \cdot K)}$ and a specific volumetric heat capacity of $C = 0.97\,\mathrm{MJ/(m^3 \cdot K)}$.

During detailed design, we recommend to verify these assumptions with a thermal response test.

6.0 CONFIGURATIONS

In this section, we will describe the configurations that we will further examine as potential candidates to provide space heating, DHW preparation and space cooling, as well as end-use electricity for buildings. We will describe each configuration and their control intent before we optimize and compare their performance in Section 7.0.

6.1 TERMINOLOGY

We will use the following terminology in this and the subsection sections:

- We call a configuration a specific energy system, such as a TEN, or a system with geothermal heat pumps and borefield thermal energy storage (borefield) in each building.

  These configurations describe the equipment type and schematic configuration (piping, valves, pumps, control intent), but are not yet sized.

  The configuration also restrict what components can be part of a system. For example, the configuration with building installed gas boiler and chiller excludes the use of a central plant with geothermal borefield, as this is not applicable for this type of system.

Terminology that will later be used is introduced in Section 7.1.

6.2 DEFINITION OF THE CONFIGURATIONS

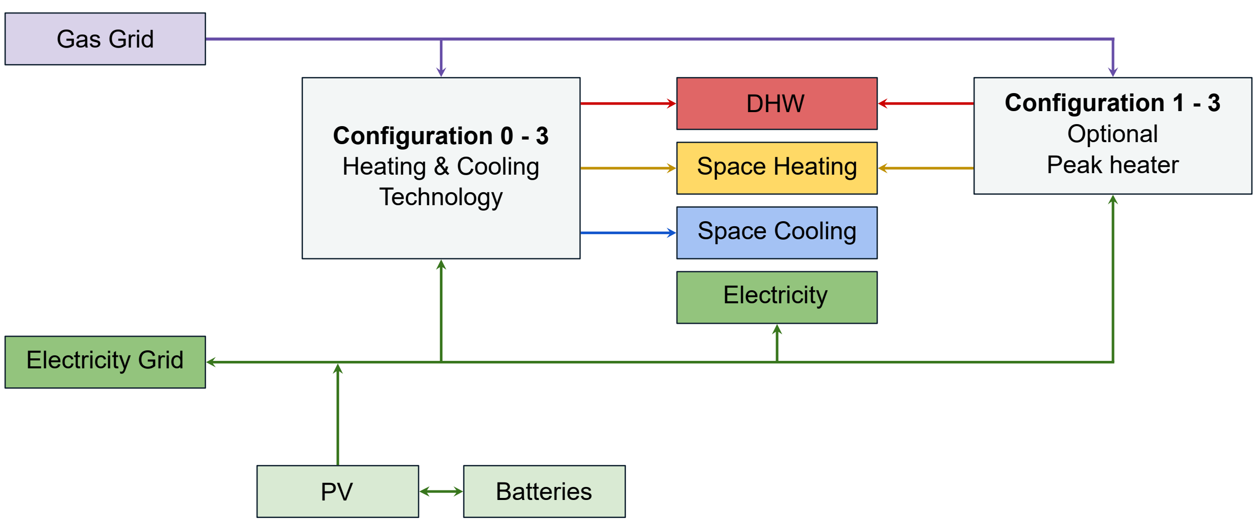

Figure 7. Possible configurations to satisfy building energy loads.

We identified the following four configurations:

- **Configuration 0 (Gas)**: A gas boiler and a chiller is used in each building. This is the base case reflecting the current configuration of the building systems.
- **Configuration 1 (AW HP)**: Individual reversible air-to-water heat pumps are used for the building to provide space heating, DHW and space cooling.

– **Configuration 2 (WW HP)**: Individual water-to-water heat pumps are used for the building to provide space heating, DHW and space cooling. The heat pumps are connected to a borefield and dry coolers.

– **Configuration 3 (TEN)**: The building is connected to a district heating and cooling network through an ETS. The district network has a borefield and dry coolers to balance the borefield.

Fig. 7 shows schematically the configurations and their energy flow connections to the utility grid, the on-site generation and the domestic hot water, space heating, space cooling and electricity load that they need to cover. For configurations 1 to 3, a gas peaker boiler may be used to produce hot water and down-size the heat pump if economically advantageous. All configurations can also have PV and batteries. In the following sections we explain these system configurations.

6.2.1 Configuration 0 (Gas): Gas Boilers & Chillers

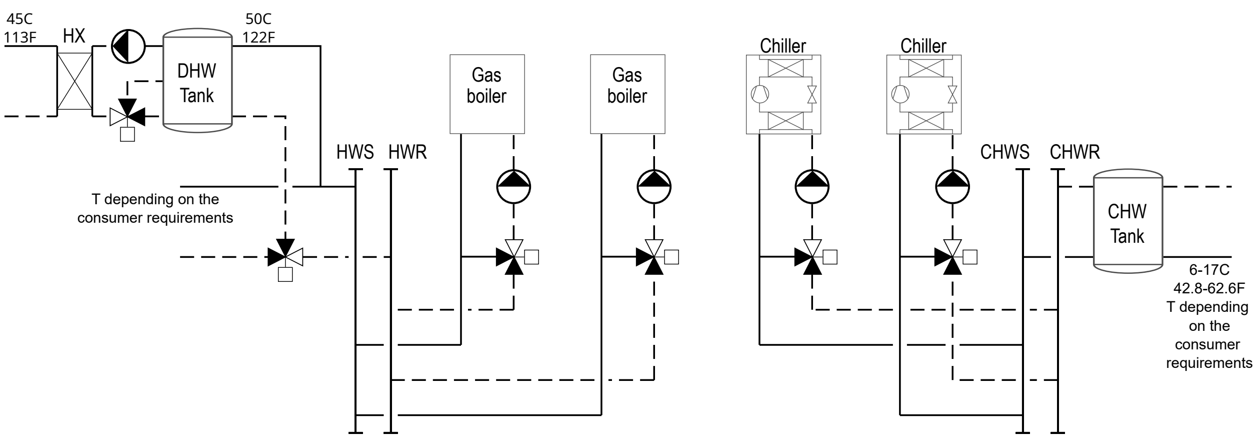

Figure 8. Schematic diagram for configuration 0 (Gas).

Figure 8 illustrates the schematic diagram of Configuration 0.

When a condensing gas boiler is utilized, the three-way valve adjacent to the boiler remains fully open during standard space heating operation, allowing maximum flow through the boiler to the heating system. However, when switching to the operating mode for charging the DHW tank, this valve becomes actively modulated. In this mode, the valve adjusts to maintain the boiler's outlet water temperature at or above 50 °C (122 °F), thereby preserving the thermal stratification within the DHW tank.[3]

If a non-condensing boiler is employed, the three-way valve is controlled to ensure the minimum return water temperature required to prevent condensation within the boiler's heat exchanger, as specified by the manufacturer's guidelines. This control avoids potential corrosion and damage due to condensation, ensuring the longevity and proper functioning of the boiler. This configuration depends on the design of the load-side heating circuits to maintain adequate flow through the boiler under all operating conditions.

[3]It is important to note that the DHW tank in this context contains heating water, not potable water supplied to showers and faucets. Therefore, operating at lower temperatures does not pose a risk of *Legionella* bacteria proliferation, but it does enhance system efficiency by facilitating condensing operation of the boiler.

The three-way valve near the on the hot side of the DHW tank is utilized for charging of the DHW tank. This valve is either open or close, depending on whether heat needs to be served for the DHW or the space heating.

The three-way valve located to the left of the DHW tank serves to maintain optimal stratification within the DHW tank. This valve leads the return water to the middle connection of the DHW tank if the entering water temperature exceeds 45 °C (113 °F), and to the lower connection if the temperature is below this threshold. By controlling the inflow position based on temperature, the valve enhances thermal stratification, which improves the efficiency and responsiveness of the hot water supply.

For the chiller system, the three-way valve is employed to prevent warm water from entering the chilled water (CHW) tank during the chiller's startup phase. By modulating this valve, the system maintains the stratification within the chilled water tank, ensuring that chilled water at the setpoint temperature is supplied to the cooling loads. This control is crucial for maintaining the desired supply temperature during ramp-up.

For simplicity, the schematic does not include ancillary components such as thermal expansion devices required to accommodate water volume changes due its thermal expansion, and safety relief valves designed to protect the boiler from overpressure or overheating conditions. These components are essential for system safety and compliance with relevant codes and standards but are omitted here for clarity in illustrating the primary flow and control strategies.

6.2.2 Configuration 1 (AW HP): Reversible Air-To-Water Heat Pumps

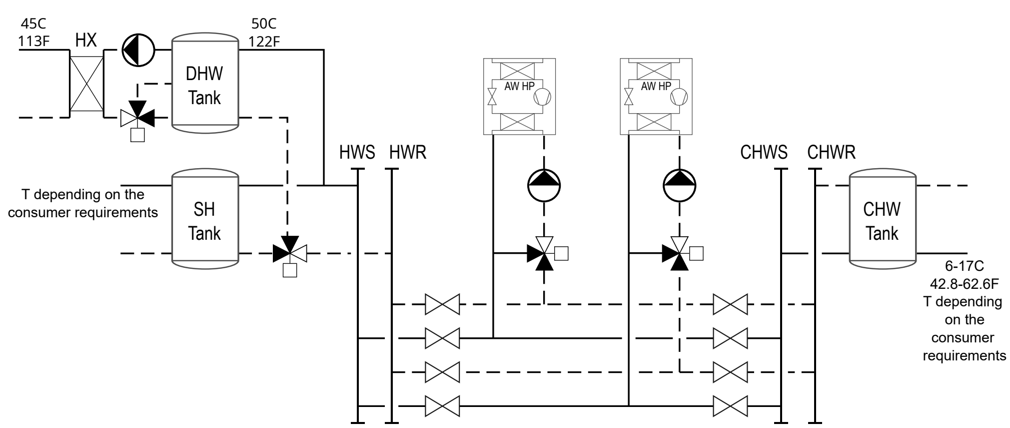

Figure 9. Schematic diagram for configuration 1 (AW HP).

Figure 9 shows the schematic diagram of the configuration that employs reversible air-to-water heat pumps to serve the building loads. These heat pumps are installed within the buildings they serve, providing localized heating and cooling capabilities.

To enhance operational flexibility, improve part-load efficiency and allow simultaneously serving heating, or DHW, and cooling loads, we assume the installation of at least two heat pumps per building. This arrangement allows one heat pump to operate in cooling mode while the other serves space heating or DHW loads. By having multiple units, the system can better modulate capacity to match varying load conditions, reducing cycling losses and improving overall efficiency.

The two-way valves positioned in the horizontally drawn pipes are utilized to control the operational mode of each individual heat pump. These valves effectively index each heat pump into heating mode, cooling mode, or shut-off (off mode) as required. By selectively opening or closing these valves, the system directs the flow of water to the appropriate circuits.

Adjacent to each heat pump, three-way valves are installed and used to maintain the required supply temperatures for the heating and cooling circuits. In heating mode, the three-way valve modulates to ensure a minimum heating supply temperature is delivered to the space heating (SH) tank, thereby preserving its thermal stratification. Conversely, in cooling mode, the valve regulates to maintain a maximum chilled water supply temperature to the chilled water tank, also preserving its stratification.

The control strategies for the other components in the system, such as tank charging priorities, minimum flow rate maintenance, and safety features, are implemented as described in Section 6.2.1.

6.2.3 Configuration 2 (WW HP): Water-To-Water Heat Pumps

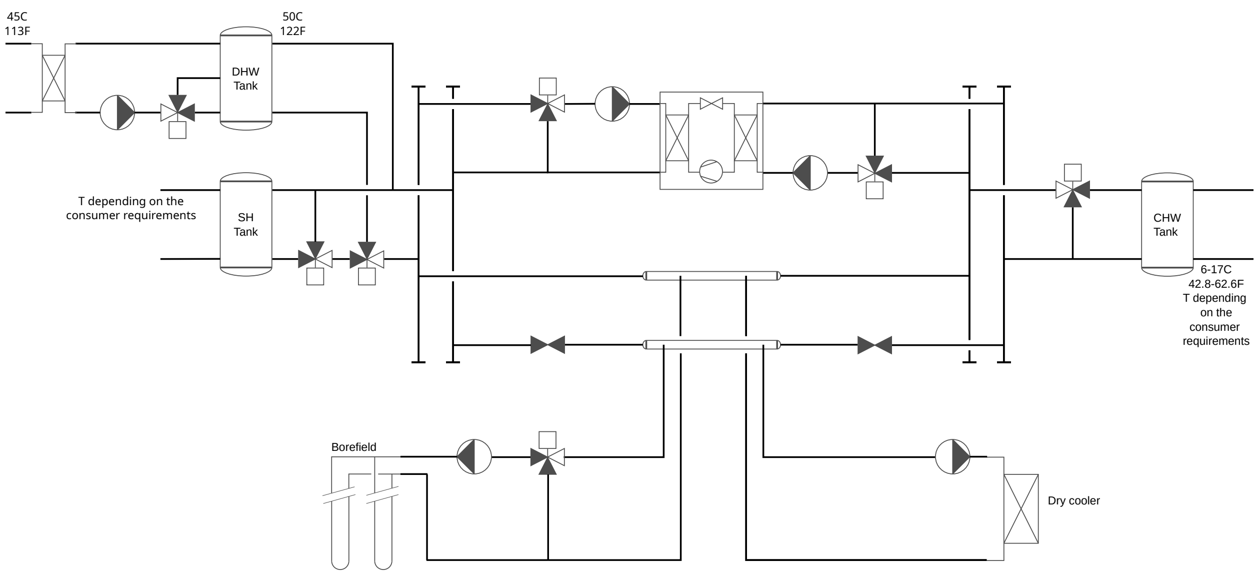

Figure 10. Schematic diagram for configuration 2 (WW HP).

Figure 10 illustrates the schematic diagram of the configuration employing water-to-water heat pumps.

In this setup, the chiller – functioning as a reversible water-to-water heat pump – can simultaneously serve heating loads (including space heating and DHW) and cooling loads. When there is a demand for both heating and cooling, the chiller operates in a mode that allows heat extracted from the cooling process (evaporator side) to be utilized directly for heating (condenser side), maximizing energy efficiency.

In scenarios where only heating or only cooling is required, the system rejects excess heat or absorbs additional heat through the borefield or the dry cooler. To manage this heat rejection, diversion three-way valves located adjacent to the vertically oriented manifold are employed. These valves are controlled to:

- *Prioritize charging of thermal storage tanks:* Initially, the system directs thermal energy to charge the space heating (SH) tank or the chilled water tank, depending on the mode of operation. This ensures that the thermal storage is utilized effectively to meet immediate or future loads.
- *Decouple storage tanks during heat rejection:* Once the respective tank reaches its setpoint temperature, the diversion valves decouple the tank from the circuit. This action preserves the energy content within the tank, preventing degradation of stratification and avoiding unnecessary thermal losses while the system continues to reject or absorb heat via the borefield or dry cooler.

The three-way valves in the condenser and evaporator loops are controlled as described in Section 6.2.2.

Two-way valves in the horizontally drawn lines are utilized to switch between heat rejection modes from the evaporator or condenser, respectively. The control logic for these valves is as follows:

- *Heat supply to evaporator:* The two-way valve in the evaporator loop is opened, allowing heat supply to the evaporator from the borefield or the dry cooler.
- *Heat rejection from condenser:* The two-way valve in the condenser loop is opened to enable heat rejection from the condenser side.
- *Isolation mode:* Both two-way valves are closed when neither heat rejection path is required, preventing unwanted water flow and maintaining system efficiency.

In cooling mode, prioritizing heat rejection to the borefield over the dry cooler allows heat to be stored in the geothermal field for later use via the heat pump when the system is in heating mode. However, if a building is cooling dominated, or depending on season and outside conditions, heat rejection via the dry cooler may be prioritized to increase the system efficiency. This is particularly true in the Spring season when outdoor conditions are mild and the cold temperature of the borefield should be preserved for use in summer. In winter, when outdoor conditions are cold, priority is given to extract heat from the borefield. Optimizing the borefield and dry cooler usage allows increasing the system performance.

The three-way valve in the borefield loop serves to limit the maximum water temperature entering the borefield. By modulating this valve, the system ensures that the temperature of the water circulated through the borefield remains below a maximum allowed borefield inlet temperature.

The tree-way-valve in the dry cooler loop limits the minimum cooling water return temperature to the condenser, thereby guaranteeing the minimum thermal lift across the heat pump.

Other control strategies and operational parameters are implemented as described in Section 6.2.2.

6.2.4 Configuration 3 (TEN): Thermal Energy Network

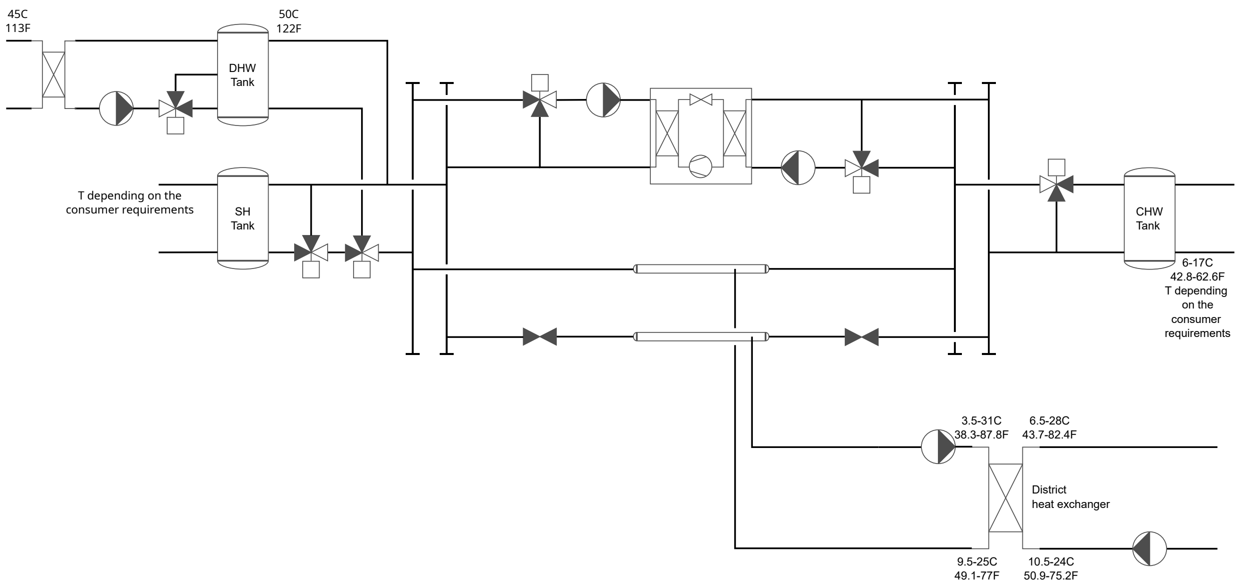

Figure 11. Schematic diagram of the ETS for configuration 3 (TEN).

Fig. 11 shows the schematic diagram of the configuration that employs a thermal energy network (TEN), with energy transfer stations (ETS) to connect the thermal systems of the buildings to the service lines of the TEN. In this configuration, there is no building-level borefield; instead, the borefield is integrated within the district loop, serving multiple buildings connected to the TEN. This centralized approach to geothermal exchange allows a large borefield to be used by multiple buildings. This shared use facilitates investing into heat pumps, piping and control to actively regenerate the borefield, and it simplifies the thermal infrastructure at the building level.

The ETS incorporates a district heat exchanger that hydraulically decouples the building's internal thermal systems from the district energy system. This decoupling allows the building to operate independently while facilitating the transfer of thermal energy to and from the district loop without direct mixing of fluids. The hydraulic separation ensures that pressure fluctuations, flow variations, or maintenance activities on one side do not adversely affect the other side.

The operation of heat rejection, or heat supply, and the management of the thermal storage, is similar to the controls described for the water-to-water heat pump system in Section 6.2.3.

For a comprehensive and detailed description of this configuration's control strategies, implementation considerations, and performance analysis, we refer to Gautier, Wetter, and Sulzer (2022). This reference provides an in-depth explanation of the control algortithms of the ETS and the dynamic response under various load conditions.

Fig. 12 shows the district loop that connects the buildings with a central plant. The district loop is designed based on the reservoir network concept (Sommer et al., 2020; Wetter and Hu, 2019). In this configuration, central plant and buildings, illustrated with two buildings connected through their respective service lines, are connected in series to the district loop. The series connections facilitate efficient thermal energy exchange among the buildings, optimizing the utilization of low-temperature heat sources and sinks. By arranging the components in series, the network can dynamically balance

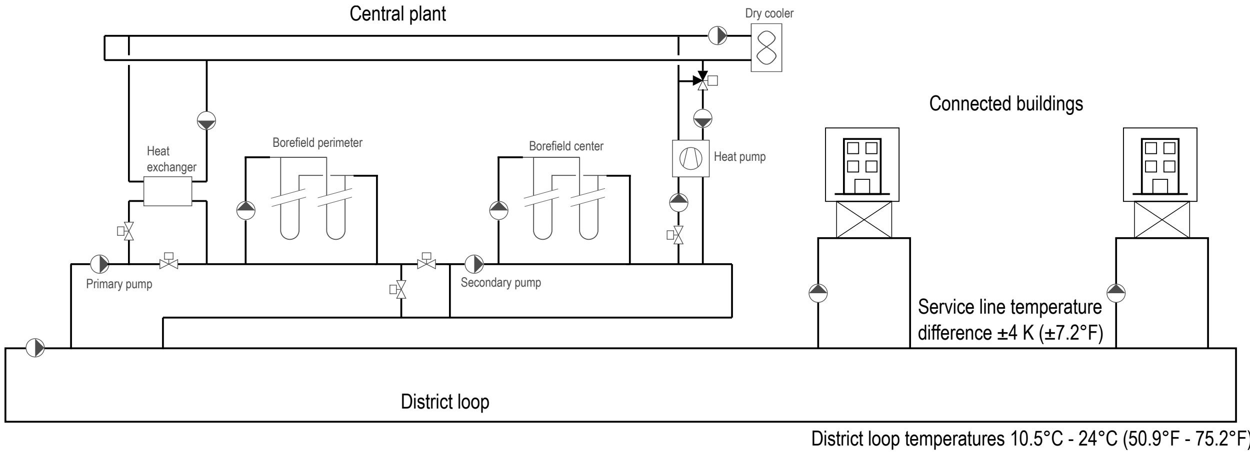

Figure 12. Schematic diagram of the district loop and central plant for configuration 3 (TEN).

thermal loads and sources, and the series connection simplifies future integration of DERs technologies, additional plants, storage and heat sources such as a data center as described in Sommer et al. (2020).

A key feature of this design is the implementation of a variable-speed pump in the district loop. The pump adjusts its speed in response to real-time thermal demand and flow requirements, significantly reducing pumping energy consumption compared to constant-speed pumping systems (Sommer et al., 2020).

7.0 IDENTIFICATION OF CANDIDATE SOLUTIONS: MILP PLATFORM

In this section, we will identify which configuration should be selected for further design, verification and derisking in Section 8.0. This will be done by selecting for each configuration their equipment sizes and operational schedules that lead to Pareto-optimal candidate solutions whose performance is compared against each other, and against the performance objectives from Section 4.0, which are expanded with additional requirements that will be described in Section 7.3. We will start with introducing terminology and giving an abstract overview of all configurations, then describe performance calculations that are common to all systems and present equipment costs. Next, we describe how each configuration has been parameterized for the MILP optimization, and present the results of the MILP optimization.

7.1 TERMINOLOGY

In Section 6.1, we introduced the term configuration. In this and the subsequent sections, we will use the following additional terminology:

- We call a candidate solution a configuration that has equipment sized and control determined and that is Pareto-optimal.

  Some of the candidate solutions, which are identified in Section 7.0, are then selected for refinement in Section 8.0, whereas the refinement includes detailed design, performance verification and robustness analysis through detailed dynamic simulations.

- We call a component an equipment or a subsystem that is used to compose an energy system. A component could be for example a heat pump will all the required piping, valves, pumps and control.

7.2 ABSTRACTION OF COMPONENTS AND OF ENERGY FLOWS

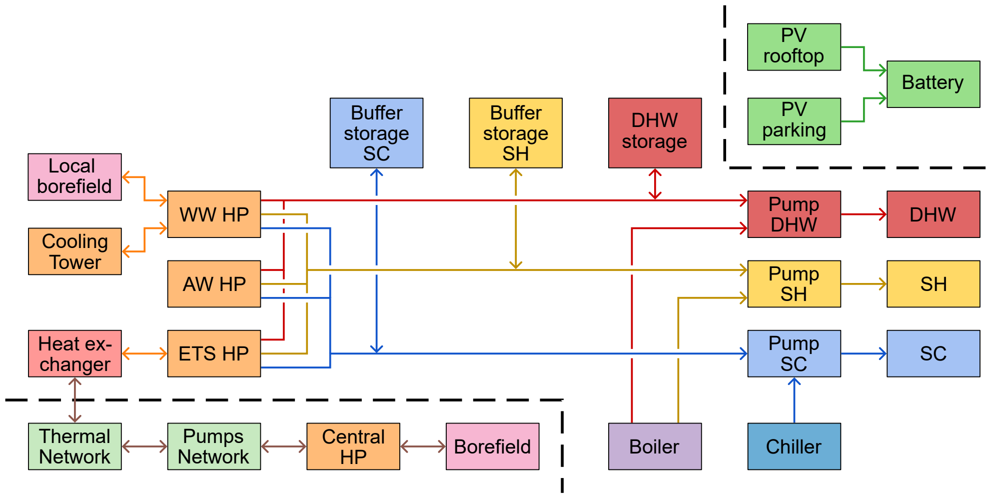

Figure 13. Abstraction of the thermal flows, the energy conversion technologies, the energy storage technologies, and the thermal network that were considered in the MILP optimization solution space. The electricity grid is not shown in this figure; only the building-level technology candidates PV and Battery are shown.

Fig. 13 shows an overview of all candidate technologies considered in the MILP optimization. This figure illustrates the wide array of energy conversion, storage, and distribution technologies evaluated to determine the optimal configurations and sizing for the site. Note that the central plant consists of a reversible air-to-water heat pump, which can also be operated in free cooling/heating mode. The colors used for the different technologies will be used in subsequent diagrams to group technologies into cost modules. For the MILP optimization, the objective is to select the combination of technologies and their capacities that result in the techno-economically optimal solution. This optimization is conducted under the constraint that the site's hourly thermal and electrical loads must be met at all times. The insights derived from this optimization inform the subsequent design process and guide the selection of technologies that offer the best value while satisfying the technical, operational, and economic requirements of the site.

In the next sections, we characterize the pre-configured system options—defined as configurations 0, 1, 2, and 3—upon which the MILP optimization is based. We also present simplified versions of Fig. 13 that only show components that are active for a particular configuration.

7.3 REQUIREMENTS

We now describe the requirements that the solutions have to meet to be considered valid at this level of abstraction, i.e., at the MILP optimization level.

The baseline scenario corresponds to a "business as usual" approach that involves using equipment similar to what is already on site: gas boilers for heating and air-source chillers for cooling, assuming no PVs and no batteries installed. The requirements, which are derived from Table 1, are as follows.

- Imported energy reduced by at least 50% compared to baseline.
- Imported peak energy reduced by at least 40% compared to baseline.

- Life-cycle cost no more than 120% of the baseline.
- Investment cost no more than 200% of baseline.
- Investment cost no more than 110% of baseline if central plant infrastructure, district loops, and utility-scale PV and battery systems are privatized.
- Levelized cost of energy for heating and cooling no more than 0.25 USD/kWh.
- The energy demands, which includes space heating, space cooling, DHW and electricity for auxiliary purposes must be matched at every time step.
- Solutions must be Pareto-optimal.

7.4 COMMON PERFORMANCE CALCULATIONS

We now present a detailed characterization of the techno-economic performance parameters for components that are common across all analyzed configurations. These components include technologies and infrastructure components whose operational behaviors, efficiency profiles, cost structures, and performance metrics remain unchanged regardless of the specific configuration in which they are implemented. By establishing a uniform set of assumptions and calculation methodologies for these common components, we ensure consistency and comparability in the evaluation of different solutions (system configurations and component sizing).

7.4.1 PV

The efficiency of the PV is

$$\eta_{PV} = f_{act}\, \eta_{conv}\, (1 - \eta_{loss}) = 0.171, \tag{14}$$

where $f_{act} = 0.9$ is the fraction of the active cell surface area, $\eta_{conv} = 0.2$ is the initial system conversion efficiency, considering PV panels, wiring, and inverters (NREL, 2025), and $\eta_{loss} = 0.05$ is the conversion loss after 10 years (Jordan and Kurtz, 2013). The produced electricity is

$$P_{PV} = \eta_{PV}\, A\, G, \tag{15}$$

where A is the collector area and G is the total irradiation onto the PV.

7.4.2 Heat Pumps and Heat Recovery Chillers

For heat pumps, the performance is estimated using the coefficient of performance

$$COP = \frac{\dot{Q}}{P}, \tag{16}$$

where $\dot{Q}$ is the condenser heat flow rate for space heating and DHW, or the evaporator heat flow rate for space cooling, and P is the electric power consumption of the compressor.

The initial MILP input will use monthly COP estimates based on Eschmann (2021). The estimation assumes a water supply temperature reset range of 50 to 60 °C (122 to 140 °F) for space heating, 50 °C (122 °F) for DHW, and 4 to 14 °C (39.2 to 57.2 °F) for chilled water. Monthly values for COP are presented in the sections below because the different configurations have different temperature lifts across the heat pumps.

7.4.3 Gas Boiler

A gas boiler is present in the configuration 0 to serve all heating loads. For configurations 1 to 3, the optimization can also select a gas boiler as a peaker boiler. Its efficiency is

$$\dot{Q}_{use} = \eta \, \dot{Q}_{gas}, \tag{17}$$

where $\dot{Q}_{use}$ is the useful heat, $\eta = 0.9$ is the efficiency, and $\dot{Q}_{gas}$ is the gas consumption.

7.5 EQUIPMENT COSTS

		Lifetime	Initial cost (USD)	Variable cost (USD/kW)	Variable cost (USD/kWh)	Variable cost (USD/m)	O&M (% of investment)
Conversion technologies	Gas boiler [a]	20	79,670	367			3
	Chiller [a]	20		1,564			2
	AW HP [a]	20	19,671	2,064			2
	WW HP [a]	20	19,671	2,230			2
	Dry cooler [a]	20		1,627			2
	ETS HP [a]	20	19,671	2,080			2
	Heat exchanger [a]	20	258,610	243			2
	Pumping station SH [a]	20	65,479	38			2
	Pumping station DHW [a]	20	6,476	4			2
	Pumping station SC [a]	20	46,404	30			2
Network technologies	Central HP [aeb]	20		1,631			2
	Network pumps [aed]	20	71,955	42			2
	Thermal network [a]	40				1,100	1
	PV rooftop [a]	25		3,500			1
	PV parking [a]	25		4,000			1
Storage technologies	DHW storage [a]	20	13,800		33		0.5
	Borefield [e]	40			1.5		0.5
	Battery [f]	15			757		1

(a) SI units.

		Lifetime	Initial cost (USD)	Variable cost		O&M (% of investment)
Conversion technologies	Gas boiler [a]	20	79,670	458	USD/(kBTU/h)	3
	Chiller [a]	20		5,500	USD/ton	2
	AW HP [a]	20	19,671	7,259	USD/ton	2
	WW HP [a]	20	19,671	7,843	USD/ton[c]	2
	Dry cooler [a]	20		5,722	USD/ton[c]	2
	ETS HP [a]	20	19,671	7,315	USD/ton[c]	2
	Heat exchanger [a]	20	258,610	71	USD/(BTU/h)	2
	Pumping station SH [a]	20	65,479	28	USD/hp	2
	Pumping station DHW [a]	20	6,476	3	USD/hp	2
	Pumping station SC [a]	20	46,404	22	USD/hp	2
Network technologies	Central HP [aeb]	20		5,736	USD/ton[c]	2
	Network pumps [aed]	20	71,955	31	USD/hp	2
	Thermal network [a]	40		335	USD/ft	1
	PV rooftop [a]	25		3,500	USD/kW	1
	PV parking [a]	25		4,000	USD/kW	1
Storage technologies	DHW storage [a]	20	13,800	33	USD/kWh	0.5
	Borefield [e]	40		1.5	USD/kWh	0.5
	Battery [f]	15		757	USD/kWh	1

(b) IP units.

[a] Initial and variables costs calculated based on data provided by Southland Industries.
[b] 80 % of the cost of an air-to-water heat pump, as it is not installed within buildings.
[c] Capacity of the heat pump based on the cooling capacity.
[d] Initial cost to be divided by the number of hubs.
[e] Costs based on expert rules.
[f] Installed costs for projects including batteries in 2021 (Bolinger et al., 2023).

Table 6. Summary of the costs for each technology candidate.

Table 6 shows the lifetime, the investment costs consisting of initial and variable costs, and the operation and maintenance (O&M) costs for each technology candidate. The investment costs are presented as turn-key costs for each specified module, meaning they include all expenses necessary to bring the technology into operational service. This comprehensive cost assessment encompasses design, equipment procurement, piping, fittings, and installation labor costs as charged to the customer. No costs are considered for space or land usage. The colors of the technologies correspond to the colors of the components shown in Fig. 13 and in the figures of the subsequent sections.

It is important to note that the costs associated with buffer storage tanks for space heating and cooling have been incorporated into the overall expenses of the heat pumps. The rationale for this aggregation is that buffer tank designs are closely linked to heat pump designs, and the cost of the buffer tanks are relatively small when compared to the total cost of the heat pump systems.

For the DHW storage tank, the variable costs is listed per kWh energy. To compute the cost per kWh of energy, we assumed a temperature difference of $\Delta T = 40\,\mathrm{K}$, and hence 1 kWh corresponds to $0.0215\,\mathrm{m}^3$ (5.68 gallons) tank volume.

7.6 CONFIGURATIONS

We will now show the characterization of the MILP problem, following the abstraction shown in Fig. 13, highlighting only those technology options relevant to configurations 0, 1, 2, and 3. This selective pre-configuration, indicated by distinct colors, emphasizes the technologies considered in each configuration, thereby facilitating a clear understanding of the optimization framework and associated decision variables.

For each configuration, we also provide the associated hydraulic diagram, replicating those from Section 6.0, but now enhanced with color coding. The colors indicate which components of the installation correspond to specific MILP modules and their respective cost as described in Table 6. It is important to note that the gas peaker boiler, although included as a potential candidate within the configurations 1-3, is not depicted in the hydraulic diagrams. As we will discuss in Section 7.8, the MILP optimization did not select the gas peaker boiler in configurations 1,2, or 3 analyzed. Excluding it from the schematics simplifies the diagrams and keeps the focus on the technologies that MILP selected in its Pareto-optimal solutions.[4]

[4]Moreover, whether the gas peak boiler should be integrated with or without storage depends on the thermal mass of the heating system and the minimum controllable load of the gas boiler, which both are important factors to avoid short-cycling.

7.6.1 Configuration 0 (Gas)

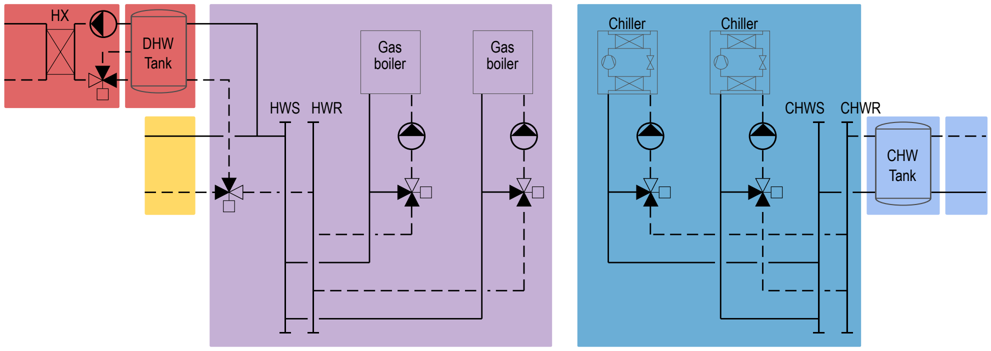

(a) Hydraulic diagram.

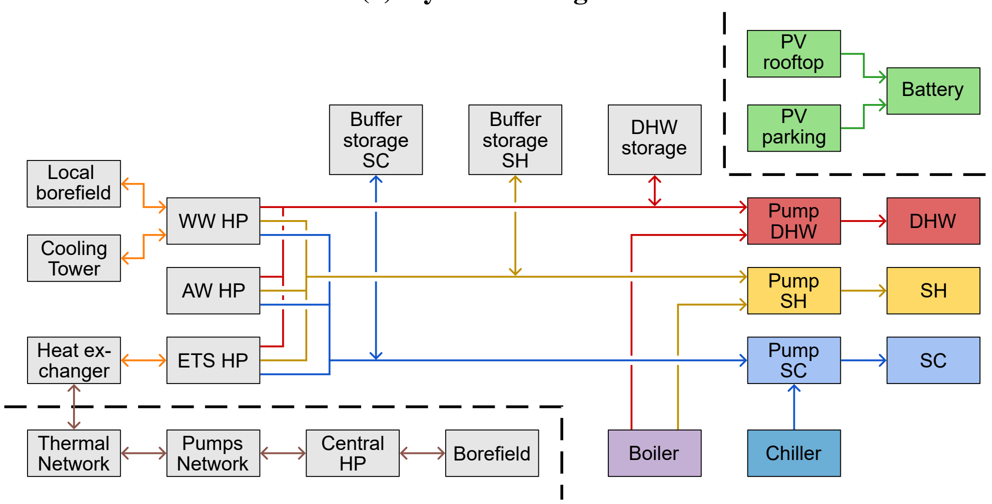

(b) MILP diagram.

Figure 14. Abstraction for the MILP optimization of the Gas configuration.

Fig. 14 shows an overview of all candidate modules associated with this Gas configuration, which serves as the baseline corresponding to the current installation.

Month	Average outdoor air temperature (°C)	(°F)	COP_{coo}
January	1.2	34.2	6.4
February	4	39.2	6.5
March	5	41	6.5
April	11.2	52.2	6.1
May	17.4	63.3	4.2
June	23.9	75	2.4
July	25.1	77.2	2.0
August	22.6	72.7	2.6
September	19.4	66.9	3.5
October	14.5	58.1	5.3
November	6.1	43	6.3
December	5.7	42.3	6.5

Table 7. Monthly COP estimates for building-level chiller.

The COP of a chiller is presented in Table 7, and the values are computed as explained below in Section 7.6.2. Note that the chiller provides only cooling, its condenser heat is rejected to ambient.

7.6.2 Configuration 1 (AW HP)

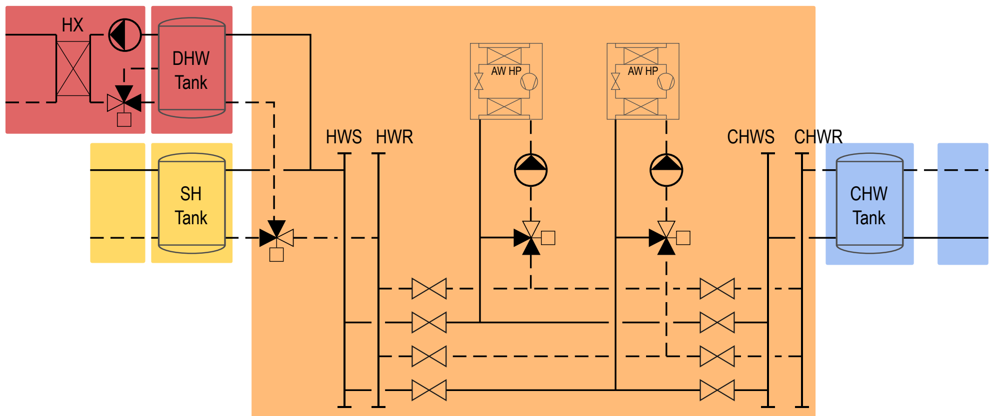

(a) Hydraulic diagram.

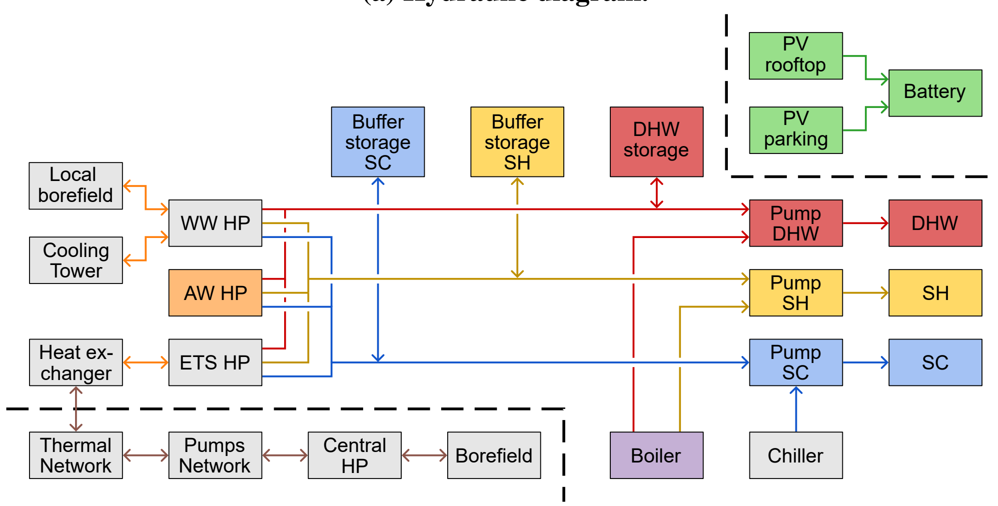

(b) MILP diagram.

Figure 15. Abstraction for the MILP optimization of the AW HP configuration.

Fig. 15 shows an overview of all candidate modules associated with this air-to-water heat pump (AW HP) configuration.

For space heating, initial COP values for the air-to-water heat pump $COP_{awhp,ini}$ are obtained from Eschmann (2021). Eschmann (2021) lists COP values for condenser temperatures varying from 30 °C to 55 °C. However, our application requires temperatures from 30 °C to 60 °C. Therefore, we adjusted the $COP_{awhp,ini}$ values as follows: We calculated the Carnot effectiveness as

$$\eta_{Car,awhp} = \frac{COP_{awhp,ini}}{COP_{Car}}, \tag{18}$$

where COP_{Car} is the Carnot COP, defined as

$$COP_{Car} = \frac{T_{con}}{T_{con} - T_{eva}}, \tag{19}$$

where T_{con} is the temperature of the condenser, which varies from 30 °C to 55 °C, and T_{eva} the temperature of the evaporator, which varies from −10 °C to 12 °C. The Carnot effectiveness $\eta_{Car,awhp}$ varies between 0.36 and 0.43, see Appendix E. As MILP optimization requires a temperature-independent COP value, we use an average value of $\overline{\eta}_{Car,awhp} = 0.385$. The COP values for space heating for the temperature regimes of our application are then

$$COP_{awhp,hea} = \overline{\eta}_{Car,awhp}\, COP_{Car}. \tag{20}$$

For domestic hot water, we calculate

$$COP_{awhp,DHW} = \overline{\eta}_{Car,awhp}\, COP_{Car}, \tag{21}$$

with $T_{con} = 60$ °C.

Eschmann (2021) does not list $COP_{awhp,coo}$. To compute $COP_{awhp,coo}$, we therefore assume the same ratio $\eta_{Car,awhp}/\eta_{Car,wwhp}$ for the heating and cooling modes, and use $\overline{\eta}_{Car,wwhp} = 0.48$, see Section 7.6.3 below. Therefore,

$$COP_{awhp,coo} = \frac{\overline{\eta}_{Car,awhp}}{\overline{\eta}_{Car,wwhp}}\, COP_{wwhp,coo} = 0.802\, COP_{wwhp,coo}. \tag{22}$$

Table 8 shows the air-to-water heat pump COP for space heating, DHW and space cooling, which were computed using the temperature reset shown in Fig. 35.

Month	Average outdoor air temperature (°C)	Average outdoor air temperature (°F)	COP_{hea}	COP_{DHW}	COP_{coo}
January	1.2	34.2	2.5	2.6	6.4
February	4	39.2	2.7	2.8	6.5
March	5	41	2.8	2.9	6.5
April	11.2	52.2	3.2	3.2	6.1
May	17.4	63.3	3.6	3.5	5.8
June	23.9	75	4	3.9	5.5
July	25.1	77.2	4.1	3.9	5.3
August	22.6	72.7	3.9	3.8	5.3
September	19.4	66.9	3.7	3.6	5.6
October	14.5	58.1	3.4	3.4	6.0
November	6.1	43	2.8	2.9	6.3
December	5.7	42.3	2.8	2.9	6.5

Table 8. Monthly COP estimates for building-level air-to-water heat pumps.

7.6.3 Configuration 2 (WW HP)

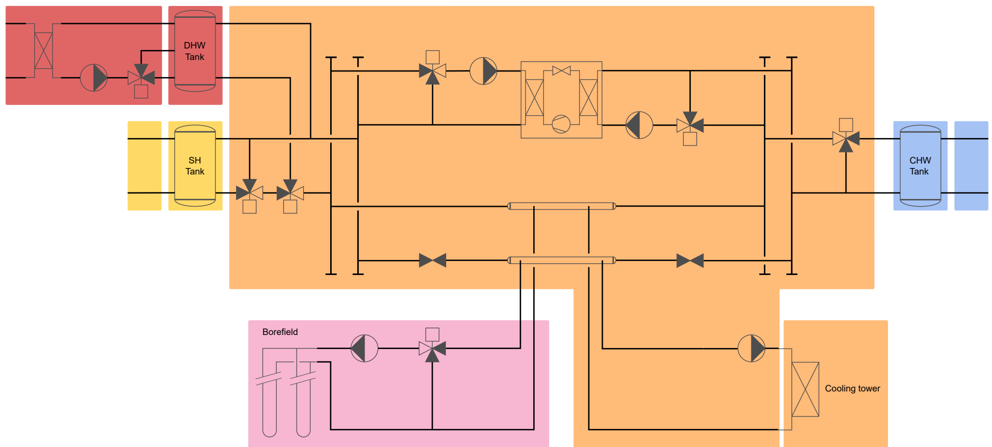

(a) Hydraulic diagram.

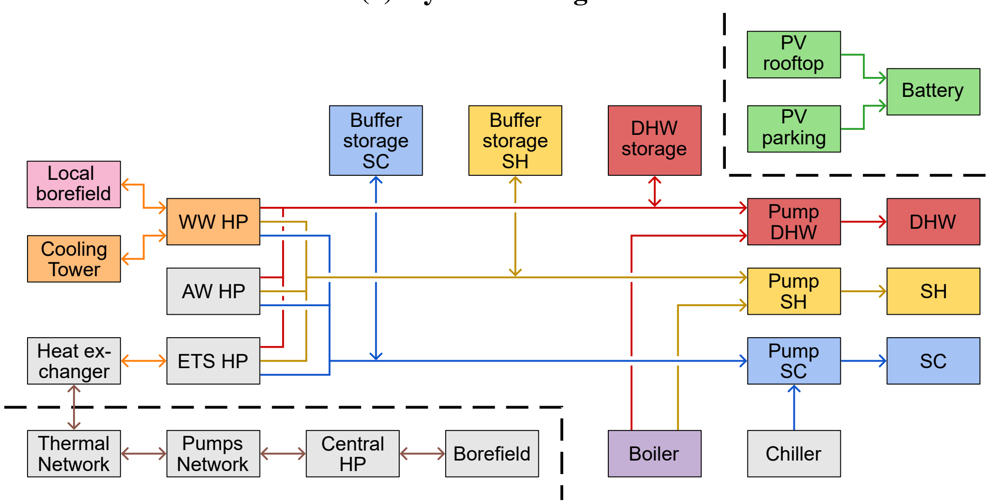

(b) MILP diagram.

Figure 16. Abstraction for the MILP optimization of the WW HP configuration.

Fig. 16 shows an overview of all candidate modules associated with the Water-Water Heat-Pump (WW-HP) configuration.

Month	Average outdoor air temperature (°C)	(°F)	COP_{hea}	COP_{DHW}	COP_{coo}
January	1.2	34.2	3.2	3.3	8.1
February	4	39.2	3.4	3.5	8.3
March	5	41	3.5	3.6	8.2
April	11.2	52.2	4	4	7.7
May	17.4	63.3	4.5	4.4	7.3
June	23.9	75	5.1	4.9	6.9
July	25.1	77.2	5.2	5	6.7
August	22.6	72.7	4.9	4.8	6.7
September	19.4	66.9	4.7	4.6	7.0
October	14.5	58.1	4.3	4.3	7.8
November	6.1	43	3.6	3.7	8.0
December	5.7	42.3	3.6	3.7	8.2

Table 9. Monthly COP estimates for building-level water-to-water heat pumps.

Table 9 shows the water-to-water heat pump COP for space heating, DHW and space cooling. We use the same method as in Section 7.6.2 to calculate the COP_{hea} and COP_{DHW}.

For the water-to-water heat pump in heating mode, the Carnot effectiveness $\eta_{Car,wwhp}$ varies between 0.422 and 0.506, see Appendix E, with an average value of 0.48. Therefore we assume $\overline{\eta}_{Car,wwhp} = 0.48$. For the water-to-water heat pump in cooling mode, we use the same values as for the ETS heat pumps, see Section 7.6.4.

The heat transfer effectiveness of the dry cooler is assumed to be 90 %.

7.6.4 Configuration 3 (TEN)

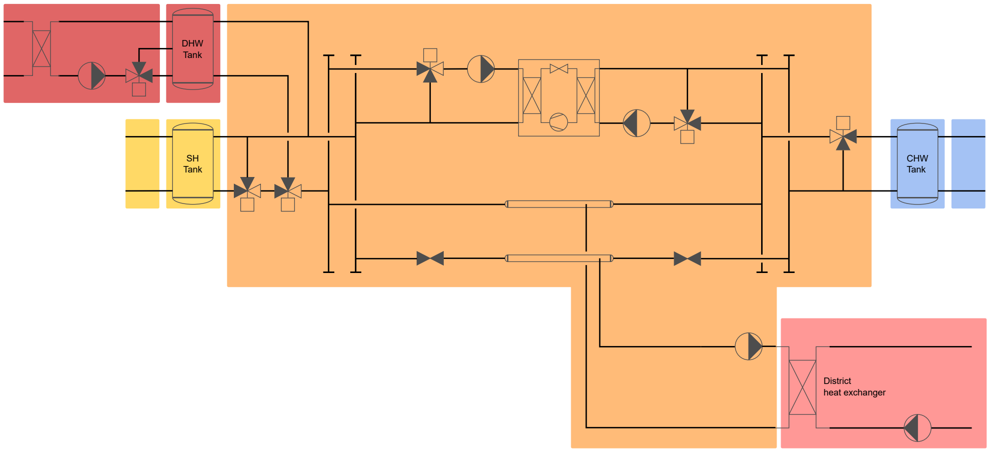

(a) Hydraulic diagram of ETS and connection to district service line.

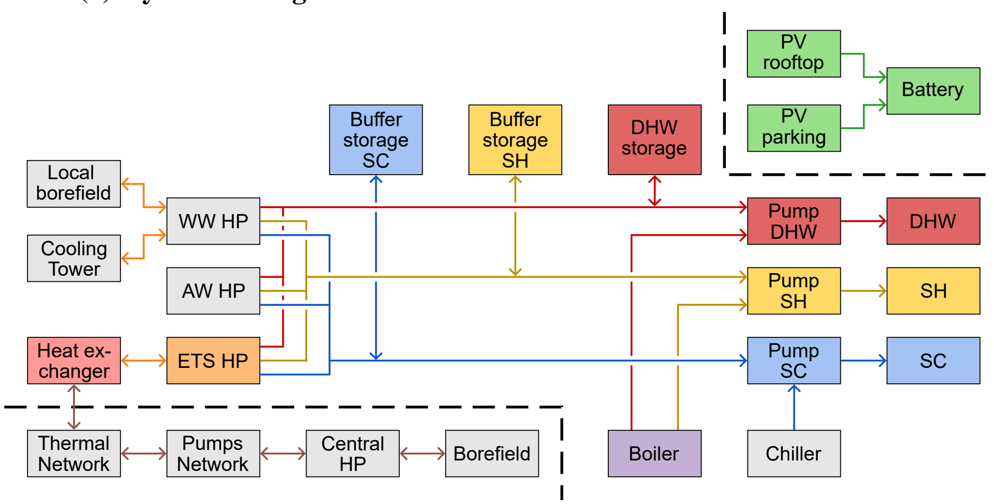

(b) MILP diagram.

Figure 17. Abstraction for the MILP optimization of the ETS and district service line of the TEN configuration.

Figure 17 presents an overview of all candidate modules associated with the TEN configuration. This configuration integrates individual buildings with a district heating and cooling network through an ETS, enabling efficient thermal energy distribution across the site. There is also a central plant, which is shown in the dashed lower left corner of Fig. 18b, connected to the TEN.

Each building within the district is connected to the district loop through an ETS, which acts as an interface between the building's internal thermal systems and the TEN. The ETS is connected using a heat exchanger, which hydraulically decouples the ETS from the TEN.

7.6.4.1 Energy Transfer Station Heat Pump (ETS HP) In the first MILP optimization, we estimated the COP values of the ETS heat pump for space heating and cooling. As this configuration was later simulated with Modelica, which uses a heat pump model whose COP is computed in detail, we then refined the COP values that are used in MILP by using the monthly average COP values of the Modelica simulations, and solved the MILP optimization problem again. These refined COP values are shown in Table 10. The COP value for DHW is selected to be constant and corresponds to the lowest value of the COP_{hea}.

Month	Average outdoor air temperature (°C)	(°F)	COP_{hea}	COP_{DHW}	COP_{coo}
January	1.2	34.2	4.1	4.1	8.1
February	4	39.2	4.5	4.1	8.3
March	5	41	4.8	4.1	8.2
April	11.2	52.2	5.4	4.1	7.7
May	17.4	63.3	6.0	4.1	7.3
June	23.9	75	6.7	4.1	6.9
July	25.1	77.2	6.7	4.1	6.7
August	22.6	72.7	6.8	4.1	6.7
September	19.4	66.9	6.9	4.1	7.0
October	14.5	58.1	5.6	4.1	7.8
November	6.1	43	5.0	4.1	8.0
December	5.7	42.3	4.5	4.1	8.2

Table 10. Monthly COP estimates for ETS heat pumps.

7.6.4.2 District Plant Fig. 18 shows the hydronic configuration of the district loop and of the district plant.

The district loop is a reservoir network (Sommer et al., 2020; Wetter and Hu, 2019).

At the district plant, a borefield serves the entire district, providing utility-scale thermal energy storage capabilities. The borefield enables seasonal storage of thermal energy, allowing excess heat or cold to be stored when available and retrieved when needed, thereby improving the system efficiency. The thermal network can be balanced by operating the borefield, by operating reversible heat pumps, or by operating the plant in free-cooling or free-heating mode.

The borefield can be balanced by operating the central plant reversible heat pumps, which are connected to a dry cooler, to provide heating and cooling, or by operating a heat exchanger that is connected to the same dry cooler to provide free-cooling or free-heating without running the heat pumps.[5] Thus, we assume that the dry coolers can operate in two different modes: (i) They can operate to reject or harvest heat for the reversible heat pumps. (ii) They can operate directly connected to the central plant hydronic loop to reject heat from the TEN or to harvest heat from the outside and inject it to the TEN, depending on the temperature differential of the district loop and the outdoor dry bulb temperature.[6] These two modes of operation are mutually exclusive.

[5] If a system is clearly heating or cooling dominated, a chiller or heat pump rather than a reversible heat pump may be used to balance the borefield system.

[6] Rejecting heat may be done during cold times when the TEN is cooling dominated and needs to reject heat. Conversely, when the TEN heating dominated and its temperature falls towards its lowest allowed temperature, the dry coolers may operate to inject heat from the outside air to the TEN on a mild winter day when the outside temperature is

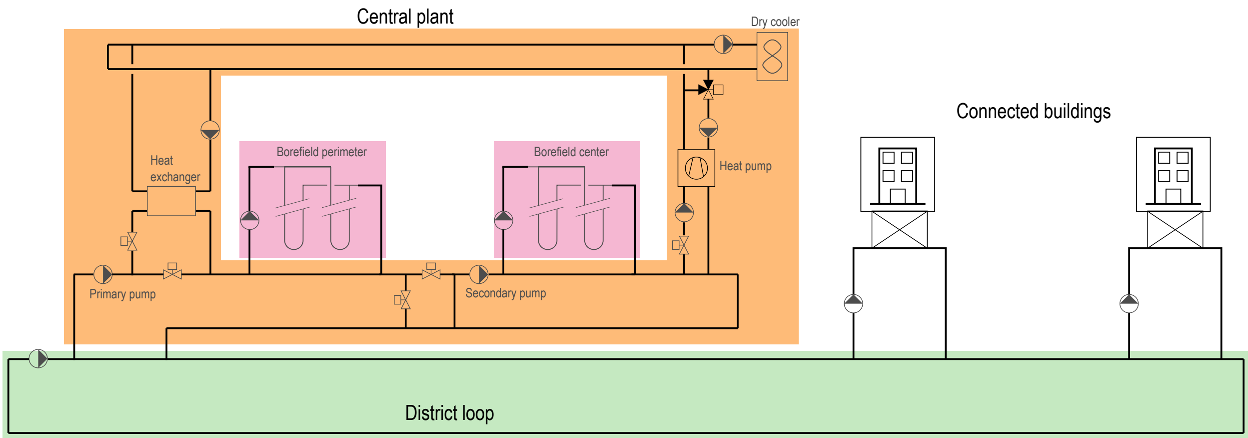

(a) Hydraulic diagram. Each part labeled "Connected buildings" consists of a service line and an ETS as shown in Fig. 17a.

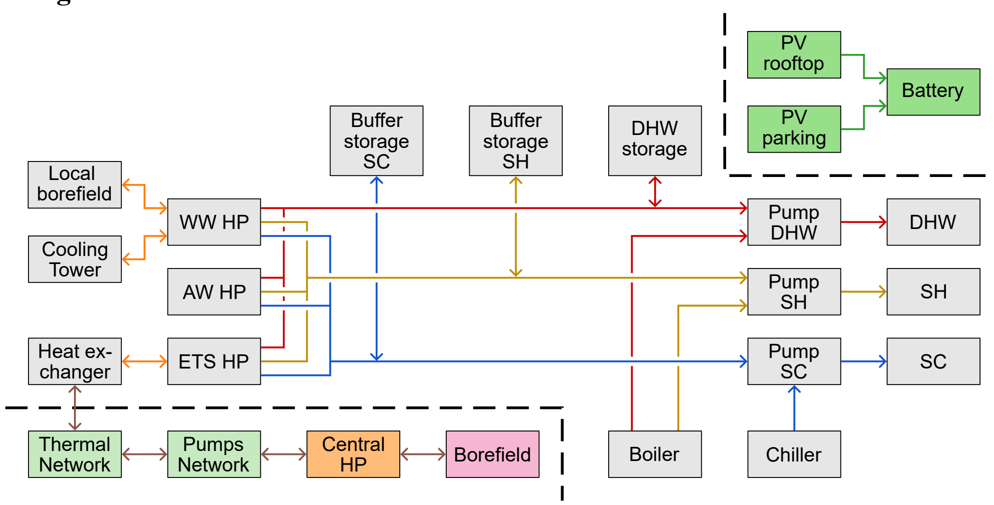

(b) MILP diagram.

Figure 18. Schematic diagram of the district loop and the district plant that is used for the TEN configuration.

For the detailed control sequence of the central plant, we refer to section Section 8.4.2 below.

As MILP does not compute the water temperatures in the system, we need to simplify these operation modes through an abstraction that retains the linearity of the model. Therefore, for the MILP model, we assume that the central plant only operates in two modes to accommodate varying thermal demands and maximize energy efficiency. These modes include:

- Heat Pump mode (Heating)
- Chiller mode (Cooling)

considering free-cooling and free-heating by adjusting the COPs of the reversible heat pump at the central plant.

Each mode of operation is characterized by specific monthly COP values, which are critical for accurately modeling the performance of the central plant and for optimizing operational strategies. To adequately determine these critical parameters, we performed an iterative analysis between the MILP optimization and the Modelica simulation platform. The COP values of the main plant heat pump are extracted from the monthly average COP values of the central plant heat pump from the Modelica simulation. Table 11 describes the COP for each mode. Interestingly, the refinement in the Modelica platform in Section 8.0 showed that the contribution of the free-cooling and free-heating is marginal for the system at Joint Base Andrews. Therefore, in the updated MILP model, the adjustments of the COPs for the central plant heat pump are not necessary.

Month	Average outdoor air temperature (°C)	(°F)	$COP_{Heating}$	$COP_{Cooling}$
January	1.2	34.2	4.1	9.5
February	4	39.2	4.7	9.5
March	5	41	5.2	5.6
April	11.2	52.2	6.2	5.4
May	17.4	63.3	6.3	5.3
June	23.9	75	6.3	5.4
July	25.1	77.2	6.3	4.2
August	22.6	72.7	6.3	4.4
September	19.4	66.9	4.8	5.6
October	14.5	58.1	4.5	8.8
November	6.1	43	4.6	9.5
December	5.7	42.3	4.9	9.5

Table 11. Monthly COP for the central plant heat pump.

above the TEN temperature.

7.6.5 Hubs and Network

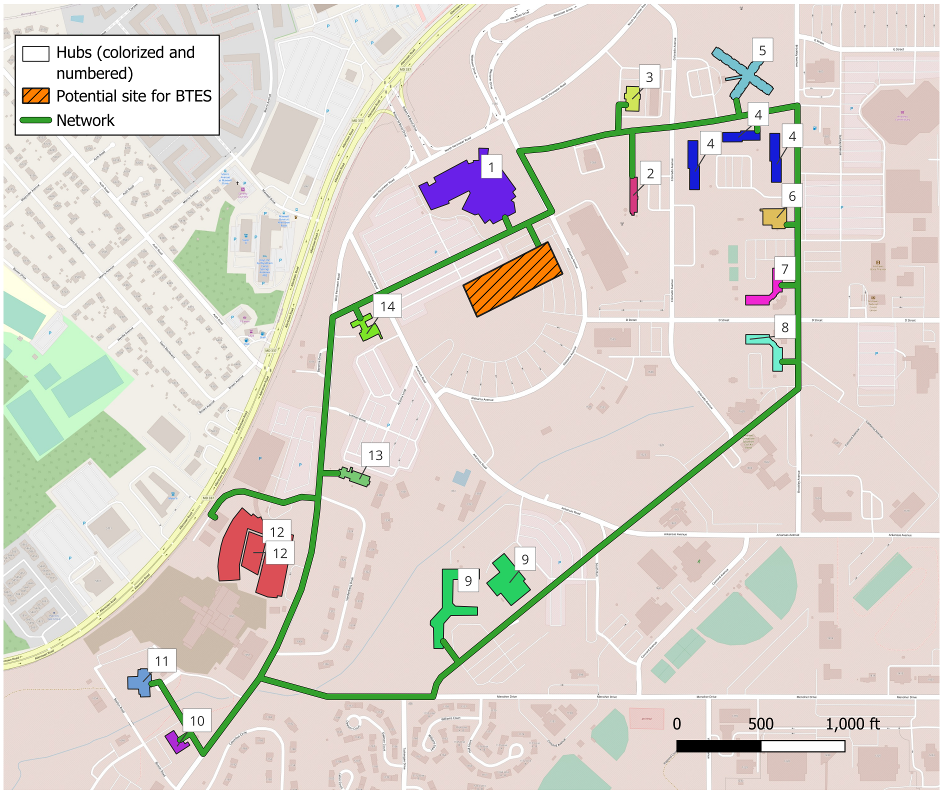

Figure 19. Location of energy hubs, district loop and borefield.

Fig. 19 shows the layout of the network of Configuration 3 (TEN). This network mostly follows the roads as it is common practice for district heating and cooling networks. Additionally, we also show the site for a potential borefield. The central plant, although not shown in the figure, is located next to the borefield. For each hub, the ETS shown in Fig. 17a is applied. Most hubs are composed of a single building, but some buildings are combined to create a hub. We combined buildings into the same hub if the buildings are close to each other and may be served by a single ETS.

7.6.6 Borefield

As an initial estimate, the maximum storage capacity of the borefield is determined by the highest cumulative load of space heating and DHW or space cooling over a three-month period. The maximum value pertains to space cooling and is equal to $E = 9.5$ GWh. The maximum heat extraction was set so that the borefield is discharged in one hour by 0.1% based on the selected storage capacity. The maximum heat extraction rate was therefore $\dot{Q} = 0.001\, E = 9{,}500$ kW. With 2,376 wells at an average length of 91 m, this gives a maximum heat extraction rate of 44 W/m, which is within typical values for borefield heat extraction rates. However, verifications with Modelica showed that this heat storage capacity is too optimistic for the temperature range in which the TEN operates. We therefore reduced the storage content by 50% and also the maximum heat extraction rate by 50% and recomputed the MILP optimization. The maximum storage capacity is 4.75 GWh and the maximum heat extraction is $\dot{Q} = 2{,}138$ kW. This gives a maximum heat extraction rate of 10 W/m. See Section 8.7.1.5 for a detailed discussion about the importance of obtaining such values through a detailed, coupled geothermal, energy and control simulation.

To put the maximum heat to be stored in the borefield in context of a soil temperature change, we can compute the following estimated average change in soil temperature: First, we note that the borefield specification was obtained from the Navy Geothermal Office Project team, with a borefield length of 495 m, width of 57 m and depth of 91 m. See also Fig. 30 for detailed borefield configuration. Adding a perimeter of 3 m around the borefield gives a volume of $V = 2.97 \cdot 10^6$ m^3. The soil has a specific volumetric heat capacity of $C = 0.97$ MJ/(m$^3 \cdot$ K) (see Section 5.6). Therefore, if we assume the soil temperature were to change uniformly, the temperature difference that corresponds to 4.75 GWh change in energy is

$$\Delta \overline{T}_{soi} = E/(V\,C) = 5.9\,\text{K}. \qquad (23)$$

This is highly idealized as the temperature change is more pronounced around the wells, but it nevertheless shows that the assumed energy content is reasonable.

7.6.7 Heat Pump in Central Plant

The heat pump size depends on the heat extraction rate of the borefield, and MILP strongly simplifies this aspect as explained in Section 3.4.3. Therefore, based on the verification with Modelica, we require MILP to use a reversible heat pump with a cooling capacity of at least 6.0 MW.

7.7 OPTIMIZATION OBJECTIVES

The two objectives of the optimization are to minimize energy imports and life cycle costs. Those objectives increase energy security while reducing the overall cost, to achieve the performance objectives defined in Section 4.0.

Minimizing the energy import: This aims to reduce the electricity and/or gas consumption and to increase energy efficiency and the use of on-site energy, all three measures decrease the reliance on imported energy by the grid and therefore increase the energy security of the installation.

Minimizing life cycle costs: As explained in Section 4.0, minimizing life cycle costs ensures that the system is financially viable for the duration of the project.

7.8 RESULTS OF THE MILP OPTIMIZATION

7.8.1 Optimal Solutions and Selection

The MILP optimization is applied to each of the four configurations that were introduced in Section 7.6. The four configurations are optimized independently as having a single type of system across the base eases maintenance, reduces operator training, simplifies logistics of supply chain management and replacement part inventory, and through this improves reliability.

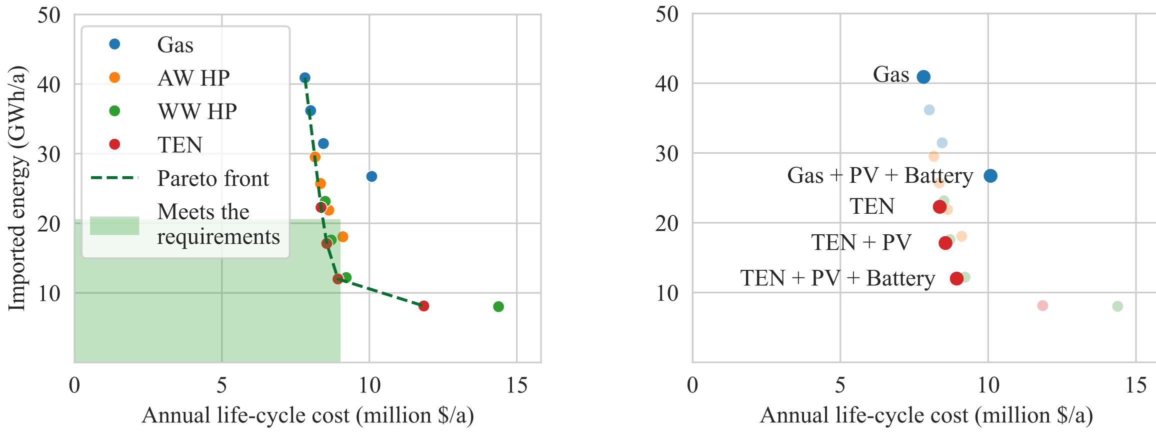

(a) Solutions from MILP optimization for the different configurations.

(b) 5 solutions selected to be discussed in more detail.

Figure 20. Solutions of the MILP optimization.

For each of the four configurations, we obtain a Pareto front, represented through four solutions of the respective configuration. Increasing the number of solutions would increase the number of points comprised between the two extreme solutions of a given configuration, without adding more insight into the optimal configurations. Fig. 20a shows all these 16 solutions. The solutions that meet the requirements defined in Section 7.3 – except for the investment cost, which are explained further below – are contained in the green rectangle of Fig. 20a. Among the solutions from the different configurations, only the ones that are on the Pareto-front are optimal. Fig. 20b shows five of these 16 solutions that are further analyzed.

The solution **Gas** corresponds to the configuration 0 (see Section 6.2.1) without PV nor batteries. This solution was selected as it is the baseline scenario as described in Section 7.3. It is the solution with the lowest life cycle costs, lowest investment costs, but with the highest energy imports. The solution **Gas + PV + Battery** also corresponds to the configuration 0, with the presence of PVs and batteries to store the excess PV production. This presence leads to a life cycle cost increase of more than 27.8 % and a decrease of the imported energy by almost 34.7 % compared to the solution **Gas**. This solution was selected as it is the one with the lowest imported energy for the configuration 0.

The solution **TEN** corresponds to the configuration 3 (see Section 6.2.4) with no PV and no batteries. Compared to the solution **Gas**, the life cycle cost is higher (7.0 %) but the imported energy is lower (−45.5 %). Also, compared to **GAS + PV + Battery**, the **TEN** solution has both, lower life cycle costs and lower imported energy, it Pareto-optimal whereas the **GAS + PV + Battery** is not. The other solutions **TEN + PV** and **TEN + PV + Battery** also correspond to Configuration 3. Compared to the **TEN** solution, **TEN + PV** includes the use of PV panels, and **TEN + PV + Battery** also includes the use of batteries. Both additions moderately increase the life cycle costs but they decrease the import of energy. On-site energy generation and storage through PVs and batteries also improves resilience and energy supply security, which were not monetized in the life cycle costs. Those solutions were selected as they meet the requirements defined in Section 7.3.

7.8.2 Life Cycle Costs

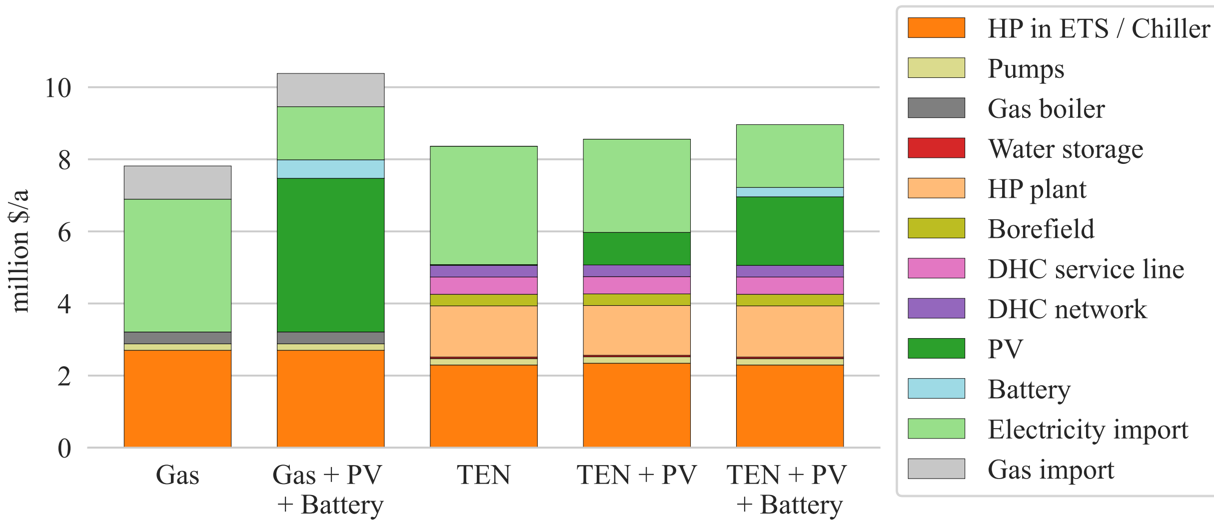

Figure 21. Annualized life cycle costs.

Fig. 21 presents the annual life cycle cost of the different solutions.

The **Gas** solution has the lowest life cycle cost, most of it being related to the import of gas and electricity (58.9 %) and to the individual chillers, installed at every building, cost (34.6 %).

By contrast, the **Gas + PV + Battery** solution has the highest annual life cycle costs. The contribution of chillers, boilers and pumps is similar than for the **Gas** solution, but it has lower costs related to energy imports (−48 %) and but higher overal life cycle costs due to the PV and batteries, which account for 46 % of the total life cycle cost.

For the different TEN solutions, the annual life cycle costs differ because of their varying contributions in PV, batteries and energy import. Other equipment cost is around $4 million for all TEN solutions.

7.8.3 Energy Imports

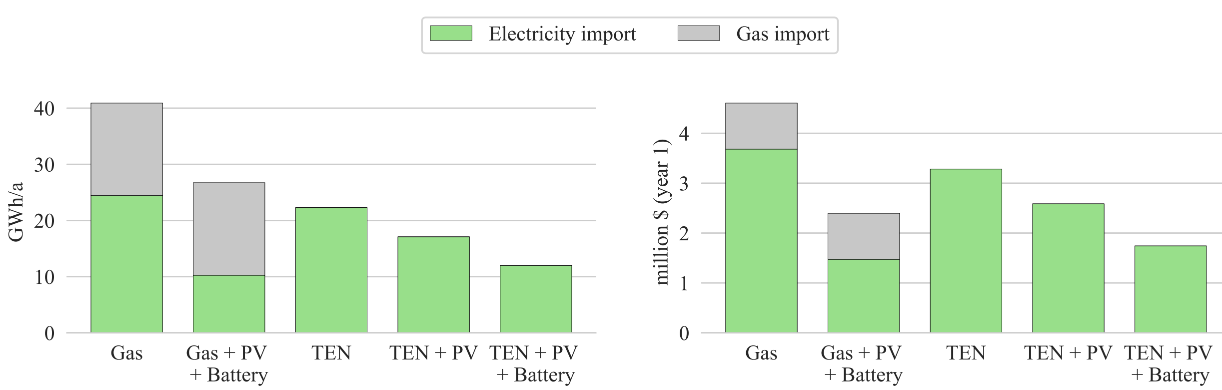

Figure 22. Energy import (left) and cost of the imported energy (right) for each solution.

Fig. 22 shows that half as much electricity is imported in the **Gas + PV + Battery** as in the **Gas** solution, leading to a 59 % reduction of the electricity cost, as the batteries store electricity for later use when electricity rates are high.

Compared to the **Gas** solution, the **TEN** solution has 45 % lower energy imports due to the higher system efficiency.

Compared to the **TEN** solution, adding PV and batteries decreases the energy import by 21 % for the **TEN + PV** solution and by 47 % for the **TEN + PV + Battery** solution, with a similar decrease in energy costs.

Overall, the TEN configuration has higher system efficiency than the gas solution, as reflected in the reduced import of energy. Moreover, thermal and electrical storage permits to store energy when cost or system efficiency is high, thereby further reducing energy costs.

The share of self-production is the ratio of energy produced on-site over the energy consumed. Over the year, the self-production is 34.7 % for the **Gas + PV + Battery** solution, 23.8 % for the **TEN + PV** solution, and 46.9 % for the **TEN + PV + Battery** solution. The higher self-production values observed for the **Gas + PV + Battery** and **TEN + PV + Battery** solutions result from their substantial photovoltaic (PV) energy generation capacity.

7.8.4 Investment Costs

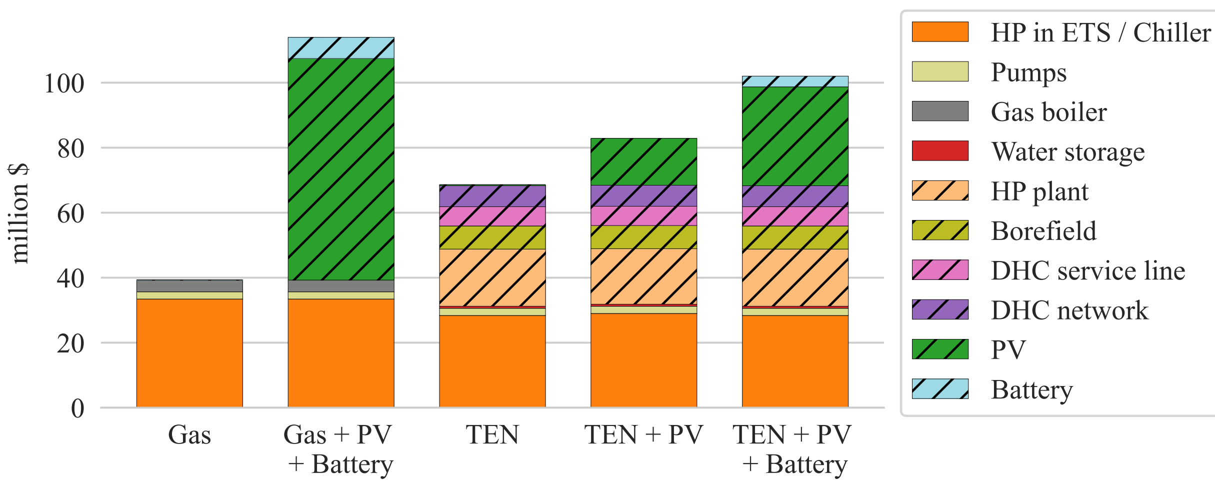

Figure 23. Investment costs, with the hashed values indicating assets that may be suitable for privatization to reduce DoD investments. As the same ECM are applied to all solutions, and part of the baseline assumption, their investment cost is not included in the figure.

Fig. 23 shows the investment costs of each solution, not accounting for the ECMs, listed in Table D, that are the same for all solutions. The investment costs are the lowest for the **Gas** solution. The second lowest investment cost has the **TEN** solution, with investment costs of +75% compared the **Gas** solution. For the **Gas + PV + Battery** solution, 65.6 % of the cost is associated to the presence of PV panels, making the **Gas + PV + Battery** more expensive than the **TEN** solution, while still importing more energy than the **TEN** solution.

For the TEN solutions, the investment cost is almost evenly split between the overall cost of the ETS that represents around \$31 million and the network related costs that also represent around \$37 million. For the **TEN + PV** solution, the PV account for 17 % of the investment cost, leading to a 21 % increase compared to the **TEN** solution, and PV and batteries account for 33 % of the investment costs for the **TEN + PV + Battery**, leading to a 49 % increase compared to the **TEN** solution.

An important point to note is that compared to the **Gas** solutions, the DoD investment for the **TEN** solutions are even lower if PV, batteries, TEN service line, TEN distribution line and central plant are being privatized. The **Gas** solutions require DoD investments of \$39 million, wheras the **TEN** solutions, excluding the privatized components, require \$31 million.

7.8.5 Maximum Equipment Capacity

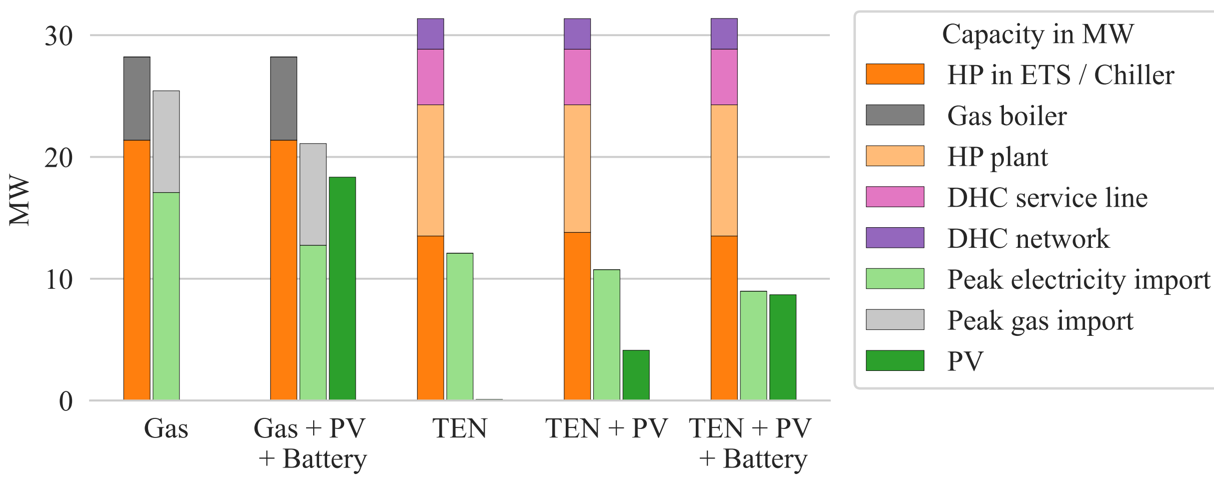

Figure 24. Capacities associated with the different elements and peak energy imports.

Fig. 24 shows that the maximum capacities of the different equipment remain the same for each configuration as they meet the same demand. Note that the capacities of the service lines are excluded from this comparison, as they do not directly contribute to meeting the demand.

The peak electricity import is lower in the **TEN** solutions compared to the **Gas** solutions as the heat pumps in the **TEN** solution have higher efficiency than the air-cooled chiller in the **Gas** solutions. We also observe a decrease of the peak electricity import for the **TEN + PV** solution and for the **TEN + PV + Battery** solution compared to the **TEN** solution. This reduction is attributed to the increased self-consumption of electricity generated by the photovoltaic (PV) system.

7.9 SENSITIVITY TO ENERGY PRICE

The Energy Outlook 2023 (EIA, 2023b) list energy rates for different economic growth and technology costs. To assess the sensitivity of the MILP results to the energy price, we consider two cases that represent the range of potential energy price evolution as shown in Fig. 4. We also accounted for an electricity price variation depending on the season and the time of the day as shown in Fig. 5.

As explained in Section 5.4.1, the prices of energy follow the reference case, with an average electricity rate of 14.6 ¢/kWh and a gas rate of 5.6 ¢/kWh. The high economic growth scenario leads to a slight decrease in electricity and gas prices, compared to the reference scenario, with an average price of 14.1 ¢/kWh for electricity and 5.35 ¢/kWh for gas. For electricity, the high rates are in 20.7 ¢/kWh in winter and 24.5 ¢/kWh in summer, the low rate is 11.4 ¢/kWh all year. This case was selected as it represents a low price scenario.

The low economic growth and low zero-carbon technology cost scenario represents a high energy price increase, with the average electricity price being 18.66 ¢/kWh for electricity and 7.29 ¢/kWh for gas. For electricity, the high rates are in 27.5 ¢/kWh in winter and 32.6 ¢/kWh in summer, the low rate is 15 ¢/kWh all year. This scenario was selected as it represents a high price scenario.

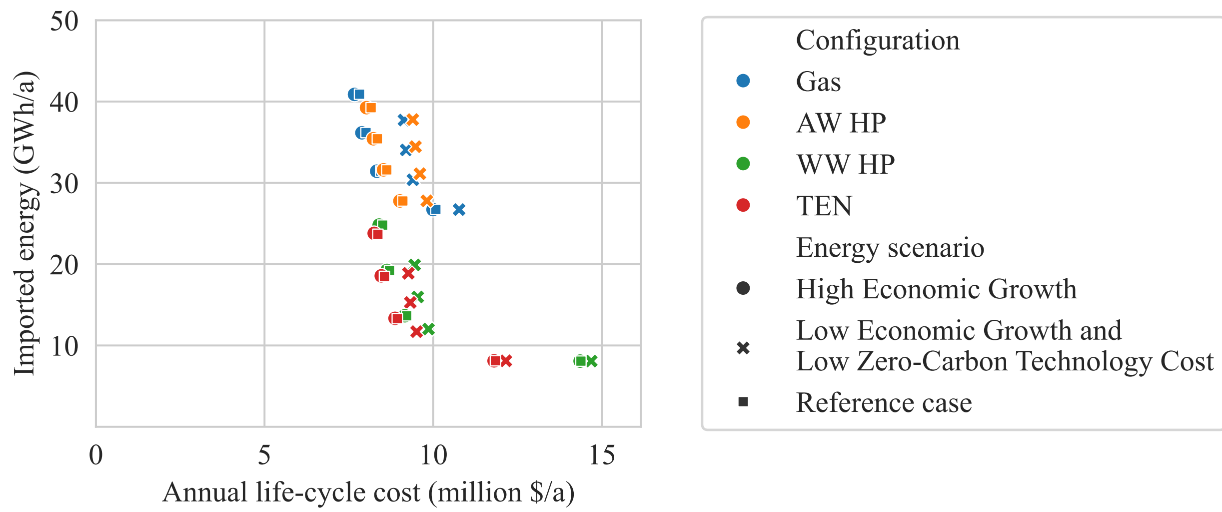

Figure 25. Life-cycle costs and energy imports for different energy cost scenarios.

Fig. 25 shows for each presented solution the energy imports and annual life cycle costs. The high economic growth case has no noticeable effect on the imported energy and the ALCC. For the low economic growth and low zero-carbon technology scenario, variations in energy imports are due to increased PV panel and battery sizes caused by the higher energy costs. **Therefore, an increase in energy costs makes the TEN configuration more favorable.**

7.10 SELECTED SOLUTION

In this section we will select from the above candidate solutions the one that we will use for the design, performance verification and risk reduction in Section 8.0.

Criteria	TEN + PV		TEN + PV + Battery	
Imported energy reduced by at least 50% compared to baseline.	✓	(−58.2 %)	✓	(−70.7 %)
Life-cycle cost no more than 120% of the baseline.	✓	(109.5 %)	✓	(114.3 %)
Investment cost no more than 200% of baseline.	✓	(174 %)	✗	(259 %)
Investment cost no more than 110% of baseline if central plant infrastructure, district loops, and utility-scale PV and battery systems are privatized.	✓	(79.5 %)	✓	(81.1 %)
Levelized cost of energy for heating and cooling no more than 0.25 USD/kWh.	✓	(0.227 $/kWh)	✓	(0.239 $/kWh)
The energy demands, which includes space heating, space cooling, DHW and electricity for auxiliary purposes must be matched at every time step.	✓		✓	
Solutions need to be Pareto-optimal.	✓		✓	

Table 12. Success in meeting the requirements for the selected solutions.

From all MILP candidate solutions, the two candidate solutions that satisfy most of the criteria are the **TEN + PV** and the **TEN + PV + Battery**. We selected the solution **TEN + PV + Battery** as it results in the lowest energy imports, and as the batteries further improve resilience and energy supply security. Table 12 shows the verification of this solution relative to the requirements defined in Section 7.3.

	ALCC (million $/a)	Investment (million $)
HP in ETS / Chiller	2.29	28.37
PV	1.90	30.40
Electricity import	1.74	0.00
HP plant	1.42	17.57
DHC service line	0.48	5.93
DHC network	0.32	6.46
Borefield	0.32	7.12
Battery	0.26	3.30
Pumps	0.18	2.21
Water storage	0.04	0.64
Electricity export	−0.03	0.00
Total	8.94	102.02

Table 13. Annualized life cycle costs and investment costs by components for the selected solution.

Table 13 shows a breakdown of the annualized life cycle costs and the investment cost for the selected solution.

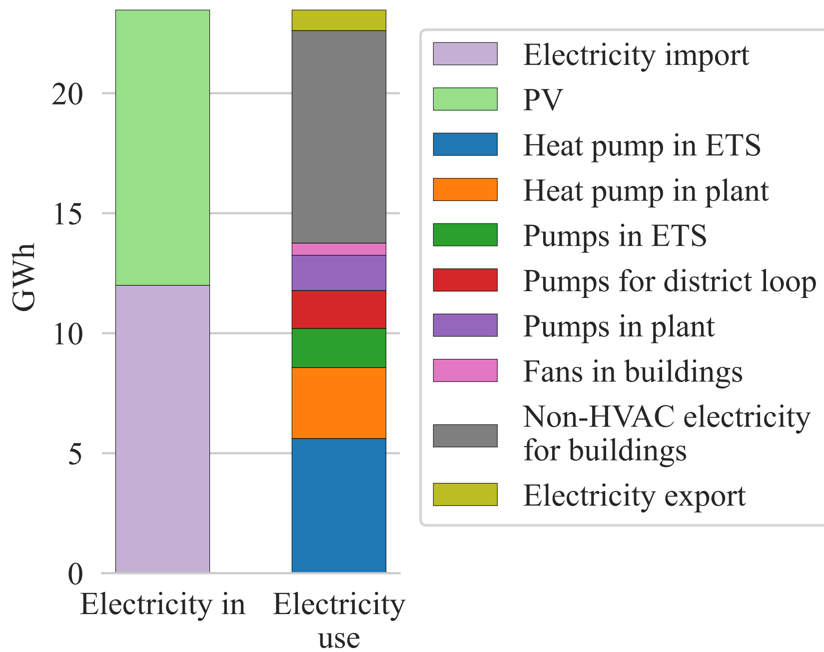

Figure 26. Electricity use for the selected solution TEN + PV + Battery.

Fig. 26 shows the electricity use for the selected solution **TEN + PV + Battery**. The electricity use, life cycle costs, and size of main equipment for each hub is available in Appendix F.

Fig. 27 shows the Sankey diagram of the selected **TEN + PV + Battery** solution, and, for comparison, the Sankey diagram of the **Gas** candidate solution which is the baseline. The Sankey diagram shows that the significantly higher performance of the **TEN + PV + Battery** solution is obtained through system integration. Specifically, for the **TEN + PV + Battery** solution, 12 GWh/a electricity import can cover the whole demand, compared to the **Gas** baseline, which would require twice the electricity import and 16 GWh/a gas import. **From an energy security point of view, this is a substantial reduction, and only small backup plants could operate the energy system in autarky mode.**

Comparing the two Sankey diagrams also shows that the **TEN + PV + Battery** solution has significantly more energy flows among the energy system components. Managing these energy flows requires more advanced design and control, which is being done and verified in the subsequent Section 8.0.

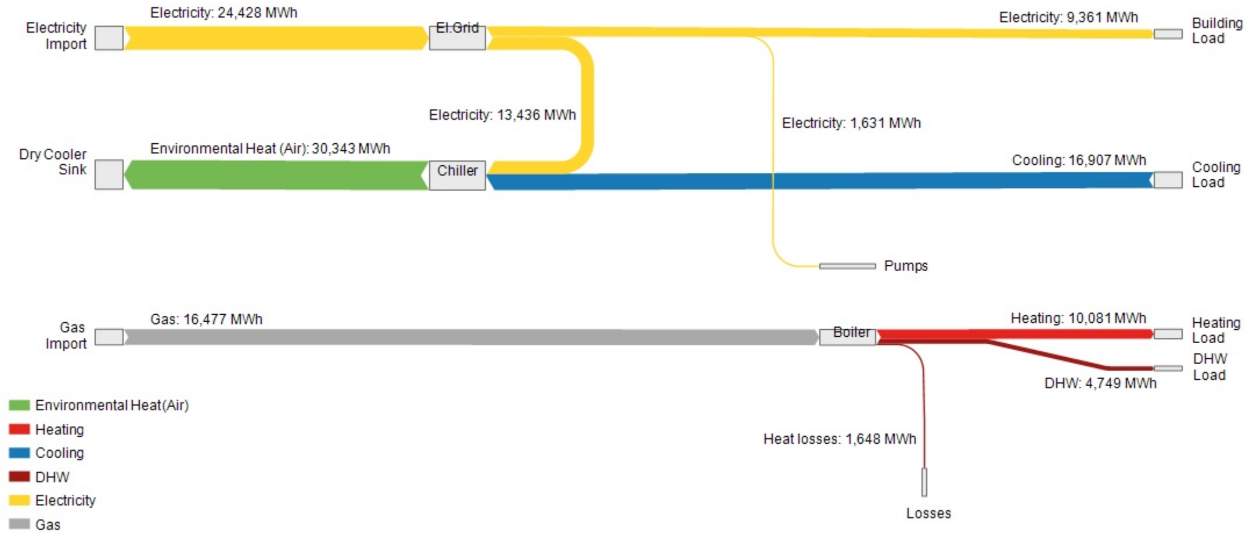

(a) Gas baseline.

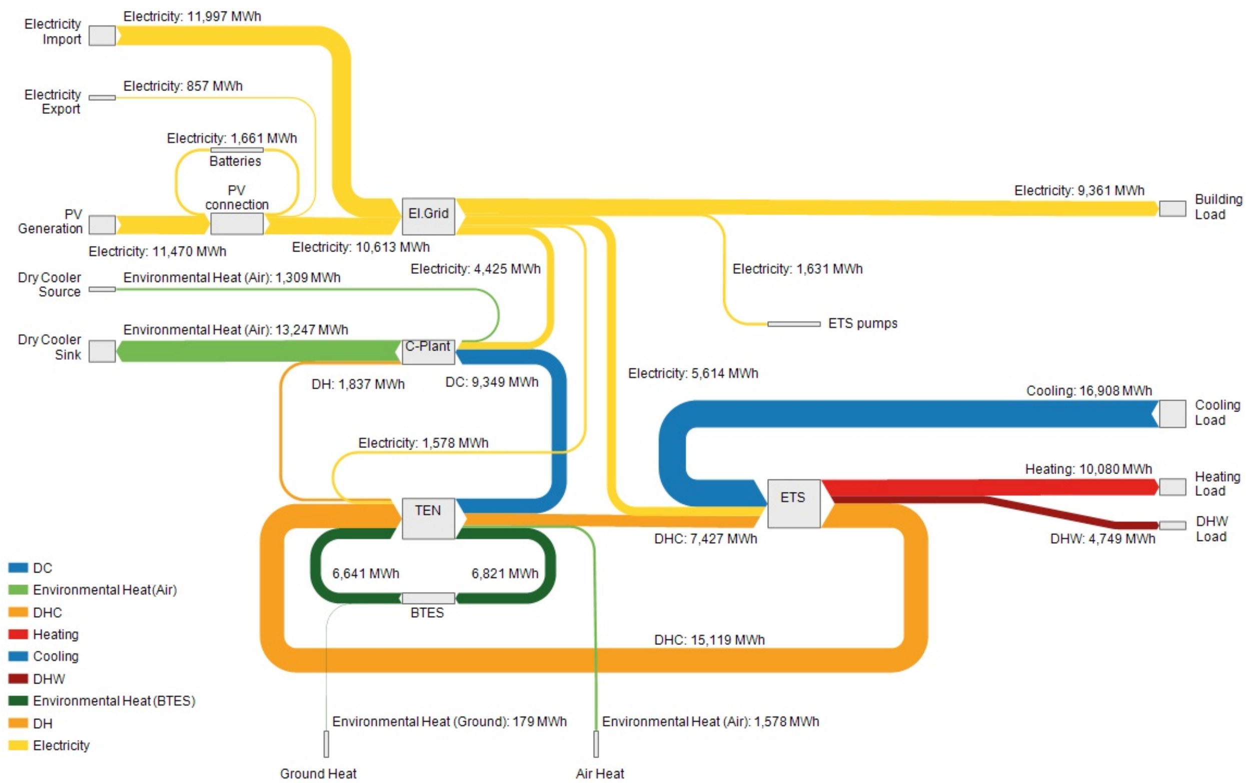

(b) TEN + PV + Battery solution.

Figure 27. Sankey diagram of the annual energy flows as obtained by the MILP optimization.

8.0 DESIGN, VERIFICATION AND RISK REDUCTION: MODELICA PLATFORM

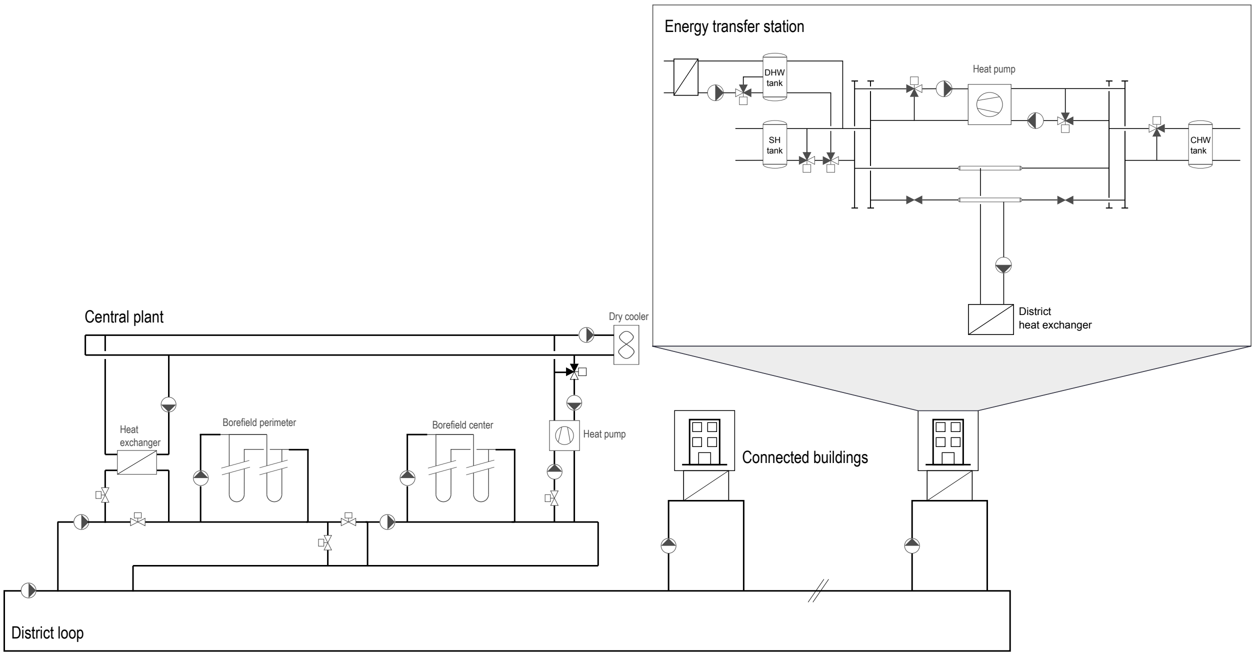

Figure 28. Schematic diagram of the TEN with central plant, district loop and ETS.

In this section, we will select the most suitable candidate solution from Section 7.0. We will then do a detailed design of the mechanical system, develop and implement control logic, and verify the performance and reduce operational risks through detailed dynamic simulations of the heat and power flows, pressure-driven water flow distributions and feedback control logic. The outcome will be a solution that is designed in terms of equipment, valve, pipe and pump sizes, that has detailed feedback control logic which has been verified for proper operation. This will then represent the specification for how to build such a system.

In Section 7.0, we identified using MILP the solution for the case **TEN + PV + Battery**, which is the Configuration 3 (ETS) in Section 6.2.4. Fig. 28 shows the schematic diagram of this configuration. For this system, we built a detailed model that coupled geothermal borefield, central system, district loop and ETSs, all having feedback control systems at a level of detail that it can be used as a specification for how to operate the system. Throughout this section, we refer to this model as the *base case*. The PV and batteries are sized and operated as determined by the MILP optimization in Section 7.10. In other words, we did not explicitly model the PVs and batteries in Modelica, but rather incorporated their electricity generation into the Modelica energy system simulations. Therefore, results in this section do contain the energy flow from the PVs and batteries.

We consider the same 17 buildings as has been used in the MILP optimization. However, to keep the detailed simulations manageable from a computing resources point of view, we group these 17 buildings into 5 hubs as shown in Fig. 29.

For the **TEN + PV + Battery** solution, MILP computed a total cost of imported energy of $29.1

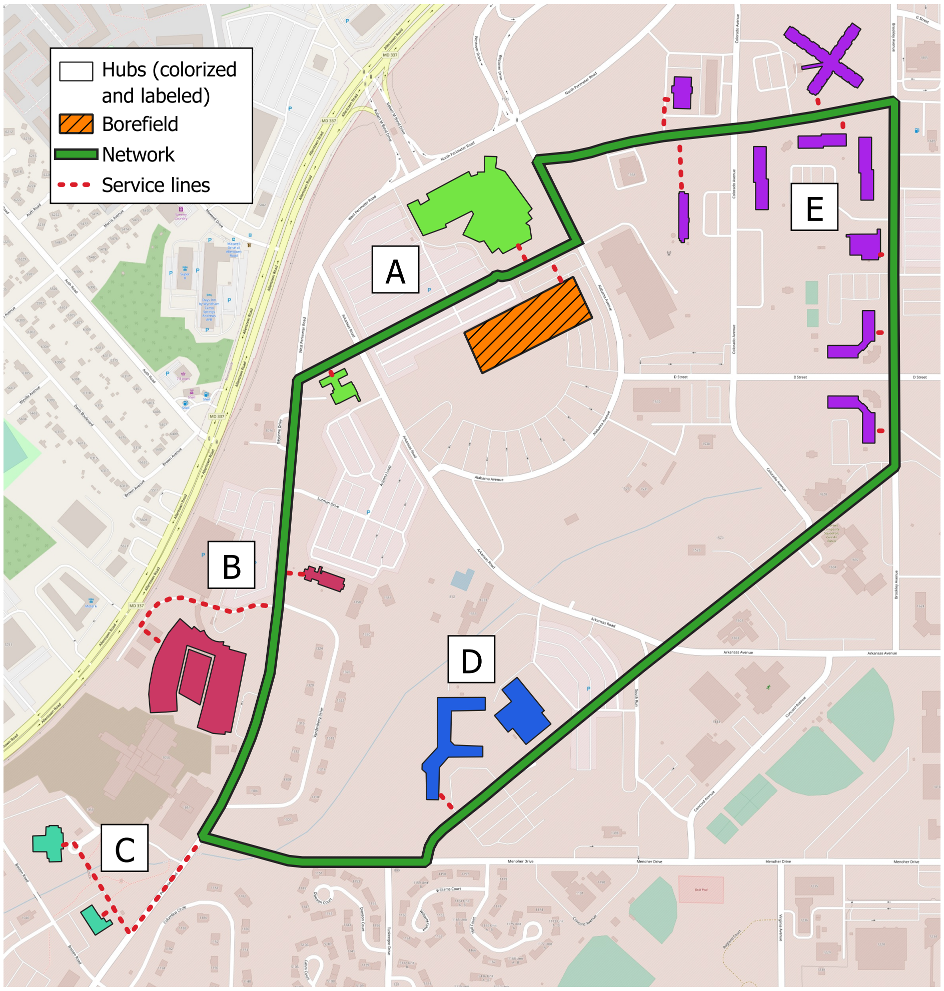

Figure 29. Buildings grouped to five larger hubs to reduce computational load in the Modelica model.

million for operating the HVAC system, which includes the central plant, the TEN and all HVAC systems in the ETSs. Also included are electricity for plug loads, lighting, and air handler unit fan operation. The associated annual energy use is 12.12 GWh/a. Normalized by the floor area, this corresponds to 15.8 $\$/(m^2\,a)$ energy costs and 108.2 $kWh/(m^2\,a)$ electricity use. These are the imported energy and cost budgets that we need to meet in this verification as described below, together with additional requirements that are added at this level of refinement of the PBD process.

We will first present formal requirements, then describe the selected candidate systems, state the analyzed scenarios, explain the sizing and finally present results of the verification.

8.1 REQUIREMENTS

We will now state verifiable requirements that system must satisfy at this abstraction layer of the PBD workflow in order to be considered a valid specification. These requirements will be verified with the system simulation to ensure that the design meets the specifications at that layer of abstraction.

We denote with the letter C a requirement for capital, D for design and O for operation. The numbers that follow the last dash are used to track them across the analysis.

Some requirements for this abstraction layer are flowing down from the above optimization layer, such as requirement on life cycle costs and imported energy. Other requirements are added at this layer because the refined design needs to satisfy them and they would be too detailed to be taken into account at the upper layer, such tracking of temperature set points and minimum equipment run times.

We will now state the requirements for the system level, for the ETSs, for the district loop and the central plant. The requirements need to be met for future weather data, and requirements related to set point tracking also need to be met with TMY3 weather data.

These requirements are to be understood in addition to requirements from DOD, such as Unified Facilities Criteria (UFC), local jurisdiction and professional organizations. As we are not designing the electrical system and not designing for sound attenuation, these requirements are not stated.

8.1.1 System Level

The requirements for maintaining the objectives on life cycle costs and imported energy are as follows:

- O-101: Imported energy reduced by at least 50% compared to baseline.
- O-102: Imported peak energy reduced by at least 40% compared to baseline.
- O-103: Life-cycle cost no more than 120% of the baseline.
- C-104: Investment cost no more than 200% of baseline.
- C-105: Investment cost no more than 110% of baseline if central plant infrastructure, district loops, and utility-scale PV and battery systems are privatized.
- O-106: Levelized cost of energy for heating and cooling no more than 0.25 USD/kWh.
- C-107: Capacities of the generation and storage no higher than in the MILP platform.
- O-108: Energy cost no more than 110% of the MILP platform.

  Note: We allow some slack as the above platform layer assumes perfect control, and perfect knowledge of the system.
- O-109: Imported annual energy no more than 110% of the MILP platform.

  Note: We allow some slack as the above platform layer assumes perfect control, and perfect knowledge of the system.

The requirements for maintaining equipment durability are as follows:

- O-201: The heat pumps must operate at least 30 min when activated, and remain off for at least 10 minutes.
- O-202: All control valves must show stable operation.

8.1.2 Energy Transfer Stations

The requirements for ensuring that the design constraints, such as temperature set points at the ETS, are satisfied are as follows:

- O-301: The DHW supply temperature must be 45°C ± 1 K (113°F ± 1.8°F).

- O-302: The heating water temperature that serves the DHW tank must be no less than 1 K (1.8°F) below and 10 K (18°F) above the heating water temperature set point once the tank charging is on for 10 minutes.

  Note: The higher upper limit is to account for the following situations: (i) the heat pump has a minimum controllable capacity that may cause some temperature overshoot if its condenser inlet temperature is close to the set point. (ii) A set point changes from the set point being determined from the space heating tank to the DHW tank can cause overshoots until temperatures are settled.

- O-303: The space heating water supply temperature set point must be tracked within ±1 K (±1.8°F) once the system is in space heating mode for 10 minutes.
- O-304: The space cooling water supply temperature set point must be tracked within ±1 K (±1.8°F) once the system is in space cooling mode for 10 minutes.
- O-305: At the district heat exchanger in the ETS, the secondary side leaving water temperature that serves the heat pumps must be between 9.5°C and 25°C (49.1°F and 77°F).

  Note: The lower limit avoids freezing in the evaporator, assuming a temperature difference of 4 K (7.2°F) over the evaporator. Both limits are used for designing the heat recovery heat pumps.

- O-306: At the district heat exchanger in the ETS, the primary side leaving water temperature that is fed back to the district loop must be between 6.5°C and 28°C (43.7°F and 82.4°F)).
- O-307: The heat pump evaporator leaving water temperature must be at least 3.5°C (38.3°F), and be preferably higher, once the system draws heat from the district for at least 5 minutes.

  Note: This ensures that the heat pump evaporator has no risk of freezing, and is a condition used for sizing the ETS heat exchanger.

- O-308: The heat pump condenser leaving water temperature must not exceed 31°C (87.8°F) once the system rejects heat to the district for at least 15 minutes.

  Note: This ensures that the temperature is set back, and is a condition used for sizing the ETS heat exchanger.

8.1.3 Load Tracking

The requirements for the room air temperature set point tracking are as follows:

- O-351: The room temperature should not fall more than 0.5 K below the heating set point during any 60 min window.

  Note: This verifies that the system has sufficient capacity for space heating.

- O-352: The room temperature should not raise more than 0.5 K above the cooling set point during any 60 min window.

  Note: This verifies that the system has sufficient capacity for space cooling.

- O-353: During heating or cooling, the bias of the room temperature control error, averaged over the year, should be no more than 0.05 K.

  Note: This verifies that the annual heating and cooling loads are matched.

8.1.4 District Loop

The requirements for the district loop are as follows:

- O-401: The water that is served to each service line must be between 10.5°C and 24°C (50.9°F and 75.2°F).

  Note: This is a design contract on which the ETS design is based on.

- O-402: The pressure drop in the district loop and the service line must be no bigger than 125 Pa/m at full load.

  Note: This is from option RN3 in Sommer et al. (2020).

8.1.5 Central Plant

The requirements for the central plant are as follows:

- D-501: The dry cooler loop must use propylene glycol with freezing point of −23°C (−10°F).

  Note: This is the 50 year annual extreme temperature according to ASHRAE, and corresponds to a 41.6 volumetric % mixture. In the simulations, we used a 45 volumetric % mixture, which has a freezing point of −25.8°C (−14.4°F), to allow a 2 K (3.6°F) dry cooler approach temperature.

- O-502: The supply temperature to the borefield must be between 8.5°C and 26°C (47°F and 79°F).

- O-503: The mixing water temperature in the district loop after the central plant must be between 10.5°C and 24°C (50.9°F and 75.2°F).

  Note: This is the design contract for the supply temperatures to the ETSs.

8.2 ANALYZED SCENARIOS

We conducted the following scenarios:

1. **Load increase during a 14-day heat wave.** In this scenario, we model the hypothetical scenario of a heat wave that lasts 14 days. This is simulated by repeating the weather data and load data on the hottest day from the fTMY weather file for 14 days. We then operate the system to try to meet the respective heating and cooling load. The increased cooling or heating load is compared against the base scenario to find how much energy needs to be provided during the 14-day resilience event, as this affects system reliability and resilience. This energy may come from an emergency generator, such as an onsite diesel generator. As the type of emergency generation can vary and because this represents a rare operational case, we are not modeling the emergency generation. Rather, we compute how much emergency power needs to be provided for a given candidate solution. See Section 8.7.4.1 for results.
2. **Load increase during a 14-day cold snap.** This scenario is the same as the heat wave, except that the coldest day from the fTMY file is repeated instead. See Section 8.7.4.2 for results.
3. **Requirements for backup power.** This scenario evaluates the requirements for the TEN and/or building-sited thermal systems to serve critical loads in the event of an electrical utility power outage. This scenario evaluates how much energy needs to be stored to serve the critical

building loads if utility power is interrupted for 7 days, starting at the coldest and hottest day of the year. The assumption is that 50% of all building loads are deemed to be critical loads, and hence the following requirements need to be satisfied:

- O-601: Serve all building loads, with loads being assumed to be 50% of their regular values, starting at the coldest day and the hottest day of the year.
- Satisfy all other requirements stated earlier, such as maintaining of system temperatures.

See Section 8.7.4.3 for results.

We will also conduct the following scenarios to evaluate the sensitivity of key performance indices:

4. **Sensitivity to central plant heat pump size.** The central plant heat pump is a cost-intensive equipment. In this scenario, we will evaluate the sensitivity of the cost, maximum loop temperature and the Kelvin hours of violating the maximum loop temperature. See Section 8.7.4.4 for results.
5. **Performance of central plant economizer.** In this scenario, we discuss the performance change if the central plant economizer were to be removed. See Section 8.7.4.5 for results.
6. **Sensitivity to borefield depth.** In this scenario, we change the borefield depth by increasing and decreasing it by 20% increments to show the sensitivity of investment cost, life cycle cost and imported energy. See Section 8.7.4.6 for results.
7. **Sensitivity to distribution pipe dimension.** In this scenario, we change the distribution pipe diameter by increasing and decreasing it by 20% increments to show the sensitivity as described above. See Section 8.7.4.7 for results.
8. **Sensitivity to ETS heat recovery heat pump minimum condenser leaving temperature.** In this scenario, we change the heat recovery heat pump minimum condenser leaving temperature of the ETS to show the sensitivity of the results to this control variable. See Section 8.7.4.8 for results.

8.3 SIZING

This section describes the sizing of the main components as used in the Modelica model. An overview of the sizing results is given in Table G.1.

8.3.1 Design Mass Flow Rates

The district loop, the heat pumps in the ETS and in the central plant, the borefield loops and the economizer in the central plant were all sized for a temperature difference of 4 K (7.2 F) and their respective heating and cooling capacities.

8.3.2 Borefield

The Navy Geothermal Office team designed a borefield that has two perimeter zones and a center zone for each module as shown in Fig. 30.[7] The perimeter zones have 375 wells with depth of 120 m

[7]This sizing has been obtained from the Navy Geothermal Program Office team that executes the ESTCP project EW22-D7-7483 "Grid Amplified Building Energy Seasonal Storage (GABESS) for Cost-Effective Resiliency".

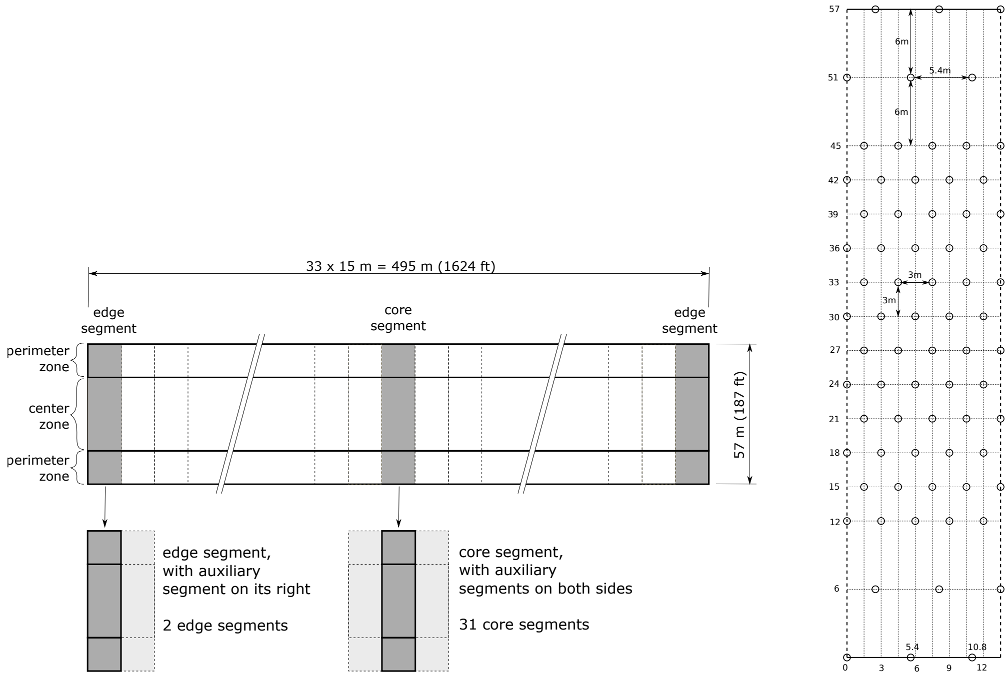

(a) Borefield layout and partitioning into edge and core segments for the Modelica simulation.

(b) Borefield segment with placement of wells.

Figure 30. Borefield layout, partitioning into segments for the simulation, and position of the wells.

(394 ft) and the center zones have 2025 wells with depth of 85 m (279 ft). For the modeling, we split the borefield along its long dimension into 33 segments that each have an identical construction, as shown in Fig. 30a.

As shown in Fig. 30b, each segment includes in the perimeter zone 12 wells and in the center zone 60 wells. We used 33 segments, and hence there are in the perimeter 396 wells and in the center there are 1980 wells, for a total of 2376 wells. As the Modelica model requires all bores to be of the same length, we assumed a borehole length of 91 m (299 ft).

We sized the mass flow rate for a temperature difference of 4 K (±7.2°F) at a specific heat flow rate of 40 W/m (41.6 BTU/h/ft).

8.3.3 Energy Transfer Station Heat Recovery Heat Pump

The set up of the ETS heat recovery heat pump is shown in Figure 17a. It can simultaneously provide heating from its condenser and cooling from its evaporator. Unlike a conventional reversible heat pump, it does not reverse the refrigerant cycle to switch between heating and cooling modes. For the Modelica model, we sized the component through its condenser capacity as

$$\dot{Q}_{con,0} = max(\dot{Q}_{hea,loa,0}, \dot{Q}_{hea,rej,0}), \tag{24}$$

where $\dot{Q}_{hea,loa,0}$ is the nominal heating load at this ETS and $\dot{Q}_{hea,rej,0}$ is the heating rejection capacity, i.e., the amount of heating rejection when the chiller is producing cooling at capacity. It is

$$\dot{Q}_{hea,rej,0} = \dot{Q}_{coo,loa,0} \frac{1 + COP_{hea,rej}}{COP_{hea,rej}}, \tag{25}$$

where $\dot{Q}_{coo,0}$ is the cooling capacity and $COP_{hea,rej}$ is the heating rejection COP.

8.3.4 Energy Transfer Station Heat Exchanger

The ETS heat exchanger allows the heat recovery heat pump to use the district loop as a heat source or heat sink. Its capacity is

$$\dot{Q}_{hex,0} = max(\dot{Q}_{coo,rej,0}, \dot{Q}_{hea,rej,0}) \tag{26}$$

where $\dot{Q}_{coo,rej,0}$ is the cooling rejection capacity, i.e., the amount of cooling rejection when the chiller is producing heating at capacity and $\dot{Q}_{hea,rej,0}$ is as in (25). Similar to (25), the cooling rejection capacity is

$$\dot{Q}_{coo,rej,0} = \dot{Q}_{hea,0} \frac{COP_{coo,rej}}{1 + COP_{coo,rej}}, \tag{27}$$

where $\dot{Q}_{hea,0}$ is the nominal heating load and $COP_{coo,rej}$ is the cooling rejection COP. Because $\dot{Q}_{coo,rej,0}$ increases with $COP_{coo,rej}$, for sizing, $\dot{Q}_{coo,rej,0}$ should be estimated using an unfavorable operating condition where $COP_{coo,rej}$ is low. Similarly, $\dot{Q}_{hea,rej,0}$ should be estimated using a favorable operating condition where $COP_{hea,rej}$ is high.

8.3.5 Central Plant Reversible Heat Pump

The central plant provides heating and cooling to keep the minimum and maximum loop temperature between the design limits. Some of this peak heating and cooling load can be provided by the borefield and the remaining part needs to be provided by the heat pump. Therefore, to size the central plant heat pump, we considered the peak heating and cooling loads of the combined building loads from all the ETSs as transmitted at heat exchanger between ETS and service line.

Next, to compute the capacity of the heat pump, we first selected a rather large heat pump, run a simulation and measured how much heating or cooling can be provided by the borefield during the peak hours. We then took this borefield capacity into consideration to downsize the heat pump. Lastly, we run parametric simulation, which are shown in Section 8.7.4.4 to see how different heat pump sizes affect investment costs, maximum district loop temperature, and Kelvin hours for which the maximum district loop temperature is violated if a smaller heat pump is selected.

8.3.6 Central Plant Economizer

We sized the central plant dry cooler for a heat exchanger effectiveness of $\epsilon = 0.9$ and the design flow rate of the district loop.

8.3.7 Central Plant Dry Cooler

The central plant dry cooler was sized for the glycol mass flow rate of the reversible heat pump, using a heat transfer effectiveness of 0.9 and a temperature difference on the glycol side of 4 K (7.5 F).

8.3.8 Network Piping

The district loop and the borefield pipes are sized for a specific pressure drop of 125 Pa/m at the design flow rate, which is the same value as was used in Sommer et al. (2020). We used a pipe roughness of 0.0015 mm (Kolahi et al., 2025). For the district loop, the resulting pipe diameter is 0.50 m(1.66 ft).

Note that the sensitivity analysis in Section 8.7.4.7 shows that a larger pipe diameter would have been more economical.

8.3.9 Circulation Pumps

All circulation pumps are sized for a nominal flow rate of

$$\dot{m}_0 = \frac{\dot{Q}_0}{c_p\, \Delta T_0}, \tag{28}$$

where $\dot{Q}_0$ is the nominal thermal load, c_p is the specific heat capacity of the fluid, either glycol or water, and ΔT_0 is the nominal temperature difference.

8.4 CONTROL SEQUENCES

The control intent for the ETSs is described in Section 6.2. Here, we describe the control of the central pump in the district loop, and then the control of the central plant.

8.4.1 Control of District Loop Pump

For the control of the district loop pump, we use the controller developed in Sommer et al. (2020). This controller reduces the pump speed unless the water temperature at the mixing points after the ETSs feed-in into the district loop is too high or too low, in which case the pump speed is increased to keep the loop temperature between a lower and upper bound.[8]

Fig. 31 shows the pump speed reset, which is as follows: Let $T_{mix,min}$ and $T_{mix,max}$ be the minimum and maximum measured mixing temperatures after all the ETSs except the last one[9] and let $T_{dis,loo,des,min}$ = 10.5°C (50.9°F) and $T_{dis,loo,des,max}$ = 24°C (75.2°F) be the design minimum and maximum district loop temperatures, let T_l and T_u be the lower and upper bounds for the mixing temperatures and let $\Delta T_{dis,mar}$ = 2 K (3.6°F) is an adjustable parameter to allow staging the

[8]Note that the reservoir loop design rules requires controlling the inlet to the energy transfer stations rather than the temperature after the energy transfer return is mixed with the district loop bypass. Using the mixing temperatures leads to a shorter feedback time. This simplifies control tuning. It is also the more conservative choice because of the heat transfer between the distribution pipes and the ground.

[9]The last ETS is excluded as we do not need to give a guarantee on the water temperature after this station.

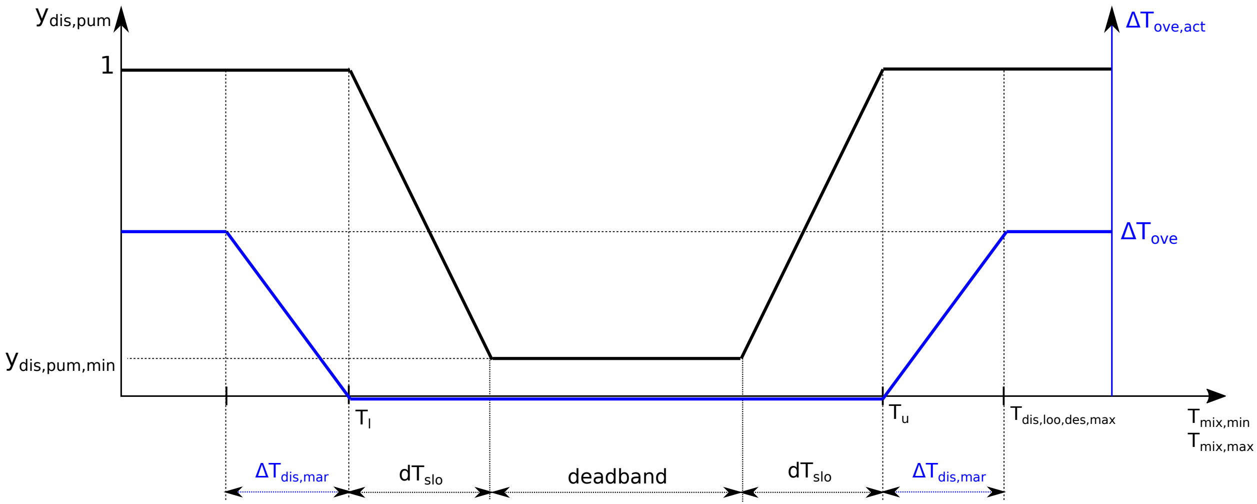

Figure 31. Controller for distribution pump speed, and controller for district loop setpoint overshoot, which is sequenced with the distribution pump speed. On the horizontal axis is the district temperature. On the left vertical axis is the district loop pump control signal as a function of the minimum and maximum of the measured temperatures after the prosumer outlets mixed with the district loop bypass. On the right vertical axis is the overshoot value that is used to provide a margin for the plant heating and cooling set point temperatures, which is needed as the dynamics of the control loop, which includes the water transport delay in the district loop, can lead to some overshoot.

equipment in the central plant after the district loop pump speed is maximized.[10] We set the limits as[11]

$$T_l = T_{dis,loo,des,min} + \Delta T_{dis,mar}, \quad (29a)$$
$$T_u = T_{dis,loo,des,max} - \Delta T_{dis,mar}, \quad (29b)$$

where $T_{dis,mar} = 2$ K (3.6°F, adjustable) is a margin that ensure that first the pump speed can be maximized, and then the heat pump in the central plant is staged. If $T_{mix,min} - T_l > 2$ K (3.6°F) or $T_u - T_{mix,max} > 2$ K (3.6°F), then the pump speed is set to the minimum speed $y_{dis,pum,min}$. Otherwise it is linearly increased to the full speed until $T_l = T_{mix,min}$ or $T_u = T_{mix,max}$. This calculation is done for the lower and upper bound, and the actual pump speed is the larger of the two pump signals.

[10]During the verification, it showed that some overshoot of the mixing temperatures can occur as it takes around 1 hour for water to travel around the loop. Therefore, we introduced this parameter to maintain slightly tighter temperature control at the mixing point after the central plant.

[11]The limits could be changed dynamically as long as

1. $T_l, T_u \in [T_{dis,loo,des,min}, T_{dis,loo,des,max}]$,
2. $T_l < T_u - 2\, dT_{slo} + \Delta T$, where ΔT is a deadband, and
3. $T_l < T_{bor,out} < T_u$ where $T_{bor,out}$ is the measured borefield outlet temperature.

to move the district loop temperature up (in winter) or down (in summer). The third condition must be satisfied as the central plant control is based on this condition. In the base line controller we are not changing the limits as we already move the borefield temperature up and down.

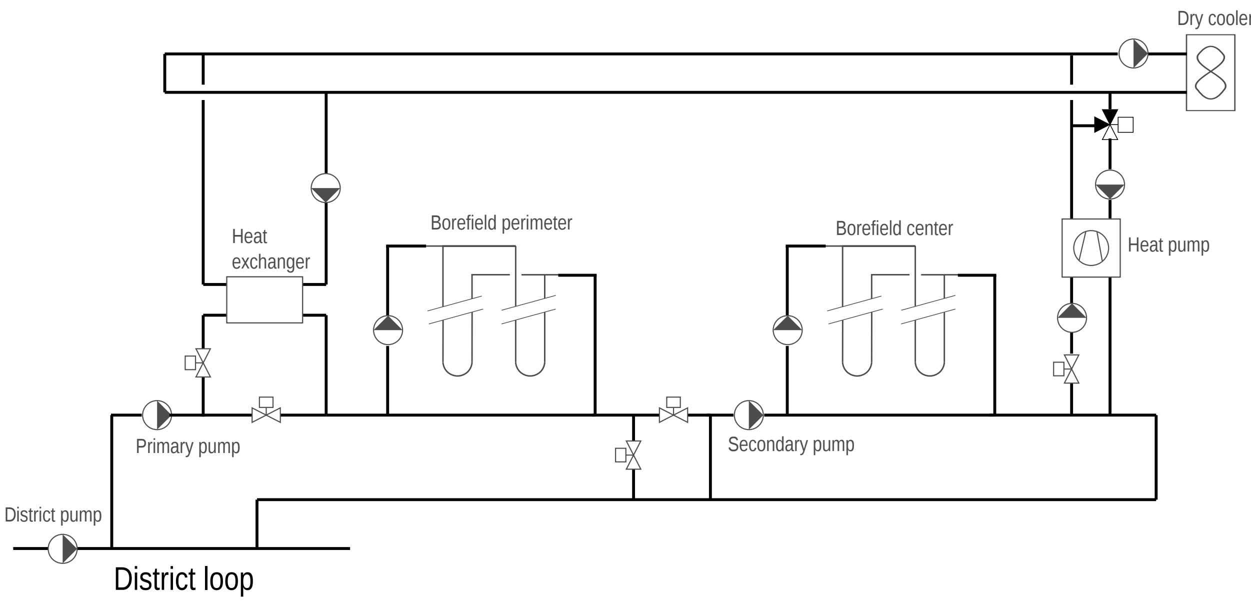

Figure 32. Schematic diagram of central plant.

8.4.2 Control of Central Plant

The central plant shown in Fig. 32 and, as part of the whole district loop in Fig. 12, contains several modules: A water-to-glycol economizer to provide compressor-less cooling, two sections of the borefield, and a reversible water-to-glycol heat pump. For this plant, we developed the rule-based controller below and used this controller for the Modelica simulations.[12]

The high-level control intent is as follows, and a more detailed specification is given below.

The district loop pump speed is modulated based on how close the mixing temperatures (i.e., the temperatures after the district service lines that connect the district loop to the ETS feed into the district loop) are to the minimum and maximum loop temperature. If they are close, the pump speed is increased to reduce the temperature changes across the district loop. If they are far from the limit, the pump speed is reduced to save energy. This was as introduced in Sommer et al. (2020).

The plant is controlled as follows: During spring and fall, if the center borefield and the heat pump are not needed to stabilize the district loop temperature, they are operated during normal electricity rates (but not during high electricity rates) to cool the center borefield in spring, and heat it in fall. This increases the capacity of the borefield, and it allows adding or removing heat from the system when outdoor conditions are more favorable than during winter or summer. When temperature conditions allow, the economizer is also adding or removing heat from the system. The pump speed for the perimeter of the borefield is interlocked with the district pump speed, thus increasing the flow rate if the district needs higher flow rate, and reducing pump energy otherwise (while maintaining turbulent flow in the borefield pipes). If the economizer and the perimeter borefield are insufficient to stabilize the loop temperature, then the center borefield and the heat pump are activated. Both are regulated to increase their load based on the plant leaving temperature.

[12]Note that we call the equipment dry cooler, even though in mild winter days it is used to add heat to the system. Also note that for an actual demonstration, this controller may be refined with a predictive controller that increases the utilization of the borefield, and thereby may allow downsizing this capital-intensive energy storage.

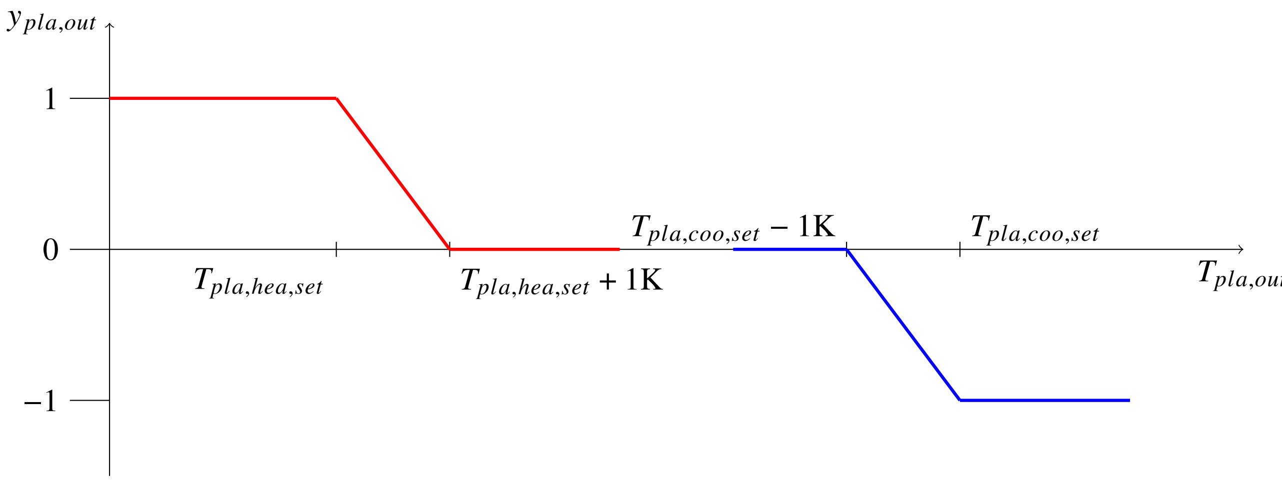

Figure 33. Heating load signal (red) and cooling load signal (blue) of the central plant to stabilize the district loop temperatures.

The controller operation is different based on the electricity rate, the load and the season. For the control sequence, we require the following indicators:

8.4.2.1 Electricity Rate Indicator Based on the current electricity rate, the electricity rate indicator is either set to normal rates or high rates. JBA has no hours with low rates.

8.4.2.2 Plant Load Indicator In Section 8.4.1, we showed how the district loop pump is controlled based on the mixing temperatures in the loop. This approach was selected as the mixing temperatures immediately react to a change in flow rate, and the approach has shown to be robust in Sommer et al. (2020). However, if we were to use the mixing temperatures after the ETSs as a controlled variable for the central plant energy input, there would be significant transport delay as it takes in the order of one hour for water to circulate through the district loop. Such long transport delays can cause control instability. Therefore, to avoid a feedback control with such transport delays, we control the central plant to meet the mixing temperature $T_{mix,pla}$ in the district loop immediately after the junction of the central plant return. If we set the central plant mass flow rate to be equal to the district loop mass flow rate, then the control objective is to keep the central plant outlet temperature $T_{pla,out}$ within the range needed to ensure the mixing temperatures in the district loop.

The control signal for the plant y_{pla} can then be computed based on the measured plant outlet temperature $T_{pla,out}$ as shown in Fig. 33. For this calculation, we introduce the plant heating set point temperature as

$$T_{pla,hea,set} = T_{dis,lop,des,min} + \Delta T_{dis,des} \frac{\dot{Q}_{hea,rej,ets,des}}{\dot{Q}_{coo,rej,ets,des}} + \Delta T_{ove,act}, \tag{30}$$

where $\Delta T_{dis,des} = 4\,\text{K}$ is the design temperature difference for the district loop. As $\Delta T_{dis,des} = 4\,\text{K}$

is for cooling, and the district loop is cooling dominated, we multiply $\Delta T_{dis,des}$ by the ratio of $\dot{Q}_{hea,rej,ets,des}/\dot{Q}_{coo,rej,ets,des}$, where $\dot{Q}_{hea,rej,ets,des}$ is the peak heat transfer at the heat exchanger of the ETS for heating, taking into account load diversity and $\dot{Q}_{coo,rej,ets,des}$ is the same for cooling. The term $\Delta T_{ove,act}$ is a safety margin to allow for some control overshoot. See Fig. 31 for how $\Delta T_{ove,act}$ is computed, where we set $\Delta T_{ove} = 2$ K (adjustable).

Similarly, the plant cooling set point temperature is

$$T_{pla,coo,set} = \begin{cases} T_{dis,lop,des,max} - \Delta T_{dis,des} - \Delta T_{ove,act}, & \text{if } T_{dry,bul} < 23°\text{C}, \\ T_{dis,lop,des,max} - \Delta T_{dis,des} - \Delta T_{ove,act} - \Delta T_{off}, & \text{if } T_{dry,bul} > 25°\text{C}, \\ T_{dis,lop,des,max} - \Delta T_{dis,des} - \Delta T_{ove,act} - \Delta T_{off}\,(T_{dry,bul} - 23)/2, & \text{otherwise,} \end{cases} \tag{31}$$

where $\Delta T_{off} = 2$ K (adjustable) is an offset to increase the cooling during hot summer days. The colder set point during hot summer days increases the capacity from the heat pump prior to a potential hot period.

With $T_{pla,hea,set}$ and $T_{pla,coo,set}$, we can compute the plant control signal $y_{pla,out}$ as shown in Fig. 33.

The plant load indicator is then

$$y_{st} = \begin{cases} 1, & \text{if } |y_{pla,out}| \in [0,\ 1/3), \\ 2, & \text{if } |y_{pla,out}| \in [1/3,\ 2/3), \\ 3, & \text{otherwise.} \end{cases} \tag{32}$$

When the mode switches from $y_{st} = 3$ to $y_{st} = 2$, the cooling capacity of the plant drops. This has shown to cause frequent mode switches because $y_{pla,out}$ reacts quickly. Hence, if y_{st} becomes 3, we enable a timer that ensures that $y_{st} = 3$ remains unchanged for 1 hour (adjustable).[13]

8.4.2.3 Season Indicator Based on the week of the year, the plant is either in *winter*, *spring*, *summer* or *fall* mode. Determining the switch-over time is done offline based on the net heating and cooling load analysis of the TEN. The season indicator is used to determine whether the central plant should add heat or cold to the system if the electrical rates are normal. Therefore, we set the season indicator to

$$y_{sea} = \begin{cases} 1, & \text{if winter,} \\ 2, & \text{if spring,} \\ 3, & \text{if summer,} \\ 4, & \text{if fall.} \end{cases} \tag{33}$$

With these three modes, we can now specify the operation of the central plant.

8.4.2.4 Control that is Common in All Modes First, we list controls that is common in all modes of operation:

1. The speeds of the primary pump and the borefield perimeter pumps, if enabled, are interlocked with the speed of the district pump, hence $y_{pri,pum} = y_{bor,per,pum} = y_{dis,pum}$. However,

[13] See discussion at `https://github.com/lbl-srg/thermal-grid-jba/issues/81`.

$y_{bor,per,pum}$ and $y_{dis,pum}$ must be larger enough to ensure turbulent flow in the pipes of the borefield.

2. Whenever the heat pump operates below 20% of the full compressor speed for 10 minutes (adjustable), switch it off, and keep it off for 1 hour (adjustable) if $y_{st} \in \{1, 2\}$, otherwise allow it to get switched on after the minimum off time of the heat pump, which is 30 minutes.
3. When the dry cooler is enabled, the fan tracks a 2K (3.6°F, adjustable) approach temperature between outdoor dry bulb temperature and leaving glycol temperature.
4. All pumps on the glycol side are operating at full speed when commanded on.
5. The glycol-side temperature control through the valves at the heat pump is tracking a maximum evaporator inlet temperature (if the heat pump is in heating mode) or a minimum condenser inlet temperature (if in cooling mode).

8.4.2.5 High Electricity Rates During high electricity rates, the central plant is operated as follows in the different stages:

1. If $y_{st} = 1$ and $y_{sea} \in \{1, 2, 3, 4\}$, the load is low, operate the borefield perimeter only. Disable the economizer, the heat pump and the borefield center.
2. If $y_{st} = 2$, the load is medium.

   Keep the heat pump off.

   Leave the borefield operation as in Item 1 and control the economizer and dry tower as follows:

   (a) If $y_{sea} = 1$ (winter), we need to add heat. If $T_{pla,in} < T_{dry,bul} - T_{app}$, where $T_{pla,in}$ is the central plant inlet temperature, $T_{dry,bul}$ is the dry bulb temperature and $T_{app} = 4$ K (7.2°F, adjustable) is the approach temperature, enable the economizer. Set the economizer pump to full speed and the dry cooler pump to full speed.

   Control the dry cooler fan to track 2 K (3.6°F) approach temperature between outlet glycol temperature and dry bulb temperature.

   If $T_{pla,in} \geq T_{dry,bul} - T_{app}$, keep the economizer off.

   (b) If $y_{sea} \in \{2, 4\}$ (spring or fall), disable both, the economizer and the heat pump.

   Although the loop load is increased, it will increase the pump of the borefield perimeter and the system tries to serve the load with the borefield perimeter only.

   (c) If $y_{sea} = 3$ (summer), we need to remove heat. If $T_{pla,in} > T_{dry,bul} + T_{app}$, with $T_{app} = 4$ K (7.2°F, adjustable), enable the economizer, and control the economizer and dry cooler as for Item 2a (but with the signs for the temperature differences adjusted accordingly).

3. If $y_{st} = 3$, the load is high.

   We run the center of the borefield and modulate the heat pump. Hence, open/close the valves to connect the primary and the secondary loop.

   Run all pumps, except for $y_{bor,cen,pum}$, with interlocked speed, $y_{pri,pum} = y_{sec,pum} = y_{bor,per,pum} = y_{bor,cen,pum} = y_{hea,pum,pum} = y_{dis,pum}$.

Control $y_{bor,cen,pum}$ to be within $y_{bor,cen,pum} \in [0.2,\ 1]$ so that the mixing temperature after the center borefield tracks $T_{pla,hea,set}$ or $T_{pla,coo,set}$, depending on whether heating or cooling need to be provided.[14]

Enable the heat pump to track a heat pump leaving set point temperature of

$$T_{hea,pum,set} = \max\left(T_{dis,loo,des,min},\, T_{hea,pum,in} + \frac{\dot m_{pla}}{\dot m_{hea,pum}}(T_{pla,set} - T_{hea,pum,in})\right), \quad (34)$$

where $T_{hea,pum,in}$ is the heat pump inlet temperature, $\dot m_{hea,pum}$ is the water mass flow rate through the heat pump, and

$$T_{pla,set} = \begin{cases} T_{pla,hea,set}, & \text{if } T_{pla,in} < \frac{T_{pla,hea,set}+T_{pla,coo,set}}{2} \text{ (heating mode)},\\ T_{pla,coo,set}, & \text{otherwise (cooling mode).} \end{cases} \quad (35)$$

Note that (34) allows the heat pump capacity to be sized smaller than the capacity of the central plant, for example to take into account that the borefield also provides heating or cooling capacity. In the special case of them being designed for the same capacity, (34) reduces to $T_{hea,pum,set} = T_{pla,set}$.

Enable or disable the economizer as in Item 2.

8.4.2.6 Normal Electricity Rates If electricity rates are normal, the central plant is operated in spring (or fall) to cool (or heat) the center of the borefield.

The control is as follows in the different seasons:

4. If $y_{sea} \in \{2, 4\}$ (spring or fall), the primary loop of the central plant is operated as in Item 2b, and the secondary loop is operated to cool (spring) or heat (fall) the center of the borefield.

   The cool or heat the borefield, close the isolation valve to form a circulation between the borefield center and the heat pump. Run the heat pump water-side pump at $y_{hea,pum,pum} = 1$, and set the borefield center pump to a speed that ensures that all water from the borefield center circulates through the heat pump, e.g, $\dot m_{hea,pum} = \dot m_{bor,cen}$.

   If $y_{sea} = 2$ (spring), cool the borefield by tracking a leaving heat pump temperature of $T_{hea,pum,set} = \max(T_{dis,loop,des,min} - \Delta T_{cha},\, T_{hea,pum,in} - \Delta T_{dis,des})$, where $\Delta T_{cha} = 4\,\mathrm{K}$ (7.2°F, adjustable) is used to sub-cool the borefield in order to have more capacity.

   If $y_{sea} = 4$ (fall), heat the borefield by tracking a leaving heat pump temperature of $T_{hea,pum,set} = \min(T_{dis,loop,des,max},\, T_{hea,pum,in} + \Delta T_{dis,des})$.

5. If $y_{sea} \in \{1,\ 3\}$ (winter or summer):

   (a) If $y_{st} = \{1, 2\}$ (low or medium load). In summer, if the dry bulb temperature is below 24°C (adjustable), operate the heat pump to charge the borefield as in Item 4. Otherwise, and also in winter, do not run the heat pump.

[14]In earlier versions, $y_{bor,cen,pum}$ was interlocked with $y_{pri,pum}$, but this added too much cooling capacity, causing the heat pump to switch to heating mode and counteract, thus causing simultaneous cooling from the borefield and heating from the heat pump. See `https://github.com/lbl-srg/thermal-grid-jba/issues/85`.

(b) If $y_{st} = 3$ (high load). Run the heat pump as in Item 3.

For all $y_{st} \in \{1, 2, 3\}$, operate the borefield perimeter and center. Control the economizer and the dry cooler as in Item 2a (winter) or Item 2c (summer).

For a more detailed specification of the control logic, we refer to the Modelica model and its documentation.

8.4.3 Control of Energy Transfer Station

Figure 34 shows the schematic diagram of the ETS and the control signals. It is adapted from Gautier, Wetter, and Sulzer (2022). We will now summarize the main operation principles.

8.4.3.1 Domestic Hot Water Tank and Buffer Tanks The chilled water and heating hot water tanks are sized for five minutes and used as buffer tanks. The DHW tank is sized for 24 hours of storage. Each tank generates a signal to request charging. If the temperature of its supply side (top for the hot tank, bottom for the cold tank) deviates from the set point with hysteresis, charging is enabled until the temperature of its return side (bottom for the hot tank, top for the cold tank) achieves the set point with hysteresis.

When the space heating or cooling tank does not request charging, the diversion valve `VAL_DIV_CON` or `VAL_DIV_EVA` to the respective tank is closed, and the isolation valve `VAL_ISO_CON` or `VAL_ISO_EVA` is opened to allow energy exchange with the district heat exchanger. The diversion valves are necessary because, for example, when the ETS operates cooling only mode, rejecting heat to the ambient loop, the condenser outputs hot water at the minimum leaving temperature is 15°C (59°F). Without the diversion valve, the cool water from the condenser would flush out the energy stored in the space heating tank. This causes energy waste. It also causes short cycling because the tank will request charging repeatedly as its temperature falls below the heating set point, bring the system into a limit cycle.

8.4.3.2 Two-tank Coordination on the Condenser Side The integration of the DHW tank is optional, as not all buildings prepare DHW using the ETS. When integrated, the space heating and DHW tank share the same condenser loop. Table 14 explains how the two loops are coordinated through valve control.

Charge signal		**Controller output**	
DHW	HHW	y_{mix}	y_{div}
on	on	0.5	1
on	off	0	1
off	on	1	1
off	off	1	0

Table 14. Control signal coordination of the DHW tank and the space heating tank. Depending on the charge signal, the control block computes the position y_{mix} of the mixing valve `VAL_MIX` (position 1 is to the space heating tank, position 0 is to the DHW tank) and y_{div} of the condenser-side diversion valve `VAL_DIV_CON`.

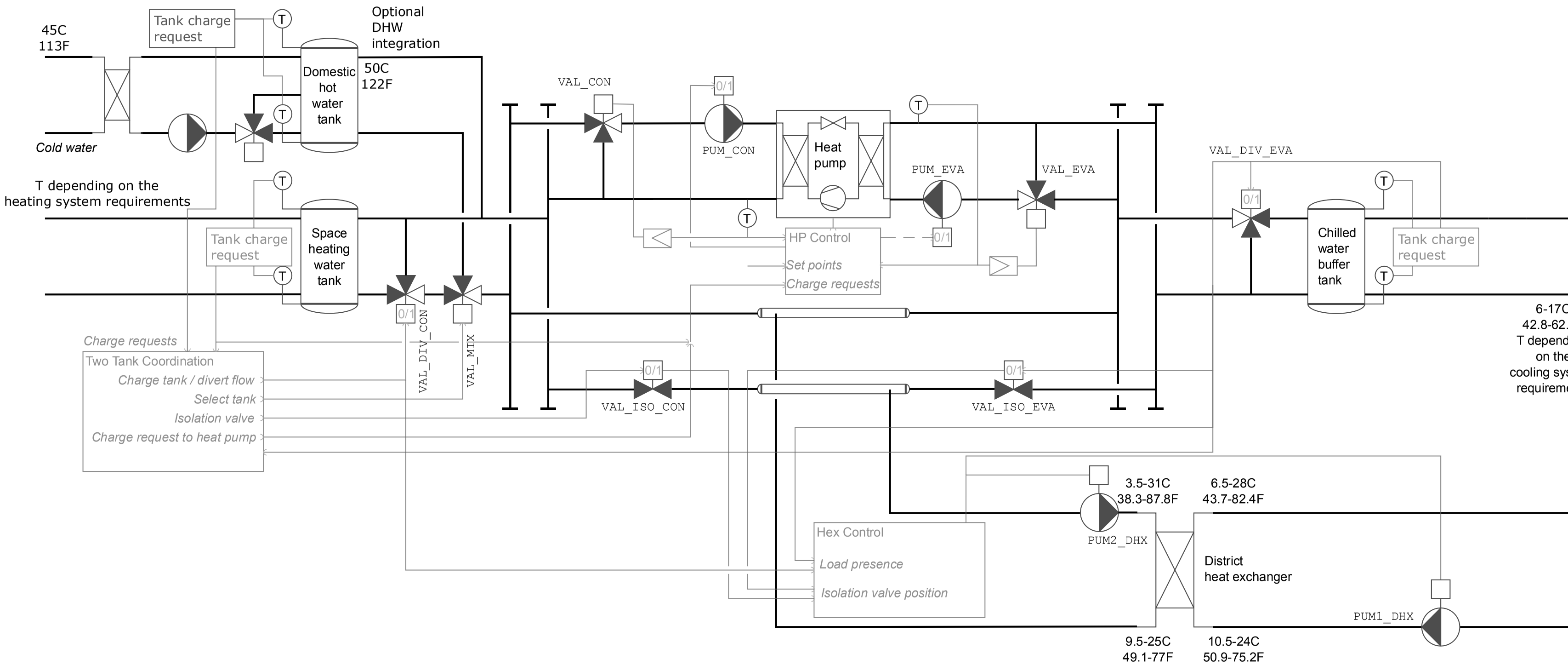

Figure 34. Schematic diagram of the ETS.

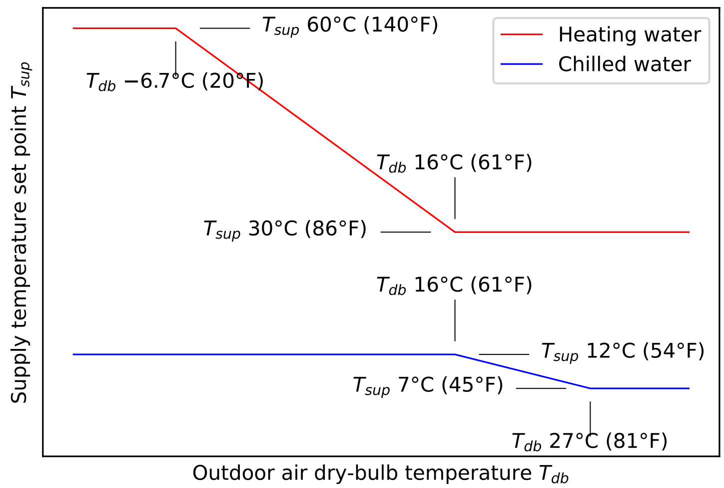

Figure 35. Heating and cooling water temperature reset schedule.

8.4.3.3 Heat Recovery Heat Pump The heat recovery heat pump can produce heating, cooling, or both simultaneously. The condenser pump `PUM_CON` and the evaporator pump `PUM_EVA` are enabled when any of the respective tanks requests charging. The heat pump is turned on 30 seconds after `PUM_CON` and `PUM_EVA` are running.

When on, the primary pumps are operated at constant speed, and the condenser (resp. evaporator) mixing valve `VAL_CON` (resp. `VAL_EVA`) are modulated with a P controller to track the set point for the water that leaves the heat pump, with a small offset to open first the valve and then ramp up the compressor speed.

The compressor speed is controlled based on the same temperature measurement as the mixing valves. Based on a moving average of the compressor speed signal for heating and cooling, the heat pump control is switched into heating or cooling dominated operation, and the respective compressor speed setpoint is sent to the heat pump.

If only heating (or only cooling) is requested from the tank, then the evaporator (or condenser) set point temperature is reset to minimize the temperature lift across the heat pump.

8.4.3.4 District Heat Exchanger The district heat exchanger hydraulically decouples the buildings system and the district system. Its primary and secondary circuits are enabled to operate if either any of the tanks request charging, and if an isolation valve `VAL_ISO_CON` or `VAL_ISO_EVA` is open. When enabled, the pumps `PUM1_DHX` and `PUM2_DHX` operate at a constant speed.

8.4.3.5 Supply Temperature Reset Fig. 35 show the heating and cooling water temperature reset schedule that are used for operating the tank and the heat recovery heat pump.

8.5 COMPONENT PERFORMANCE MODELS

8.5.1 Borefield

To simulate the borefield, we developed a new borefield model and validated it against FEFLOW simulations.

The model is a fully dynamic heat transfer model coupled to the fluid flow in the bores. The model has three main components:

- Pipe models that compute the change in temperature of the water that circulates through the wells.
- A dynamic heat transfer model in the grout, which models heat transfer and storage between the pipes and the soil.
- A dynamic model for the heat transfer in the soil that takes into account the thermal interaction of all wells. This part of the model is computed using g-functions.

The model is configured to allow operating the center and the perimeter of the borefield independent from each other, thereby allowing, for example, to use the wells in the perimeter zones for short term temperature fluctuations, while preserving the cold core for later use in summer.

For a detailed description of the model, see the model documentation of `Buildings.Fluid.Geothermal.ZonedBorefields`.

The validations are described in Section K.

8.5.2 Energy Transfer Station Heat Recovery Heat Pumps

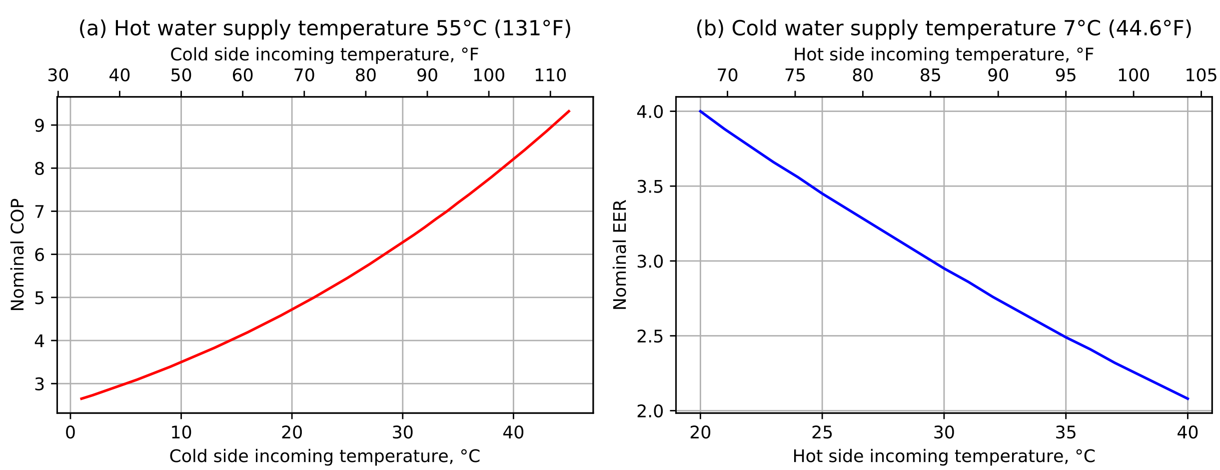

Figure 36. Performance maps of the heat recovery heat pumps.

We used a modular model developed by Wüllhorst et al. (2021) to estimate the off-nominal performance of the heat recovery heat pump. Fig. 36 shows the performance data of the heat recovery heat pump WAMAK TWW 220 WHR Heavy Duty 2L2 (`https://products.wamak.eu/`) which we used in the simulation.

For a detailed description of the model, see the model documentation of `Buildings.Fluid.HeatPumps.ModularReversible.UsersGuide`.

8.5.3 Pumps and Fans

For pumps and fans, the electrical power consumption is computed as

$$P = \frac{\dot{V}\,\Delta p}{\eta}, \tag{36}$$

where $\dot{V}$ is the volumetric flow rate, Δp is the pressure rise across the pump or fan, and $\eta = 0.7$ is pump or fan efficiency, taking into account the hydraulic and motor efficiency. Note that the pressure rise is computed based on a flow resistance calculation of the entire flow network that takes into account flow friction based on mass flow rate, actuator positions and pump or fan control signals. For a detailed description of the model, see the model documentation of `Buildings.Fluid.Movers.UsersGuide`.

8.5.4 Heat Exchangers

For the heat exchangers, we used a heat exchanger model that computes the heat transfer as

$$\dot{Q} = \epsilon\,\dot{Q}_{max}, \tag{37}$$

where $\dot{Q}_{max}$ is the maximum heat that can be transferred based on the inlet temperature difference and the minimum capacity flow rates, and ϵ is the heat transfer effectiveness, which we set to a value of around 0.9. For a detailed description of the model, see the model documentation of `Buildings.Fluid.HeatExchangers.ConstantEffectiveness` that is used for the central plant and for the DHW, and `Buildings.Fluid.HeatExchangers.PlateHeatExchangerEffectivenessNTU` that is used for the energy transfer heat exchanger.

8.5.5 Storage Tanks

For the chilled water, space heating water and DHW storage tank, we used a tank model that vertically discretizes the tank into different segments to take into account the thermal stratification. For a detailed description of the model, see the model documentation of `Buildings.Fluid.Storage.Stratified`.

8.5.6 Domestic Hot Water Preparation

For the DHW preparation, we used a fresh water station as shown in Fig. 37. The fresh water station allows to store heat in the heating rather than the domestic hot water, therefore avoiding the potential problem of Legionella bacteria getting from the hot water tank to the DHW circuit. This allows to operate the storage at a lower temperature, thereby increasing the heat pump COP. For a detailed description of the model that was used, see the model documentation of `Buildings.DHC.Loads.HotWater.StorageTankWithExternalHeatExchanger`.

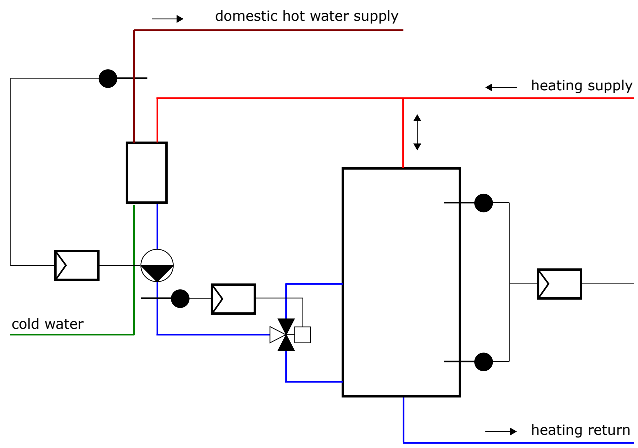

Figure 37. Schematic diagram of fresh water station.

8.6 IMPLEMENTATION OF THE SYSTEM MODEL

For the TEN, coupled to the central plant that has the borefield, and coupled to 5 ETSs, we built a Modelica system model using the Modelica Buildings Library (Wetter, Zuo, et al., 2014), version 12.1.0, and additional models that are available on `https://github.com/lbl-srg/thermal-grid-jba`, from which we used the commit c0bdb5.

This system model captures all heat flow rates in equipments such as storage tank, subsurface heat transfer and storage, heat exchangers and heat pumps. It also models the water flow rates in the whole piping network based on water or glycol pressure in the network, and these pressures are dependent on pump speeds and control valve positions, as well as on pressure drops of non-regulated resistances such as pipes, heat exchangers and heat pumps. To illustrate these models, Fig. 38 shows the model that represents the central plant, with the gray insert showing its corresponding schematic diagram. The figure shows that there is a one-to-one correspondence between equipment, pipes, valves, pumps and sensors, and how the components are connected to blocks, arranged on the top of the figure, that implement the feedback control algorithms.

For more detailed about what is represented in such a model, we refer the reader to Wetter, Zuo, et al. (2014).

The model consists of

- 16,000 components,
- 179,000 variables, of which are
- 22,500 time varying variables, and
- 965 continuous states (such as for temperatures, valve positions, pump speed, PI controllers and energy meters).

An annual simulation of the system model takes with Dymola 2025x 10 hours with the CVode solver and a tolerance of 10^{-7} on a desktop computer.

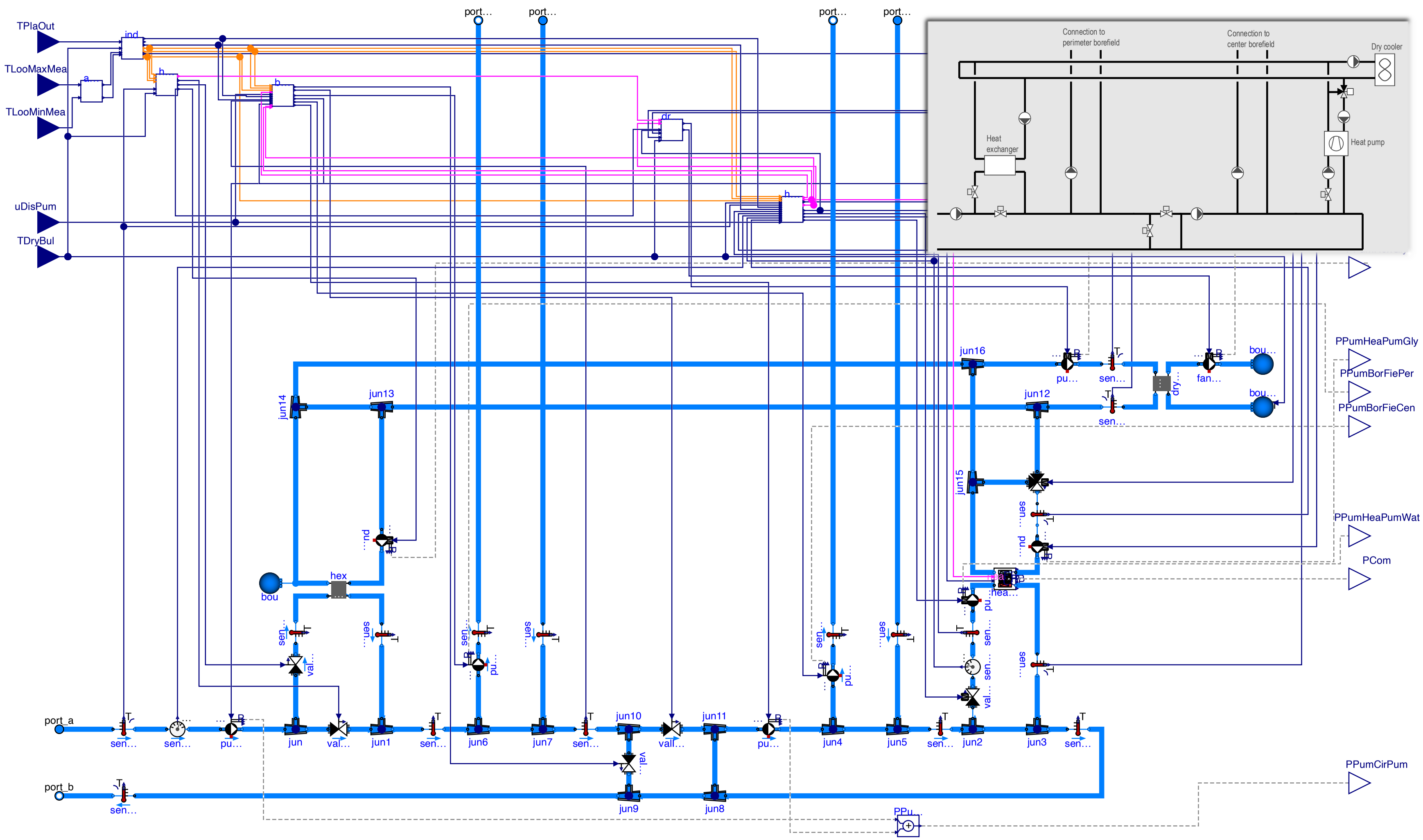

Figure 38. Schematic model view of the central plant model, which is one of the component of the whole system model. The top-right insert shows the schematic diagram of the system represented by this model.

8.7 RESULTS OF THE NONLINEAR SYSTEM SIMULATIONS

In this section, we will present the outcomes of the nonlinear system simulation conducted to validate the performance of the MILP optimization. This simulation was instrumental in derisking the design of the geothermal borefield, the energy system, and its control mechanisms. Moreover, it helped identify the design parameters that are highly sensitive to the techno-economic performance.

8.7.1 Technical Performance

We will now present the annual electricity use, the electricity as a function of time, and comment on the district loop temperatures and the central plant operation and the borefield energy.

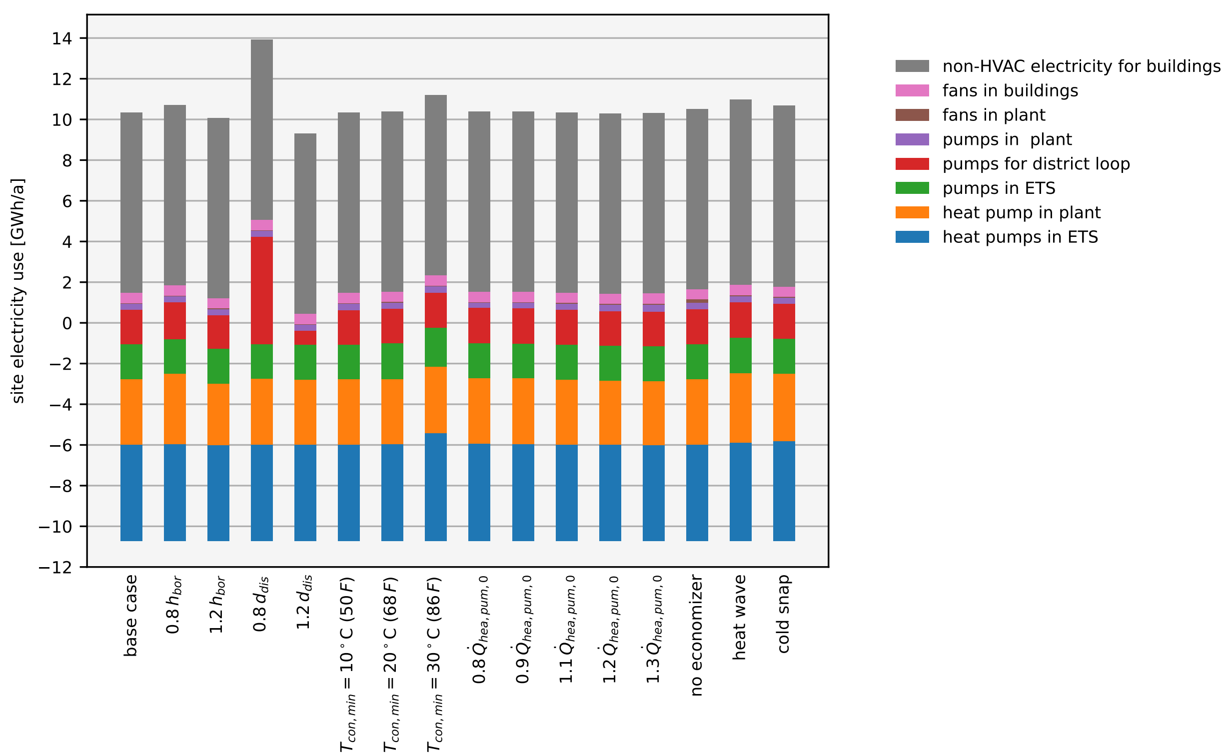

Figure 39. Energy consumption of the different components. Note that *electricity buildings* accounts for plug loads, lighting and air handler unit fan, which are all inputs to the simulation and not subject to ETS control.
The column *base case* refers to the Modelica results of the configuration *TEN+PV+Battery*. The columns with h_{bor} varied the borefield depth by ±20% (Sec. 8.7.4.6). The columns with d_{dis} varied the district loop pipe by ±20% (Sec. 8.7.4.7). The columns with $T_{con,min}$ varied the minimum condenser leaving temperature (Sec. 8.7.4.8). The columns with $\dot{Q}_{hea,pum,0}$ varied the design capacity of the central heat pump (Sec. 8.7.4.4). The column with *no economizer* removed the economizer in the central plant (Sec. 8.7.4.5), *heat wave* simulated a heat wave (Sec. 8.7.4.1), and *cold snap* simulated a cold snap (Sec. 8.7.4.2).

	Energy [GWh/a]	Specific energy [kWh/(m2 a)]
Heat pumps in ETS	4.75	42.4
Heat pumps in plant	3.22	28.8
Pumps	3.76	33.5
Fans	0.59	5.3
Non-HVAC electricity for buildings	8.85	79.1
PVs and batteries	−10.61	−94.8
Total	10.56	94.3

Table 15. Energy use of base case as shown in Fig. 39.

8.7.1.1 Annual Electricity Use Fig. 39 and Table 15 illustrate the energy contributions of the various components within the TEN. These scenarios will be further elaborated in the subsequent sections. Note that in Fig. 39, the site electricity consumption starts below zero to account for the electricity provided by the PV and battery system.

From the comparative analysis across the scenarios, it can be seen that the sizing of the district loop pipe exhibits a significant sensitivity. This observation aligns with the findings reported by Sommer et al. (2020), who also analyzed a reservoir network. Furthermore, the depth of the borefield emerges as another sensitive factor. We refer to Section 8.7.4 for a the sensitivity of the performance relative to different design parameters.

Fig. 40 shows the Sankey diagrams of all energy flows computed by the Modelica simulation. Comparing Fig. 40 with the Sankey diagram of the MILP optimization shown in Fig. 27b, shows, as expected, small differences because these are different models. The differences are small, thereby confirming that the Modelica model, which is a refinement of the MILP model, accurately represents the annual energy flows.

8.7.1.2 Electricity as a Function of Time Fig. 41a shows the total electricity use, separated into

- all electrical loads, not taking into account the PV generation and battery store,
- PV generation and battery storage, and
- electricity import from the grid, which is the difference of the above two item.

The figure shows that the PV and batteries reduce the peak electrical demand in summer from the grid by about 30%. However, there is also a short peak electricity import on day 59. Further analysis, shown in Fig. 41b, reveals that during day 59, all heat pumps in the ETS run the heat recovery heat pump at full load by setting the compressor control signal to $y_{ets,hea,pum} = 1$. ETS 2, which is the hospital with the biggest load, increases compressor speed at midnight of day 59, thereby pulling down the district loop temperature as shown through the minimum loop temperature $T_{dis,loo,min}$. This causes the heat pump in the central plant to switch to full load, shown by the compressor control signals that becomes $y_{cen,hea,pum} = 1$, and the resulting compressor electricity use $P_{cen,hea,pum}$. The other smaller ETS heat pumps also increase the compressor speed to meet their loads with a lower district loop temperature, resulting in a higher temperature lift and consequently, a higher compressor speed. From the bottom of Fig. 41b, we see that the district loop temperature is low, around 10°C to 13°C (50 F to 55 F). Therefore, if a predictive controller had been used, it could

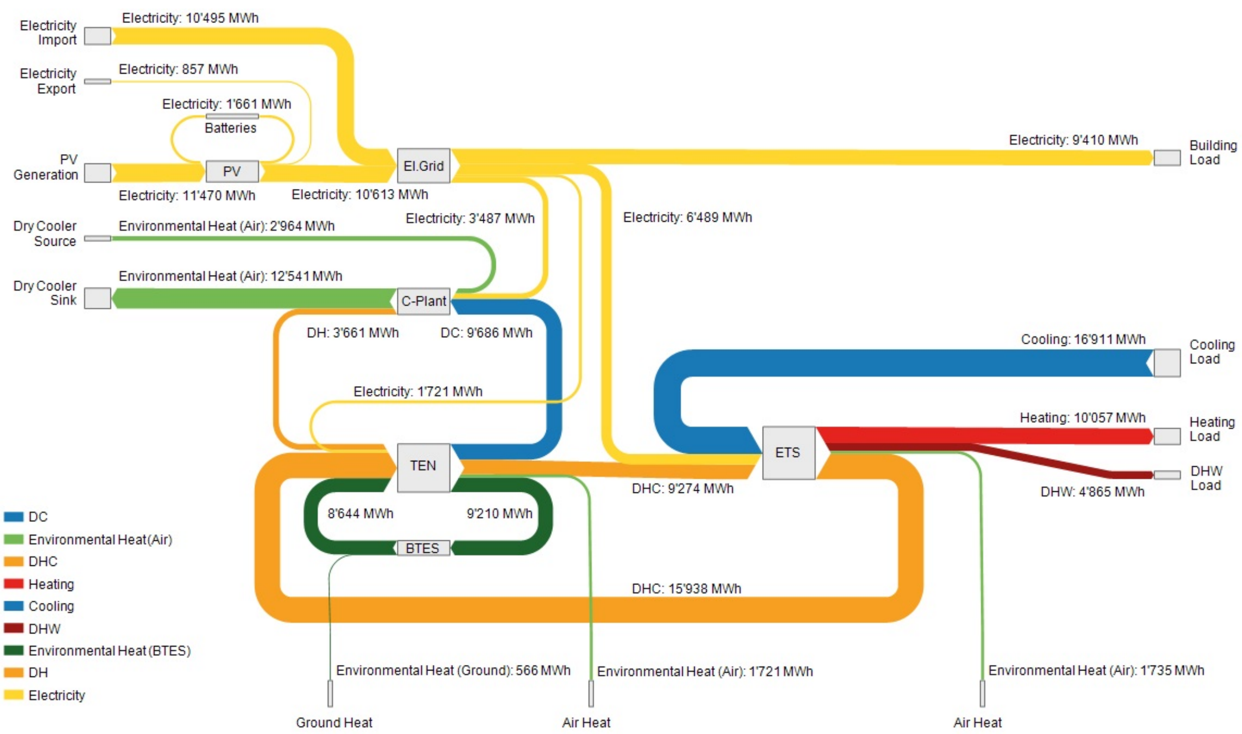

Figure 40. Sankey diagram of the system energy flow for a whole year computed by the Modelica simulation. The PV and batteries are not modelled in Modelica and the associated numbers are used directly from MILP. The PV connection node separates the batteries node from directly interacting with the electricity import and export, meaning it can only be charged by the PV.

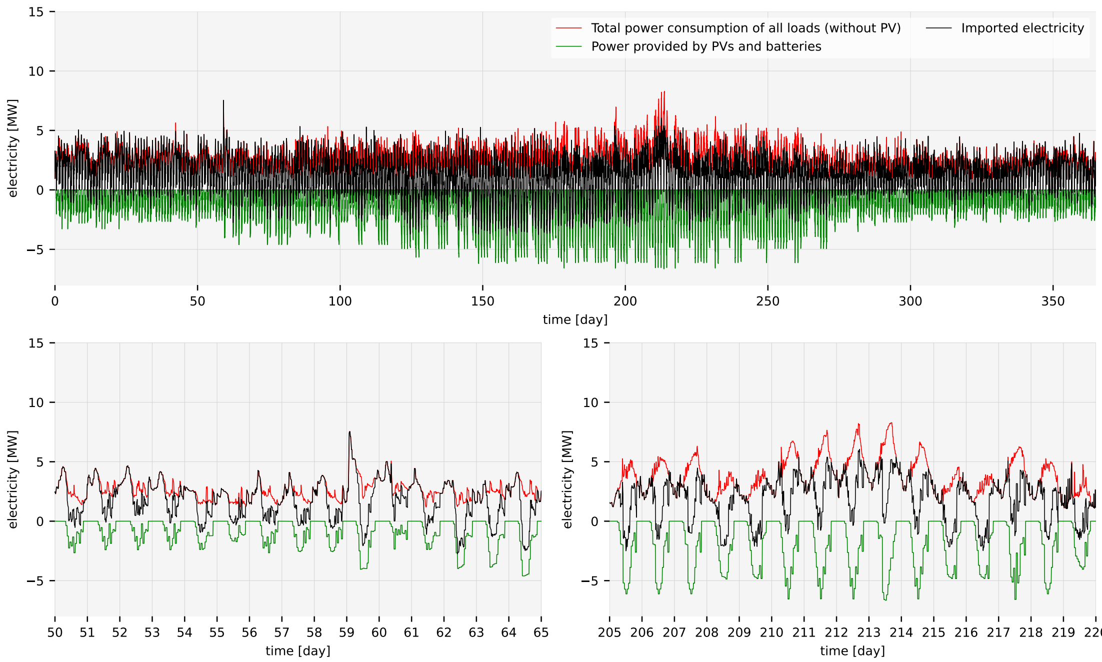

(a) Power consumption for all electrical loads, power generated by PVs, including battery storage, and power import from electrical grid. The results are averaged over each 5 minute interval.

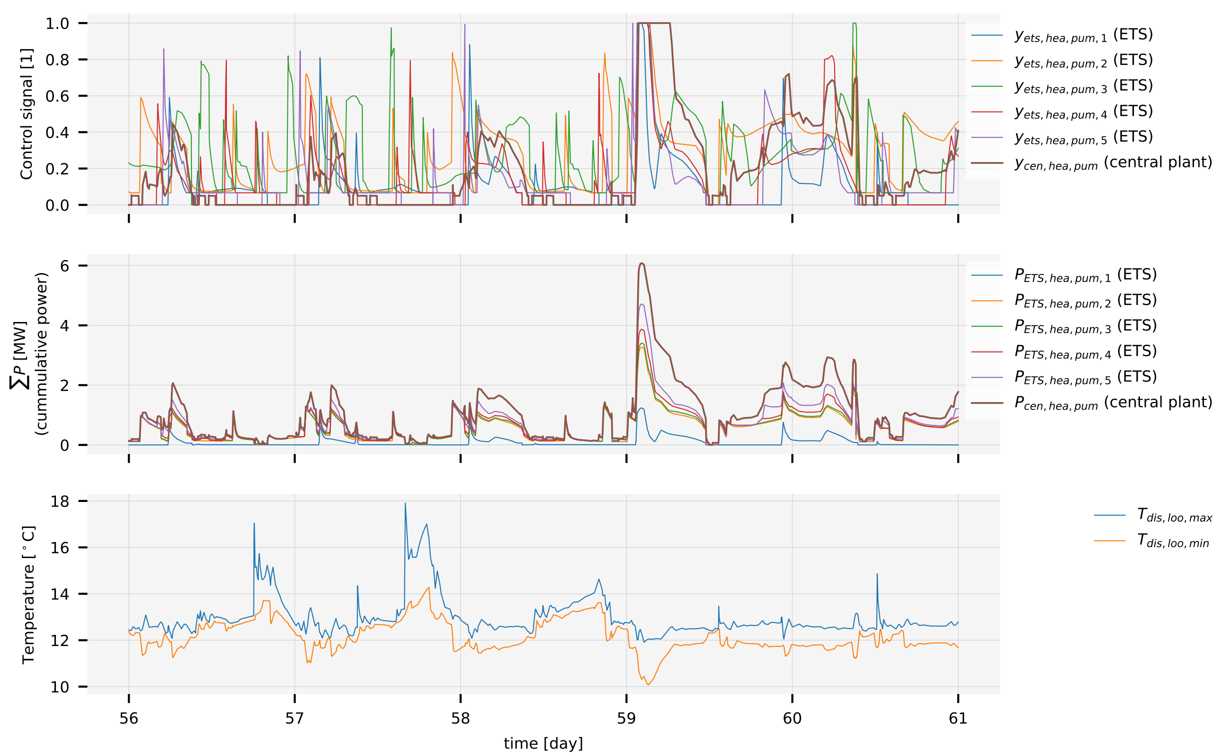

(b) Heat pump control signal, cumulative compressor power use (summed over each heat pump), and minimum and maximum loop temperature during peak power in February.

Figure 41. Analysis of electricity import.

have adjusted the district loop temperature up before this high load event, preventing the cascading ramping up of heat pump loads that leads to a high peak demand.

We therefore recommend considering a predictive controller, especially if the site negotiates a peak power price with the electricity provider. Such a predictive controller could optimize setpoints that manage daily and seasonal operation.

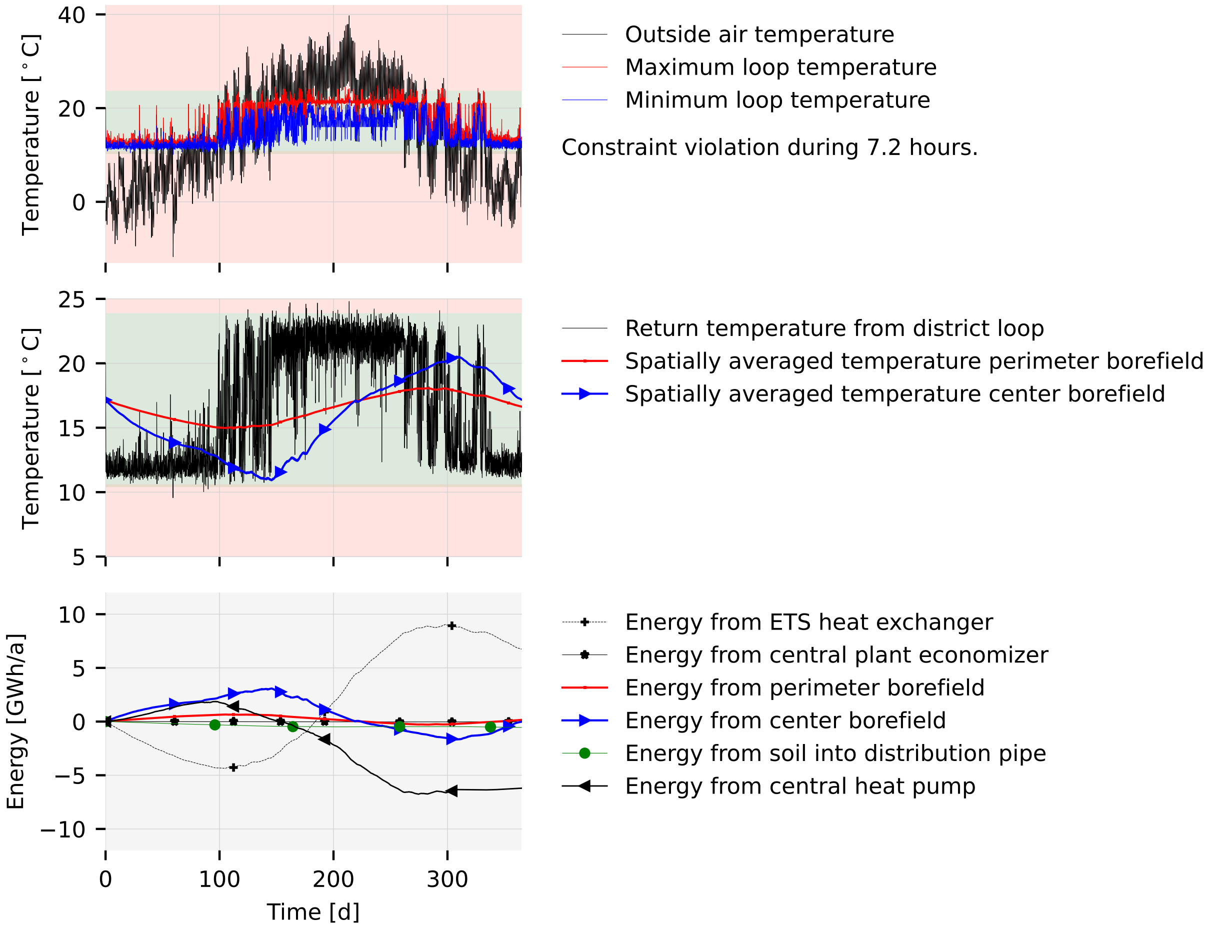

Figure 42. District loop minimum and maximum temperature and exchange of energy with the district loop. The top figure shows the temperatures, with regions beyond the design limits shown in red. The displayed soil temperature is a fictitious average soil temperature computed using (23). The bottom figure shows the energy exchanged with the district loop.

8.7.1.3 District Loop Temperatures The top plot of Fig. 42 shows that the minimum and maximum district loop temperatures upstream from the ETSs are within the allowed range for most hours of the year, with the allowed range indicated by the green background.

The middle plot shows the temperature that enters the central plant. This temperature is allowed to be outside the minimum and maximum loop temperatures as it is not a design criteria for the ETSs, and forcing it to be inside this range would require more energy and higher peak capacity. The figure also compares this temperature to the fictitious average soil temperature computed using (23).

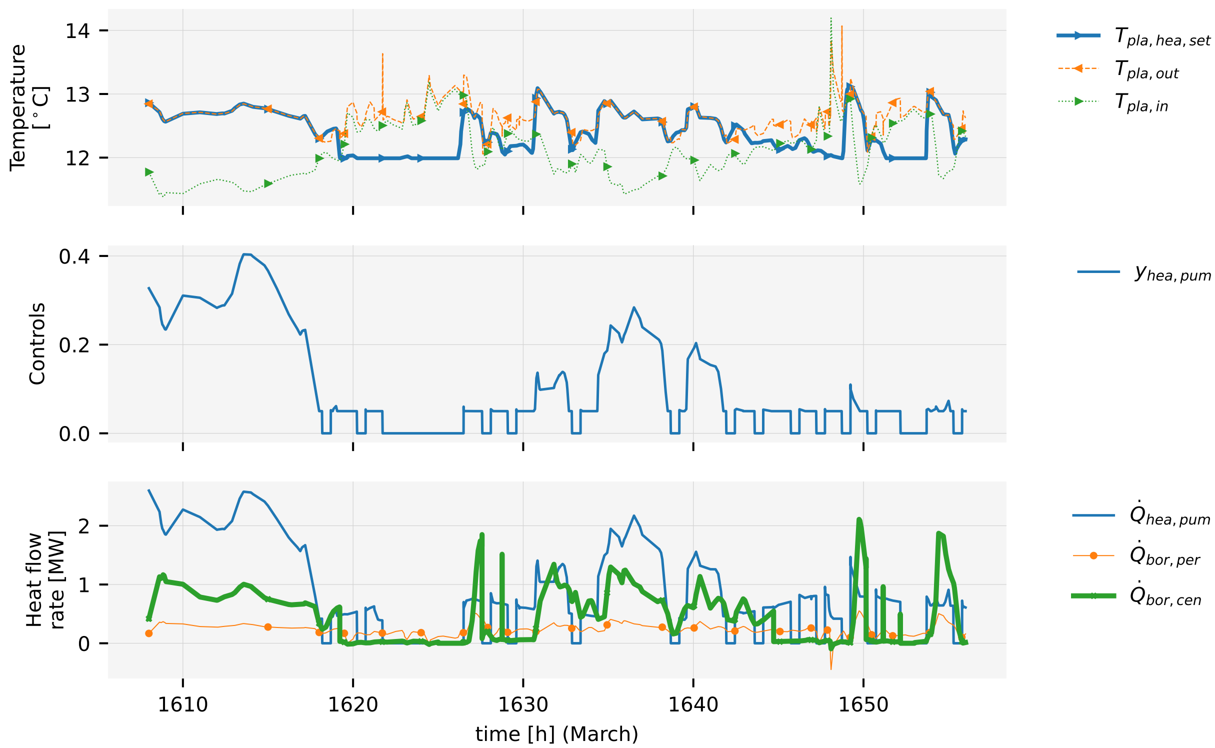

Figure 43. Operation of the central plant in spring.

While ultimately the temperature difference between grout and water determines the heat transfer rate, the grout temperature is coupled to the soil temperature, which is here represented through the fictitious average soil temperature. Comparing these temperatures highlights the dynamics that underlies the borefield heat transfer, which ultimately gives a wide range of heat extraction rates as also discussed in Section 8.7.1.5.

Comparing the energy trajectories in the bottom plot shows that most of the energy from the ETS heat exchanger is provided by the central plant heat pump and the center borefield. The perimeter borefield plays a minor role, and the energy from the central plant economizer is practically zero.

8.7.1.4 Central Plant Operation Fig. 43 shows the dynamic operation of the borefield and the heat pump, clearly illustrating that assessing the borefield performance requires a coupled simulation of the borefield, the energy system and the control. The top of the figure shows the heating temperature setpoint for the central plant leaving temperature $T_{pla,hea,set}$. This setpoint is well tracked as its comparison with the plant outlet temperature $T_{pla,out}$ shows.[15] There is only a small violation during which $T_{pla,hea,set} > T_{pla,out}$ after the heat pump switched off, because then, the controller keeps the heat pump off for a minimum time to protect the compressor. Between $t \in [1610,\ 1618]$ hours, and $t \in [1631,\ 1642]$ hours, the heat pump is modulating, whereas at other times it is off or it operates at its minimum capacity. As expected the heat pump control signal $y_{hea,pum}$ and its capacity $\dot{Q}_{hea,pum}$ is highest if the plant inlet temperature $T_{pla,in}$ is low. Similarly, during these times, the center borefield provides the most capacity, with $\dot{Q}_{bor,cen}$ around 1 MW,

[15] Note that a higher temperature is allowed if equipment operates at the minimum capacity.

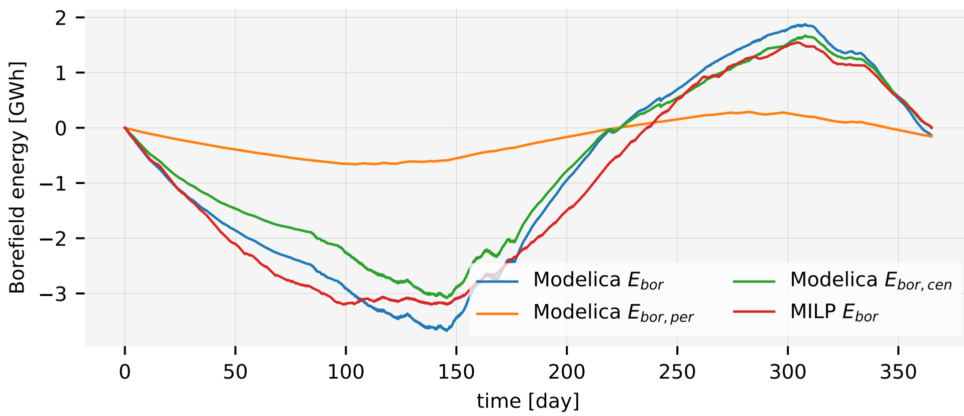

Figure 44. Energy stored in borefield for Modelica simulation and MILP optimization.

whereas at other times its capacity is around 0 to 0.5 MW only. The perimeter borefield has less fluctuation. Clearly, such a dynamic operation requires a simulation, analysis and verification that takes the coupling of the borefield, the energy system and the control into account.

8.7.1.5 Borefield Energy Fig. 44 shows the energy stored in the borefield for the Modelica simulation and the MILP optimization. The total energy E_{bor} is balanced, i.e., its value is almost the same at the start and end of the year. The rule-based controller of Modelica discharges the center of the borefield earlier and faster than the optimal charging trajectory computed by the MILP optimization, which has perfect knowledge of the whole year's energy consumption and therefore is expected to have more optimal borefield utilization. Compared the the borefield perimeter, the center of the borefield has more pronounced charge and discharge cycles, because it is actively cooled in spring and heated in fall, whereas the perimeter borefield mass flow rate is always on to add thermal inertia to the TEN.

The bottom plot of Fig. 43 shows the variation of the perimeter and center borefield heat extraction rate $\dot{Q}_{bor,per}$ and $\dot{Q}_{bor,cen}$, and Fig. 45 shows the frequency distribution of the specific heat flow rates per meter of bore for the center and the perimeter borefields. The center borefield is actively cooled in spring and heated in fall with the reversible heat pump. This leads to specific heat flow rates rates of around 40 W/m. However, discharge rates in winter and summer are only about half of that amount and seldom exceed 20 W/m, which can be explained by the small temperature difference between borefield and district loop. For the perimeter borefield, which directly obtains water from the district loop temperature (or the seldom operating economizer), heat flow rates are typically well below 20 W/m and often only around 10 W/m.

The above discussion shows strong variations which are caused by the dynamic change in loop and central plant temperatures across days and seasons. These temperature changes are caused by thermal and mass flow coupling of the buildings, district loop and the central plant, which is evolving not only based on loads, but also based on how the control strategy is programmed to operate generation, storage and mass flow rates based on these temperatures. **This strong coupling and dynamic evolution makes clear that a proper design of a TEN and its borefield, the system analysis and verification requires a coupled subsurface, energy system and controls simulation.**

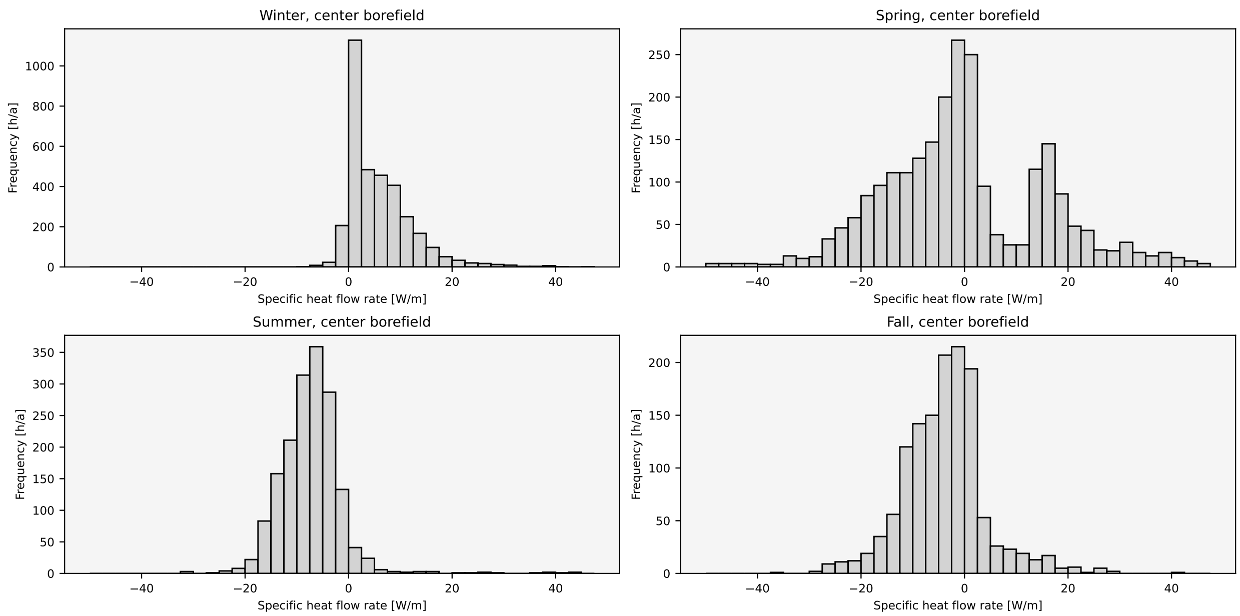

(a) Center borefield.

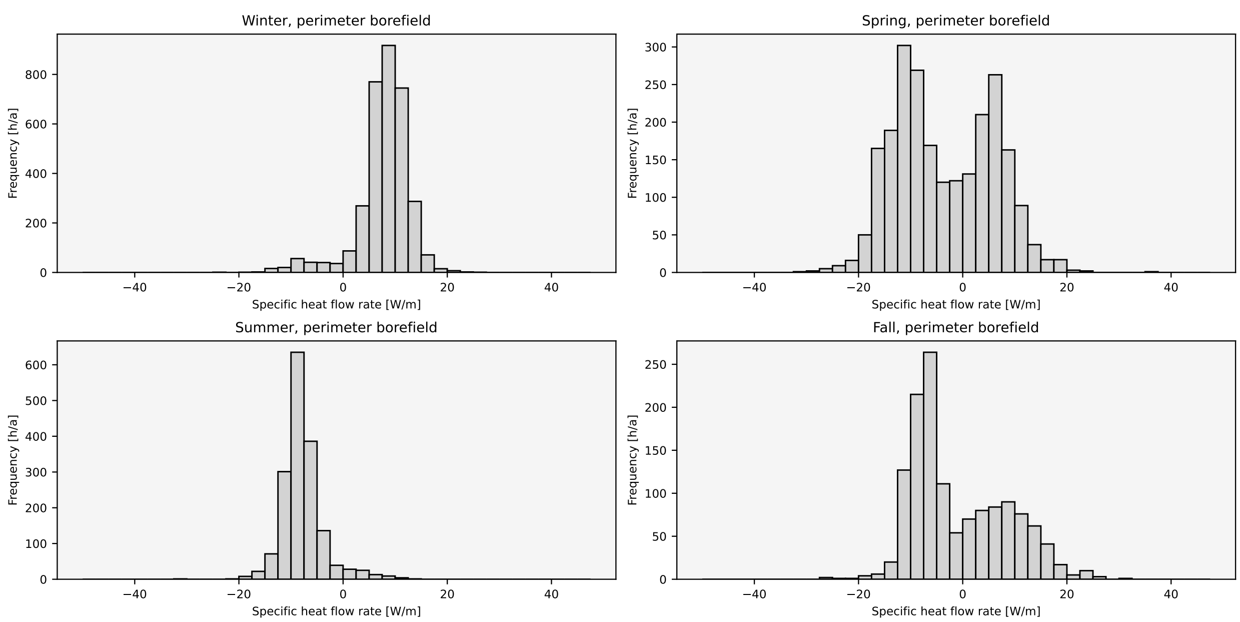

(b) Perimeter borefield.

Figure 45. Specific heat flow rate distribution for center and perimeter borefields for the four seasons.

8.7.2 Economic Performance

In this section we discuss the economic performance as computed using the Modelica model. Note that, as was also the case for the MILP optimizations in Section 7.0, we assume the ECMs discussed in Section 5.3.7 are already implemented and paid for, and hence their costs are not part of the economic calculations in this section.[16]

		MILP Gas	MILP TEN+PV+Battery	Modelica
Imported energy	[GWh/a]	40.9	12	10.6
		100%	29.3%	25.8%
Imported energy cost	[million $/a]	4.61	1.74	1.55
		100%	37.8%	33.7%
Annualized life-cycle cost	[million $/a]	7.82	8.94	8.31
		100%	114.3%	106.3%
Investment	[million $/a]	39.3	102	96
		100%	259.7%	244.4%
Levelized cost of thermal energy	[$/kWh]	0.203	0.238	0.21
		100%	117.4%	103.2%

Table 16. Comparison of economic performance metrics. The MILP baseline is the Gas solution described in Section 7.6.2 and the MILP TEN+PV+Battery solution and the Modelica model is the configuration described in Section 7.6.4.

Table 16 compares key economic metrics of the Modelica model with MILP results. In the Modelica platform, the investment is slightly lower than in the MILP platform. While the two platforms used identical sizing methods for the building ETSs, the sizing of the central plant was refined in Modelica, leading to slightly lower investment costs. Appendix H shows that the temperature-dependent heat pump models used in the Modelica simulations resulted in higher COP values than the time-averaged COP values used in the MILP optimization, in particular for ETS cooling. This reduced cost in energy import.

Note that the MILP platform and the Modelica platform both had to combine some buildings to reduce the number of energy hubs in the model to keep the computations tractable. The MILP platform used fourteen energy hubs and the Modelica platfrom used five. As a result, the ETS part of the system cannot be directly compared in this economic analysis. But since the two platforms used identical sizing methods for the ETS, their costs are the same. The central plant, the district pump, and the cost of energy import are the parts that were computed separately based on the different sizing used in the MILP and the Modelica platforms.

[16] The cost of the ECM is separately summarized in Appendix D.

8.7.3 Verification Against Requirements

We verified the base case for conformance against the requirements outlined in Section 8.1. To our knowledge, this is the first time an energy system model of this size has been verified formally against such stringent operational requirements.

During the verification process, we identified several improvements to the control sequence. These improvements include:

- Avoiding fast changes in compressor speeds: Initial simulations had fast changes in compressor speed. This caused rapid fluctuations in mixing temperatures in the district loop, which the central plant controller had to compensate for, causing control challenges when the loop temperature was near its lower or upper limit. Such fast changes are now avoided through improved set point changes and the use of rate limiters, both improving operational quality.
- Improved startup behavior of ETS heat recovery heat pumps: The sequencing of the ETS heat recovery heat pump valves and the compressor speed has been refactored, leading to better set point tracking of the loads, and longer heat pump operation times.
- Improved cascading of temperature set points: This improvement involves better cascading of set points from heating (cooling) loads to the heat pump temperature condenser and evaporator valve control, as well as the compressor speed. This results in fewer heat pump cycles, which is beneficial for increasing efficiency and compressor durability.
- Improvements to the central plant control: These improvements involve pre-cooling the center borefield before peak summer, thereby increasing its capacity and reducing the risk of exceeding district loop temperatures set points.

However, certain requirements, such as tracking set points at all times, are occasionally violated during short periods after operation mode changes. We consider these violations to be not problematic. In future work, we recommend revisiting the requirement verification and potentially formulating requirements in a way that allows for occasional minor violations if they do not negatively impact operation. This approach seems more pragmatic compared to over-engineering the system to ensure that requirements are met at all times, which would lead to higher costs and likely increased energy use.

The TEN meets the high level requirements for all but one of the criteria defined in Section 8.1 as shown in Table 17.

Criteria	Success
Imported energy reduced by at least 50% compared to baseline.	✓ (-74%)
Life-cycle cost no more than 120% of the baseline.	✓ (106%)
Investment cost no more than 200% of baseline.	✗ (244%)
Investment cost no more than 110% of baseline if central plant infrastructure, district loops, and utility-scale PV and battery systems are privatized.	✓ (100%) [17]
Levelized cost of energy for heating and cooling no more than 0.25 USD/kWh.	✓ ($0.210/kWh)
Generation capacity no higher than in the MILP platform for the *TEN+PV+Battery* configuration.	✓ (87%)
Storage capacity no higher than in the MILP platform for the *TEN+PV+Battery* configuration.	✓ (79%)
Energy cost no more than 110% of the MILP platform for the *TEN+PV+Battery* configuration.	✓ (89%)
Imported annual energy no more than 110% of the MILP platform for the *TEN+PV+Battery* configuration.	✓ (88%)
The energy demands, which includes space heating, space cooling, domestic hot water and electricity for auxiliary purposes must be matched.	✓

Table 17. Success in meeting the requirements for the selected solution. By baseline, we mean the Gas solution computed by the MILP platform.

[17] The two platforms have the same investment cost for these assets. See explanation in Section 8.7.2.

8.7.4 Sensitivity Analysis (Reliability)

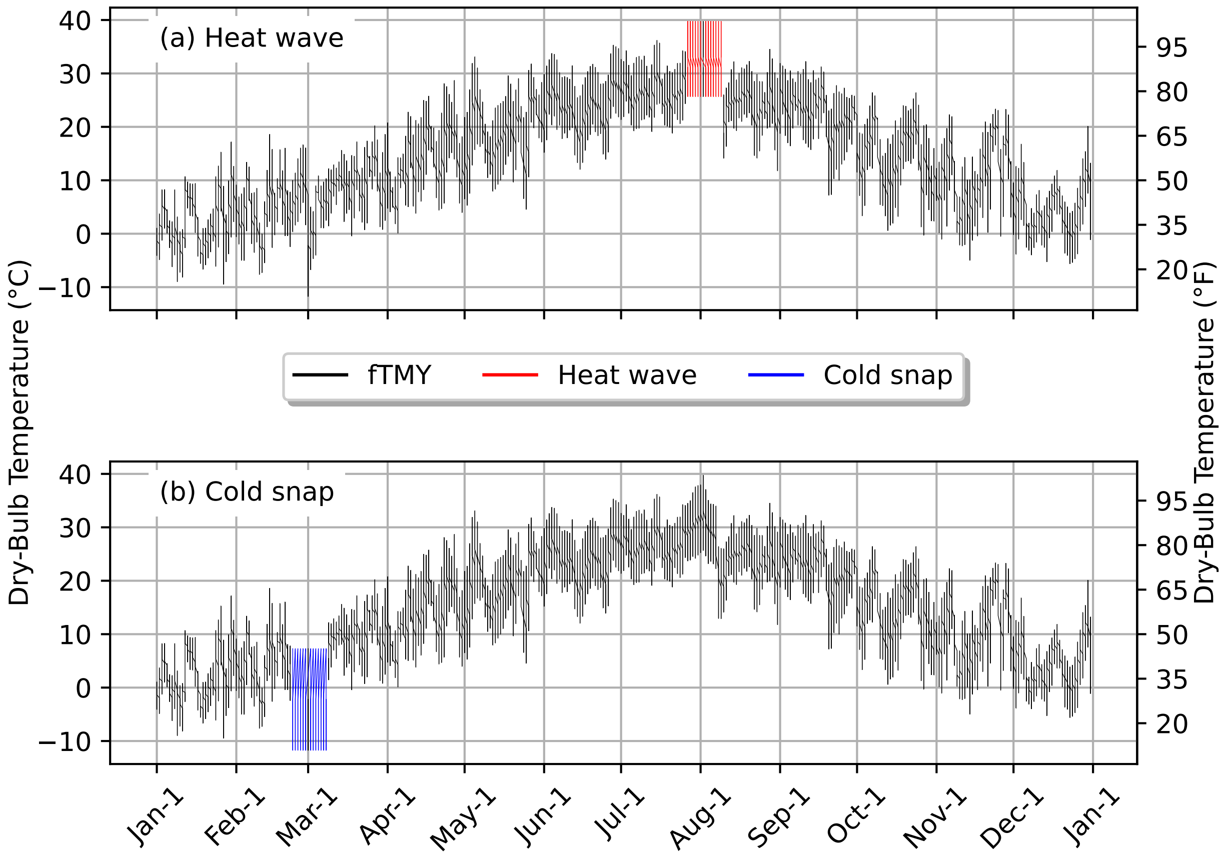

Figure 46. Extreme weather scenarios: (a) the hottest day is August 2nd with a maximum dry-bulb temperature of 39.7°C (104°F) **which is copied to replace two weeks of weather data from July 27th to August 9th, inclusive; (b) the coldest day is March 1st with a minimum dry-bulb temperature of** −11.7°C (10.9°F) **which is copied to replace two weeks of weather data from February 23rd to March 8th, inclusive.**

8.7.4.1 Load Increase During a 14-day Heat Wave In this section we analyze how the system performs under a simulated heat wave. We compare the *TEN+PV+Battery* solution against the *AW HP* solution because the *Gas* baseline also uses an air-sourced chiller, and hence has the same performance.[18]

Figure 46(a) shows how a heat wave is simulated by repeating the hottest day for a 14-day period from the original weather file. We computed the average COP when the heat pump is producing cooling as

$$COP = \frac{\int \dot{Q}_{con,coo} \, dt}{\int P_{coo} \, dt}, \tag{38}$$

[18]Using the *AW HP* solution here allows using the same system in Section 8.7.4.2 for a cold snap.

where the heat pump condenser output $\dot{Q}_{con,coo}$ and the compressor power P_{coo} is

$$\dot{Q}_{con,coo} = \begin{cases} \dot{Q}_{con}, & \text{if heat pump produces cooling,} \\ 0, & \text{otherwise,} \end{cases} \tag{39a}$$

$$P_{coo} = \begin{cases} P, & \text{if heat pump produces cooling,} \\ 0, & \text{otherwise.} \end{cases} \tag{39b}$$

		Baseline	*Heat wave*		
End-use cooling load	[MWh]	1,919	2,571	*+652*	*+34%*
	[MMBTU]	6,548	8,774	*+2,226*	
TEN+PV+Battery system					
Electric power consumed	[MWh]	769	1,123	*+354*	*+46%*
Average cooling COP	[-]	6.01	5.75		
AW HP system					
Electric power consumed	[MWh]	2,163	3,148	*+985*	*+46%*
Average cooling COP	[-]	4.45	4.08		

Table 18. Comparison between the 14-day baseline under the fTMY weather and the heat wave. The computed electric power includes the consumption by the compressors, circulation pumps, and fans for the dry cooler. The average COP is computed only when the heat pump is producing cooling.

Table 18 shows that during this 14-day period, both cooling load and electricity use increased significantly. Under the baseline operation, the ETS heat pump in the TEN system already had higher COPs compared to the air-to-water heat pump in the AW HP system described in Section 7.6.2. During the heat wave, the TEN system heat pumps also suffered from less COP degradation. When considering all auxiliary electricity consumption serving the thermal loads, the AW HP consumed approximated three times as much energy as did the TEN system.

In summary, during the heat wave, the TEN system is more resilient than the AW HP system, and it requires three times less electricity. This is significant as the electrical grid supply is typically less reliable during a heat wave, and hence provisioning of on-site backup power may be required for continuous operations.

8.7.4.2 Load Increase During a 14-day Cold Snap In this section we analyze how the system performs under a simulated cold snap. For the cold snap, comparing the *TEN+PV+Battery* against the *AW HP* solution allows to see the impact of the geothermal coupled TEN, and it allows comparing the same energy carrier.[19]

[19] To compare the *Gas* solution versus the *TEN+PV+Battery* solution for the cold snap, one could compare the "End-use heating load", divide it by the efficiency of the gas boiler, and compare this to the electric power consumed by the *TEN+PV+Battery* solution.

Figure 46(b) shows how a cold snap is simulated by repeating the coldest day for a 14-day period from the original weather file. The average COP is computed in a similar as described in Equation 38 but for when the heat pump is producing heating.

		Baseline	*Cold snap*		
End-use heating load	[MWh]	686	1,096	*+411*	*+60%*
	[MMBTU]	2,340	3,741	*+1,401*	
TEN+PV+Battery system					
Electric power consumed	[MWh]	527	819	*+291*	*+55%*
Average heating COP	[-]	4.31	3.41		
AW HP system					
Electric power consumed	[MWh]	644	1,164	*+520*	*+81%*
Average heating COP	[-]	4.27	3.02		

Table 19. Comparison between the 14-day baseline under the fTMY weather and the cold snap. The computed electric power includes the consumption by the compressors, circulation pumps, and fans for the dry cooler. The average COP is computed only when the heat pump is producing heating.

Table 19 shows that during this 14-day period, both space heating load and total electricity use increased significantly. The heat pumps in both systems suffered from significant COP degradation during the cold snap, but those of the AW HP system described in Section 7.6.2 had a larger COP drop. In the overall system, the electricity consumption of the TEN system increased by a significantly smaller ratio.

Therefore, the TEN system is more resilient than the AW HP system during a cold snap.

8.7.4.3 Requirements for Backup Power In this section we analyze how the system performs in serving critical thermal loads after a power outage. The simulated power outage lasts 7 days after the coldest day and after the hottest day in the fTMY weather file. During this time, the critical thermal load that is to be served is assumed to be 50% of the original load.

		TEN System	AW HP System		
Required backup power					
After the coldest day	[MWh]	194	222	*+28*	*+14%*
After the hottest day	[MWh]	178	527	*+349*	*+196%*

Table 20. Comparison between the TEN system and the AW HP system of backup power needed to serve critical thermal loads for a 7-day power outage. The required backup power includes all electricity required for the compressors, circulation pumps, and fans for the dry cooler.

Table 20 compares the amount of backup electricity required to serve the critical load. After the cold snap, the AW HP system requires moderately more energy to maintain the critical thermal load compared to the TEN system. Meanwhile, after a heat wave, the AW HP system as we described in Section 7.6.2 requires substantially more electricity backup compared to the TEN system.

With this analysis, we find that the TEN system is is more resilient than the AW HP system in the event of a power outage after a heat wave or a cold snap as it requires substantially less backup electricity.

One may also ask how a gas boiler with air source chiller compares for backup energy provision to the other options listed in Table 20. During summer, the backup electricity needed is as shown for the AW HP system, e.g., 527 MWh. In winter, there would also need to be sufficient gas storage (in case the gas supply is interrupted). Hence, backup power would need to be provided for two energy carriers, electricity and gas. In comparison, the TEN solution requires 194 MWh backup electricity, and hence is favorable to the gas boiler with air source chiller as well.

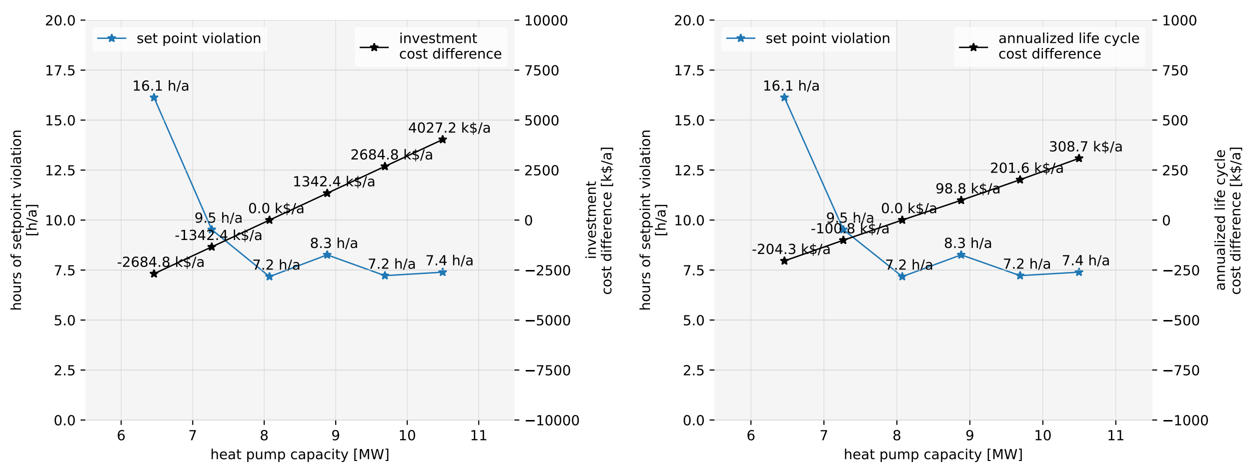

(a) Investment cost difference. **(b) Annual life cycle cost difference.**

Figure 47. Number of hours of set point violation, and differences in investment cost and annual life cycle cost relative to base case, as a function of the central heat pump capacity.

8.7.4.4 Central Plant Heat Pump Fig. 47 shows the impact of changing the central heat pump capacity on the hours that the minimum or maximum loop temperature is violated, and the impact on the difference in investment costs and annual life cycle costs relative to the base case. The figure shows the following points:

1. Increasing the heat pump capacity has no benefit on the loop temperature violation as a size above 8 MW, which is the base case, does not markably change the hours when the set point is violated.
2. Reducing the size of the heat pump leads to a moderate number of hours during which the minimum and maximum loop temperature is violated. However, downsizing the central plant heat pump would reduce investment cost by $1 million to $2.7 million, at reduced annual life cycle costs of around $100,000 to $200,000, based on the cost estimate of Table 6.

On may ask why increasing the heat pump size does not drive the number of hours of setpoint violation to zero. Inspection of the simulations showed that some violation occur due to the dynamic of the district loop, the central plant and the control logic. For example, in the base case, at full pump speed, the flow velocity in the district loop is 3.42 m/s(11.23 ft/s). As the district loop is 3500 m long, it takes around 15 min for water to circulate around the loop. As such transport delay can cause control instability if the controller reacts too fast, the transport delay together with the dynamic of the feedback control causes some overshoot before the central plant compensates for the high load. Use of a predictive or a feedforward controller could alleviate this problem.

This illustrates that through dynamic simulation, the effect of different equipment sizing on key performance indices can be evaluated, which in this case shows that relaxing the requirement can substantially reduce investment and annual life cycle costs.

In view of this cost sensitivity, we recommend considering a performance contract that allows violating the temperature constraints during a certain number of hours.

8.7.4.5 Central Plant Economizer Fig. 39 shows that there is insignificant energy contribution from the central plant economizer, which was added to increase system efficiency. However, the Modelica simulations showed that it only contributed around 0.06 GWh/a of cooling and 0.02 GWh/a of heating. This is only around 0.4% of the imported electricity and if that heat were to be provided instead by the installed heat pump, and assuming a COP of 5, it impacts on annual electricity use is below 0.1%.

Moreover, its presence does not allow downsizing the heat pump, as it did not operate during the peak load. The outdoor air and district loop water temperatures entering the central plant did not allow for its operation around peak heating or cooling conditions.

Therefore, we recommend to not install the central plant economizer to reduce costs and improve system simplicity.

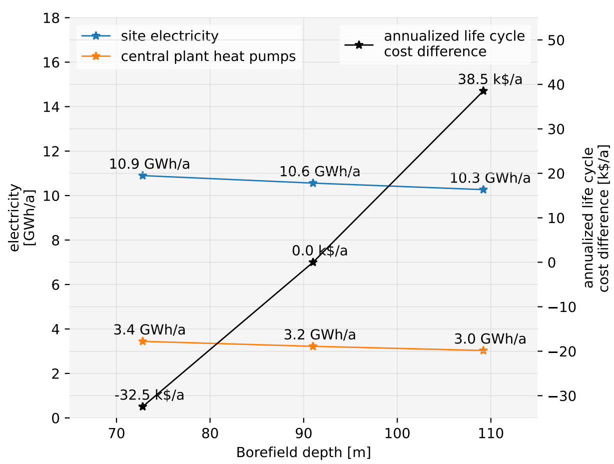

Figure 48. Energy use and change in annualized life cycle cost as a function of the borefield depth.

8.7.4.6 Borefield Depth Fig. 48 shows the sensitivity of the electricity use and the difference in annual life cycle cost if the length of the bores in the borefield is decreased and increased by

20% from their original length, which is 91 m (299 ft). This calculation is based on a unit cost of borefield installation, normalized by the length of the bore, of $42\$/m$ (Liu et al., 2018).

Based on this cost sensitivity, we recommend during detailed design to revisit the borefield design for cost-optimality, evaluated with a coupled simulation of the subsurface, the energy system and the feedback control.

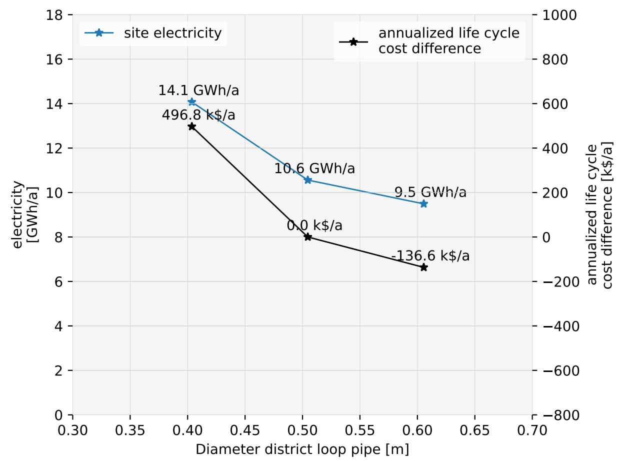

Figure 49. Energy use and change in annualized life cycle cost as a function of the district loop pipe diameter.

8.7.4.7 District Loop Pipe Sizing We will now show that decreasing the district loop pipe diameter by 20% increases the annual life cycle costs by \$0.50 million. As shown in Fig. 49 and in Fig. 39, the pump electricity use significantly contributes to the energy consumption. The pipe sizing for the base case is done to maintain a design pressure drop of 125 Pa/m. This results in a district loop pipe diameter of 0.50 m(1.66 ft). Decreasing it to 0.40 m(1.32 ft) increases energy use by 33%, with an associated increase in annual energy costs of \$0.52 million. Based on Sommer et al. (2020), the reduced pipe diameter allows investment cost savings of around 140 \$/m (42 \$/ft) per length of trench for the distribution pipe. Taking into account the reduced investment costs of the smaller pipes, the increase in annual life cycle cost due to smaller pipes would be around $\$500,000$. Conversely, increasing the district loop pipe by 20% reduces annual life cycle cost by around $\$135,000$.

Note that these calculation are based on an annual Modelica simulation and therefore take into account the dynamic control of the distribution pipe that aims to reduce pump energy when the district loop temperatures allow.

We therefore recommend to optimize the district loop sizing further once the building loads are better understood, as an increase in the district pipe diameter of 20% reduces annual life cycle costs by around $135,000.

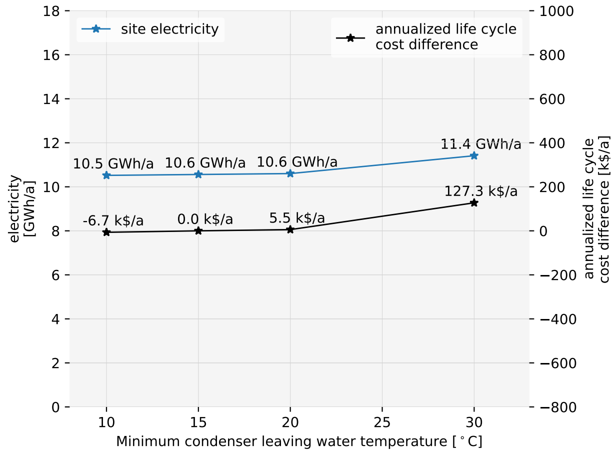

Figure 50. Energy use and change in annualized life cycle cost as a function of minimum condenser leaving temperature.

8.7.4.8 Minimum Condenser Leaving Water Temperature Fig. 50 shows the importance of reducing the minimum condenser leaving water temperature of the heat recovery heat pumps in the ETSs. Setting a too high limit of $T_{con,lvg,min}$ = 30°C (86 F) increases annual life cycle costs by around \$127, 000.

Due to the sensitivities to control settings, and because field studies have shown that control resets are often not properly applied (Crowe et al., 2020; Fumagalli et al., 2017; Raftery et al., 2024), we recommend using an Energy Management Information System that ensures sustained proper operation.

9.0 DISCUSSIONS

To retrofit the 500 DoD installations, with 300,000 buildings, at a 25 year retrofit cycle, the posing problem is to retrofit every month 1 to 2 installations with an average of 1,000 buildings each. With the PBD process, we provided a first demonstration of a process that is promising to enable data-driven sequential decision-making and derisking of system integration. For JBA, this process led to a 74% reduction of energy use, 45% reduction of peak electricity use through a geothermal coupled TEN. The reductions, compared to a base case with gas heating and air-source chiller, increase reliability and resilience to energy supply chain disruptions and extreme weather, at an increase in life cycle costs of 6%.

The PBD process allowed systematic capturing and verification of requirements, ranging from requirements from site personal to detailed engineering requirements for the energy and control system. It allowed a comprehensive design space exploration that would not have been possible had we only done a simulation-based analysis. The subsequent verification through nonlinear dynamic simulation of the geothermal system, the energy system and the controls was critically important to improve assumptions of the optimization and to correct design shortcomings in the mechanical system and the control sequences. Specifically, as part of the design verification, we made structural changes to the mechanical configuration of the ETS and the central plant, and changes to the control sequences. The coupled simulations pointed us toward these shortcomings, which were not apparent based on our design documentation. The coupled simulations also identified further optimization potential, and it enabled sensitivity analysis including the dynamic verification of component sizing. Sensitivities range in the order of a few hundred thousands of dollars in annual life cycle costs, and hence million dollars in costs over the system life cycle. Also, investment cost sensitivities are in the range of a few million dollars. These savings alone, without accounting for the previously mentioned design changes that we identified in simulation and which would have been expensive to correct in operation, warrant investment in a design process as presented here.

We also like to illustrate the importance of using a coupled simulation based on our insights about the borefield performance: In Section 8.7.1.5, we saw strong variations in geothermal heat flow rate across days and seasons. These variations are caused by thermal and mass flow coupling of the buildings, district loop and the central plant, which are evolving not only based on loads, but also on the how the control strategy is programmed to operate storage, heat pumps, valves and circulation pumps based on these temperatures.

MILP does not have the physics to represent this behavior. Consequently, in earlier MILP optimizations, we significantly overestimated the heat extraction rates of the borefield, as we used typical heat extraction rates from the literature which turned out to be not applicable for our thermal network design. The higher heat extraction rates of the borefield also led to an undersizing of the heat pump in the central plant. The verification showed this discrepancy which we subsequently corrected.

This strong coupling and dynamic evolution makes clear that a proper design requires a coupled nonlinear and dynamic subsurface, energy system and controls simulation. It also showed that verification of MILP and subsequent refinement of the assumptions that the MILP model is based on was critically important to obtain realistic MILP results and a robust design of the components.

10.0 FUTURE WORK

This section describes issues to consider for a subsequent implementation and recommends future items to consider for the PBD process and for the considered technology options. The listed items are based on our experience of conducting the feasibility study for Joint Base Andrews, and on discussions for how to prove out and eventually mature the PBD process for DoD energy system retrofits. While the listed items are not exhaustive, they describe the major points for consideration in future work.

10.1 PILOT DEMONSTRATIONS

We recommend moving forward with one or serval pilot demonstration of a thermal energy network, which may be set up to serve a small set of perhaps five buildings, and later be expanded to add other loads. Such a staged approach is beneficial to keep investments targeted towards testing the technology on a minimum viable size.

We recommend that such pilot projects follow a PBD process. If done for Joint Base Andrews, the detailed system design represents another refinement step within the PBD process, and we recommend it builds on the here presented work.

As shown in the sensitivity analysis, the system performance is sensitive to proper operation. We therefore recommend that any demonstration is accompanied with a robust monitoring project that ensures that the design intent is and remains satisfied in the operational phase.

10.2 PLATFORM-BASED DESIGN WORKFLOW

In this work, we conducted the PBD for the first time at that scale. For its successful execution, it was critical to have an interdisciplinary team that combined its expertise in design, controls, costing, modeling and optimization, with its collaboration and data-driven decision making organized by the PBD workflow.

For future work, we recommend the following main work packages.

1. **Transferability of the process:** We recommend to conduct the PBD process at different DoD sites to prove its transferability across sites that have different weather, loads, site requirements and hence resulting energy system configurations.
2. **Mature process and supporting software infrastructure:** We recommend to further formalize the process with specific sequence charts that describes how the design is done within and across the different platform layers. This is an important step towards formalizing the process, aligning it with related standards including the DoD UFCs and ISO 50001, and ultimately being able to teach it to industry in a uniform way.
   Moreover, the underlying software framework should be built out to standardize requirements formulation and verification, and to build libraries of reusable component models. Such libraries are a key aspect to achieve speed, reproducibility and ultimately reliability.
3. **Expand process with layers for detailed design:** This report conducted a feasibility study, and further refinement is recommend as part of a detailed design, both for JBA and for application at other DoD sites. For example, in detailed design, the ETSs and central plant

models should be refined to model multiple equipment in parallel, and at that point, sequences for optimal equipment staging and rotation as well as failsafe operation should be developed and verified. Within the PBD methodology, this step represents a refinement of the components that represent the ETSs and the central plant models.

4. **Training and technology transfer:** Train industry in executing the PBD process so that it can be scaled across the DoD installations, leading to a family of replicable, highly standardized energy systems that can then be increasingly prefabricated to reduce time and cost for installation and operation.

We believe that a structured approach of proving out the transferability of the process and of working on maturing and scaling of the process and the underlying computational infrastructure are strategically important investments for DoD that has a short payback time through cost-effective reliable retrofits.

10.3 TECHNOLOGY OPTIONS

Within this feasibility study, we examined a range of technologies, but also identified other technologies that would be important to consider in future work. The following shows what we recommend to consider in a future feasibility study or design.

- **Offering utility-scale grid responsive operation.** TENs offer significant opportunities to provide utility-scale grid flexibility. We recommend considering how to implement a grid flexible central plant together with predictive control, and evaluate how such a measure could allow obtaining a revenue stream for providing grid services.
- **Improve control loop for minimum and maximum district loop temperatures.** Predictive control, or feedforward control, could improve the control performance of the district loop temperatures by reducing the overshoot during fast load increases. This allows expanding the temperature range in which the central plant is controlled, which, in turn, is expected to increase system efficiency, increase the storage capacity and heat transfer rate of the borefield, and reduces the size of the capital intensive central heat pump.
- **Assess performance difference to a conventional borefield with simpler central plant control**. The borefield with its two zones, the core zone being actively managed for long term energy storage, and perimeter zone serving to add thermal capacity to the TEN, led to an inherent control complexity. We recommend to compare how this type of borefield compares to a conventional borefield.
- **6-pipe heat pump in ETSs.** An alternate design to the heat recovery chiller in the ETSs is to use a 6-pipe heat pump. Such heat pumps have two pipes for heating, two pipes for cooling, and two pipes to connect to the district loop heat exchanger. While the complexity of a 6-pipe heat pump is higher than the one of a heat recovery heat pump, it simplifies the piping of the ETSs. Future work may consider the benefits and disadvantages of using such a 6-pipe heat pump.
- **Optimization of borefield control and borefield size.** The borefield is a high capital investment. Using predictive control that optimizes its operation likely increases its utilization,

and thus downsizing it. We recommend to consider predictive control in a future detailed design and operation of the system.

Moreover, if the electricity rate difference between low and high are more pronounced, it may be justified to further decrease the minimum and increase the maximum borefield temperature. This also supports a downsizing of the borefield. This would also require changing the hydronic integration and the control to ensure that the district loop temperature is still within the required design temperatures.

- **Pit thermal storage:** An alternate solution to the borefield thermal storage is the use of a pit thermal storage (Xiang et al., 2022). We recommend to consider this technology option in future design, and evaluate the techno-economic difference compared to a borefield. Pit thermal storage may reduce cost, provide a higher storage capacity and increased rate of heat transfer compared to the borefield. This may also circumvent the relatively low heat transfer rates that we observed for the borefield due to the small temperature difference during part of the operation.

These are some of the potential design options that could be considered in future work, either at JBA or at other sites. Moreover, depending on typical weather, load profiles and site requirements, other options may be added to the design space. The PBD process allow phasing in such additional technology options by providing component models for the MILP and Modelica platforms, and then compare their benefits and derisk their deployment.

11.0 DATA AVAILABILITY

The data, models and scripts that have been used for this report are publicly available at https://github.com/lbl-srg/thermal-grid-jba.

12.0 GLOSSARY

architectural component Description of the physical, digital, or virtual component to be used to build a system[20]. 118

behavior Representation of what a system does at each level of abstraction. 3, 7, 116

candidate solution We call a *candidate solution* a configuration that has equipment sized and control determined. 39, 110

communication component Connection among architectural elements used to form a system, such as a bus or network. Communication components also include connections among functional elements that are used to decompose a high-level task, e.g., protocols, adaptors, and channels. 116

component Function, model, or communication element representing physical or computational items. 3, 5, 32, 39, 41, 116

configuration We call a *configuration* a specific energy system, such as a thermal energy network, or a system with geothermal heat pumps and borefields in each building, with component sizes not yet determined. A configuration that has components sized is a candidate solution. 32, 39, 110

COP The coefficient of performance (COP) of a heat pump (or chiller) is a measure of how much useful heat (or cold) is provided per unit of consumed electricity. 9

design space The space of all possible solutions to a problem. 5, 116

digital twin A virtual representation of an object or system that spans its lifecycle, which is updated using real-time data and uses simulation, system identification, and reasoning to assist decision-making[21]. 17

discipline A subdivision of knowledge or expertise applied to the performance of professional tasks in a particular field. 10

district loop The pipe that is installed in the ground and connects the service lines of the thermal grid. 37

domain Independent activity or system, especially one which has its own control, influence, or rights. 11

energy transfer station See ETS. 37

ETS The mechanical and control system that connects building heating loads (such as heating coils), building cooling loads (such as cooling coils) with the service line. An ETS is typically installed in a building, serving one or multiple nearby buildings. 7, 33, 110

[20] Software provides the operational support to perform a function on a chosen architecture (hardware).
[21] IBM. What is a digital twin? 2021. `https://www.ibm.com/topics/what-is-a-digital-twin` (accessed Mai 29, 2023).

library A set of components that contains available functional, architectural, communication, and virtual components that can be reused. 12, 116

model Software representing components in a virtual context using equations. 3, 5

Pareto-optimal The optimal configuration where it is impossible to reconfigure them without worsening one of the considered requirements. 8, 39

PBD See Platform-Based Design. 1, 5

platform The set of architectures that can be assembled using the library of components to generate a design. 5, 116

platform instance A specified architecture that defines the system (how the system does what is supposed to do). 117

platform layer A layer that represents an intermediate platform at a particular level of abstraction, one that structures and constrains the design space. 10, 67

Platform-Based Design The Platform-Based Design (PBD) process is a layered design process that formulates functional requirements and then composes systems from a library of components that meet those requirements. This leads to a process that moves from high-level decisions to detailed design and operations at discrete platforms. Abstraction, refinement, and reusable components enable management of design and operational complexity, leading to standardization and efficiency. 5, 111, 116

reservoir network A hydronic configuration for a thermal energy network that uses one pipe to distribute water to service lines, and in which the connection of the service line supply and return pipes have (approximately) the same pressure. E.g., they are passive connections. 4, 37

reusability A feature of PBD that allows the “recycling" of a component or a part of a component. 5

semantic domain A mathematical characterization of a language. Defining a common semantic domain between functional and architectural components allows the optimized mapping of function to architecture. 117

service line The pipes that connect a district loop with an ETS, typically using a heat exchanger that is part of the ETS. 37, 60

specification Description of what a system must do; it could include multiple layers of abstraction. 9, 10, 65, 80, 116

TEN The mechanical and control system that provides heating and cooling to multiple buildings through pipes that carry water or a water-based solution. 1, 2, 4, 93, 111

thermal energy network See TEN. 37

virtual component Placeholder in a system for a yet-to-be-developed architectural component. 116

13.0 REFERENCES

Balarin, Felice et al. (1997). *Hardware-Software Co-Design of Embedded Systems*. Boston, MA: Springer US. ISBN: 978-1-4613-7808-2 978-1-4615-6127-9. DOI: 10.1007/978-1-4615-6127-9.

Bolinger, Mark et al. (Oct. 2023). *Utility-Scale, 2023 Edition*. Lawrence Berkeley National Laboratory.

Bollinger, Andrew L., Julien F. Marquant, and Matthias Sulzer (Aug. 2019). "Optimization-based planning of local energy systems -bridging the research-practice gap". In: *IOP Conference Series: Earth and Environmental Science* 323.1, p. 012077. DOI: 10.1088/1755-1315/323/1/012077.

Chowdhury, Shovan et al. (2023). "Multi-Model Future Typical Meteorological (fTMY) Weather Files for nearly every US County". In: *Proceedings of the 10th ACM International Conference on Systems for Energy-Efficient Buildings, Cities, and Transportation*, pp. 468–471. DOI: 10.1145/3600100.3626637.

Crowe, Eliot et al. (2020). "Building commissioning costs and savings across three decades and 1500 North American buildings". In: *Energy and Buildings* 227, p. 110408. ISSN: 0378-7788. DOI: 10.1016/j.enbuild.2020.110408.

Di Natale, M. and A.L. Sangiovanni-Vincentelli (Apr. 2010). "Moving From Federated to Integrated Architectures in Automotive: The Role of Standards, Methods and Tools". In: *Proceedings of the IEEE* 98.4, pp. 603–620. ISSN: 0018-9219, 1558-2256. DOI: 10.1109/JPROC.2009.2039550.

EIA (2020). *US Census Regions Divisions*. URL: https://atlas.eia.gov/datasets/eia::us-census-regions-divisions/explore (visited on 07/15/2025).

— (2023a). *Annual Energy Outlook 2023 - Table 3. Energy Prices by Sector and Source*. URL: https://www.eia.gov/outlooks/aeo/data/browser/#/?id=3-AEO2023 (visited on 07/15/2025).

— (Apr. 2023b). *Annual Energy Outlook 2023: Case Descriptions*.

Eschmann, Michael (2021). *Test results of heat pumps*. Ed. by Eastern Switzerland University of Applied Sciences. URL: https://www.ost.ch/en/research-and-consulting-services/technology/system-technology/ies-institute-for-energy-systems/heat-pump-test-center-wpz/test-results-of-heat-pump (visited on 07/15/2025).

DHI-WASY (2010). *Finite Element Subsurface Flow and Transport Simulation System*. Tech. rep. White Paper Vol. V. Berlin, Germany: DHI-WASY GmbH.

Fumagalli, Marica et al. (2017). "Monitoring of gas driven absorption heat pumps and comparing energy efficiency on primary energy". In: *RE* 110. Increasing the renewable share for heating and cooling by the means of sorption heat pumps and chillers, pp. 115–125. ISSN: 0960-1481. DOI: 10.1016/j.renene.2016.12.058.

Gagnon, Pieter et al. (Feb. 2024). *Cambium 2023 Scenario Descriptions and Documentation*. NREL.

Gautier, Antoine, Michael Wetter, Jianjun Hu, et al. (Oct. 2023). "HVAC and Control Templates for the Modelica Buildings Library". In: *Proceedings of the 15th International Modelica Conference*. Linköping Electronic Conference Proceedings. Aachen, Germany: Modelica Association and Linköping University Electronic Press.

Gautier, Antoine, Michael Wetter, and Matthias Sulzer (Nov. 2022). "Resilient cooling through geothermal district energy system". In: *Applied Energy* 325, p. 119880. DOI: 10.1016/j.apenergy.2022.119880.

Jordan, D. C. and S. R. Kurtz (2013). *Photovoltaic Degradation Rates – an Analytical Review*. 1, pp. 12–29. DOI: 10.1002/pip.1182.

Keutzer, K. et al. (Dec. 2000). “System-level design: orthogonalization of concerns and platform-based design”. In: *IEEE Transactions on Computer-Aided Design of Integrated Circuits and Systems* 19.12, pp. 1523–1543. ISSN: 02780070. DOI: 10.1109/43.898830.

Kolahi, Mohammad-Reza et al. (2025). “Reducing pumping energy in thermal grids: A study on hydraulic modeling and design approaches”. In: *Energy* 327, p. 136410. ISSN: 0360-5442. DOI: 10.1016/j.energy.2025.136410.

Liu, Xiaobing et al. (Aug. 2018). *Analysis of Cost Reduction Potential of Vertical Ground Heat Exhanger*. Tech. rep. ORNL/TM-2018/756. Oakridge, TN: Oakridge National Laboratory.

Mattsson, Sven Erik and Hilding Elmqvist (Apr. 1997). “Modelica – An international effort to design the next generation modeling language”. In: *7th IFAC Symposium on Computer Aided Control Systems Design*. Ed. by L. Boullart, M. Loccufier, and Sven Erik Mattsson. Gent, Belgium, pp. 1–5.

Milica Grahovac Paul Ehrlich, Jianjun Hu and Michael Wetter (2023). “Model-based Data Center Cooling Controls Comparative Co-design”. In: *Science and Technology for the Built Environment* 0.ja, pp. 1–49. DOI: 10.1080/23744731.2023.2276011.

NREL (2025). *Champion Module Efficiencies*. URL: https://www.nrel.gov/docs/libraries/pv/champion-module-efficiencies.pdf (visited on 07/15/2025).

NYU Stern School of Business (Nov. 20, 2024). *Cost of Equity and Capital (US)*. URL: https://pages.stern.nyu.edu/~adamodar/New_Home_Page/datafile/wacc.html (visited on 07/15/2025).

Pritoni, Marco et al. (Aug. 2024). “Digital and Interoperable: The future of building automation is on the horizon. What’s in it for me?” In: *Proceedings of the ACEEE 2024 Summer Study on Energy Efficiency in Buildings*. ACEEE. Asilomar, Pacific Grove, CA. DOI: 10.20357/B76W3X.

Raftery, Paul et al. (2024). “Insights from hydronic heating systems in 259 commercial buildings”. In: *Energy and Buildings* 321, p. 114543. ISSN: 0378-7788. DOI: 10.1016/j.enbuild.2024.114543.

Sangiovanni-Vincentelli, Alberto (Mar. 2007). “Quo Vadis, SLD? Reasoning About the Trends and Challenges of System Level Design”. In: *Proc. of the IEEE* 95.3, pp. 467–506. DOI: 10.1109/JPROC.2006.890107.

Seland, Øyvind et al. (2020). In: *Geoscientific Model Development* 13.12, pp. 6165–6200. DOI: doi.org/10.5194/gmd-13-6165-2020. Sommer, Tobias et al. (2020). “The reservoir network: A new network topology for district heating and cooling”. In: *Energy* 199. DOI: 10.1016/j.energy.2020.117418.

Sulzer, Matthias et al. (2023). “Platform-based design for energy systems”. In: *Applied Energy* 352, p. 121955. ISSN: 0306-2619. DOI: 10.1016/j.apenergy.2023.121955.

US Bureau of Labor Statistics (Nov. 20, 2024). *Consumer Price Index for All Urban Consumers (CPI-U)*. URL: https://data.bls.gov/timeseries/CUUR0000SA0 (visited on 07/15/2025).

Wetter, Michael, Paul Ehrlich, et al. (Jan. 2022). “OpenBuildingControl: Digitizing the control delivery from building energy modeling to specification, implementation and formal verification”. In: *Energy* 238.A. DOI: 10.1016/j.energy.2021.121501.

Wetter, Michael and Jianjun Hu (Mar. 2019). *Quayside Energy System Analysis*. Tech. rep. LBNL-2001197. Berkeley, CA: Lawrence Berkeley National Laboratory.

Wetter, Michael and Matthias Sulzer (2024). n: *Journal of Building Performance Simulation* 17.3, pp. 383–393. DOI: 10.1080/19401493.2023.2285824.
Wetter, Michael, Wangda Zuo, et al. (2014). "Modelica Buildings library". In: *Journal of Building Performance Simulation* 7.4, pp. 253–270. DOI: 10.1080/19401493.2013.765506. Wilcox, S (2008). *Users manual for TMY3 data sets*. Tech. rep. NREL/TP-581-43156: 56. Wüllhorst, Fabian et al. (2021). "A modular model of reversible heat pumps and chillers for system applications". In: *Modelica Conferences*, pp. 561–568.
Xiang, Yutong et al. (2022). "A comprehensive review on pit thermal energy storage: Technical elements, numerical approaches and recent applications". In: *Journal of Energy Storage* 55, p. 105716. ISSN: 2352-152X. DOI: 10.1016/j.est.2022.105716.
Zhang, Kun et al. (Jan. 2022). "Estimating ASHRAE Guideline 36 Energy Savings for Multi-zone Variable Air Volume Systems Using Spawn of EnergyPlus". In: *Journal of Building Performance Simulation* (2), pp. 215–236. DOI: 10.1080/19401493.2021.2021286.

APPENDIX A Points of Contact

Point of Contact Name	Organization Name Address	Email	Role in Project
Michael Wetter	Lawrence Berkeley National Laboratory 1 Cyclotron Rd. Berkeley, CA 94720	MWetter@lbl.gov	Principal investigator
Eric Nyenhuis	Southland Industries 16835 West Bernardo Dr. Suite 210 San Diego, CA 92127	ENyenhuis@southlandind.com	Industrial advisor

APPENDIX B General Concept of Platform-Based Design

The Platform-Based Design (PBD) concept is well documented, both the method itself and in various case studies. The basic principles of PBD (Balarin et al., 1997; Keutzer et al., 2000; Alberto Sangiovanni-Vincentelli, 2007) are to:

1. Start at the highest level of abstraction.
2. Hide unnecessary details of the implementation.
3. Summarize the important parameters of the implementation in an abstract model.
4. Limit the design space exploration to a set of available components.
5. Carry out the design as a sequence of "refinement" steps that go from the initial specification toward the final implementation using platforms at various levels of abstraction.

An essential characteristic of the PBD paradigm is the orthogonalization of concerns, which allows the separation of the design space aspects: The functionality (what the system is supposed to do) is separated from the architecture (how the system does what it is supposed to do). This allows a more effective and efficient exploration of the architectural space that supports the required functionality. Hence, mapping functions to architectural solutions will become an essential step in the process from conception to implementation (Alberto Sangiovanni-Vincentelli, 2007).

The following description of the PBD concept, i.e., platform, mapping, design and modeling principles, is extracted from Di Natale and A.L. Sangiovanni-Vincentelli (2010), Keutzer et al. (2000), and Alberto Sangiovanni-Vincentelli (2007) and has originally been published in Sulzer et al. (2023).

B.1 PLATFORM PRINCIPLES

A platform is a library of components that can be assembled to generate a system design at a particular level of abstraction. Such a design library contains not only mathematical models, representing physical and digital components that perform in a quantifiable manner, but also communication components that are used to interconnect components to form a system.

It is important to keep physical, digital, and communication components well separated so that different methods for representing and refining systems can be applied. Design by aggregation of components (abstraction) requires great care in defining the communication mechanisms as they may facilitate or hinder design reuse. Unexpected behavior of the system configuration is often due to negligence in defining the interfaces and the communication among the components.

In general, each library component is characterized in terms of performance parameters and the functionality it can support. Not all components in the library are pre-existing components. Some library components can be virtual components, which are placeholders for yet-to-be-developed components. Virtual components provide flexibility of customization or express the need to innovate new components as part of the design process.

B.2 MAPPING PRINCIPLES

Platforms represent a particular family of solutions that share common architectural features, i.e., components of the platform. Hence, components of a platform can be reused to form various system

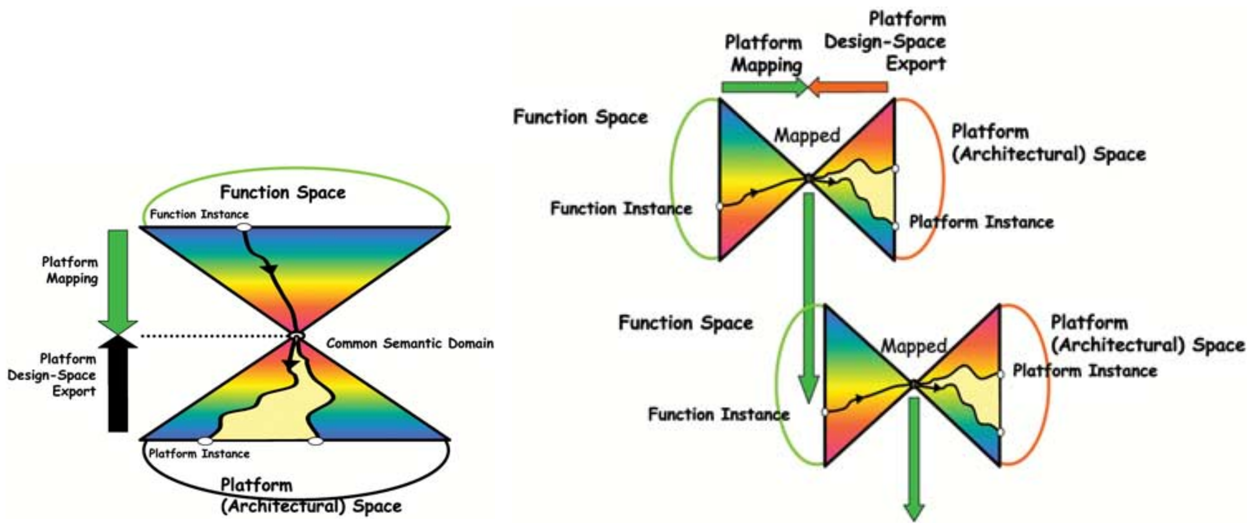

(a) PBD triangles. **(b) PBD process.**

Figure B.1. The PBD concept.

solutions. Since the notion of a platform is associated with a set of potential solutions to a design problem, the process of mapping a functionality (what the system is supposed to do) with the platform elements that will be used to build a platform instance or an architecture (how the system does what it is supposed to do) is crucial. This mapping process is the essential step for refinement and provides a mechanism to proceed toward implementation in a structured way.

The PBD design process is neither a fully top-down nor a fully bottom-up approach in the traditional sense; rather, it is a *meet-in-the-middle* process (see Fig. B.1a) as it can be seen as a combination of both:

- A top-down approach maps an instance of the required functionality of the design into an instance of the platform (architecture) and propagates constraints.
- A bottom-up approach builds a platform by choosing components of the library to form a system that characterizes it and an associated performance abstraction, e.g., a seasonal performance factor of a heat pump.

The *middle* is where functionality meets the architectural configuration, which represents the solution or instance of the platform. Given the original semantic difference between the two, the meeting place must be described with a common semantic domain so that the mapping of functionality to components of the platform, to yield an implementation, can be formalized and automated.

A prerequisite for the adoption of the PBD and of the meet-in-the-middle approach is the definition of the right models and abstractions for the description of the functional specification at the top and for the architecture solutions at the bottom of the hourglass of Fig. B.1a. The platform interface must be isolated from lower-level details but, at the same time, must provide enough information to allow design space exploration with a fairly accurate prediction of the properties of the implementation.

B.3 DESIGN PRINCIPLES

To better represent the refinement process and to stress that platforms may pre-exist the functionality of the system to be designed, we turn the triangles on their sides and represent the *middle* as the mapped functionality. Then, the refinement process takes place on the mapped functionality that becomes the *function* at the lower level of the refinement. Another platform is then considered *underneath* with the mapped instance, and the process is iterated until all the architectural components are implemented in their final form. This process is applied at all levels of abstraction, demonstrating what we call the *fractal nature of design* — the design problem repeats itself at every level of the hierarchy. The resulting Fig. B.1b exemplifies this aspect of the design methodology.

The result of the mapping process from functionality to architecture can be interpreted as functionality at a lower level of abstraction where a new set of components, interconnections, and composition rules are identified. To progress in the design, the new functionality has to be mapped to the new set of architectural components. If the previous step used an architectural component that was fully instantiated,[22] then that part of the design is considered concluded and the mapping process involves only the parts that have not been fully specified yet.

Establishing the number, location, and components of intermediate platforms is the essence of the PBD process. In fact, designs with different requirements and specifications may use different intermediate platforms, hence different layers of regularity and design-space constraints. The trade-offs involved in selecting the number and characteristics of platforms relate to the size of the design space to be explored and the accuracy of the estimation of the characteristics of the solution adopted.

The choice of the intermediate platforms may also be dictated by business concerns and by the common agreement of the supply chain in specific industrial segments. However, degrees of freedom should be exploited inside any of the companies in the supply chain and in the definition of the components even across company boundaries.

[22]The component reaches its *atomic* stage, and its decomposition stops.

APPENDIX C Energy Consumption Profiles

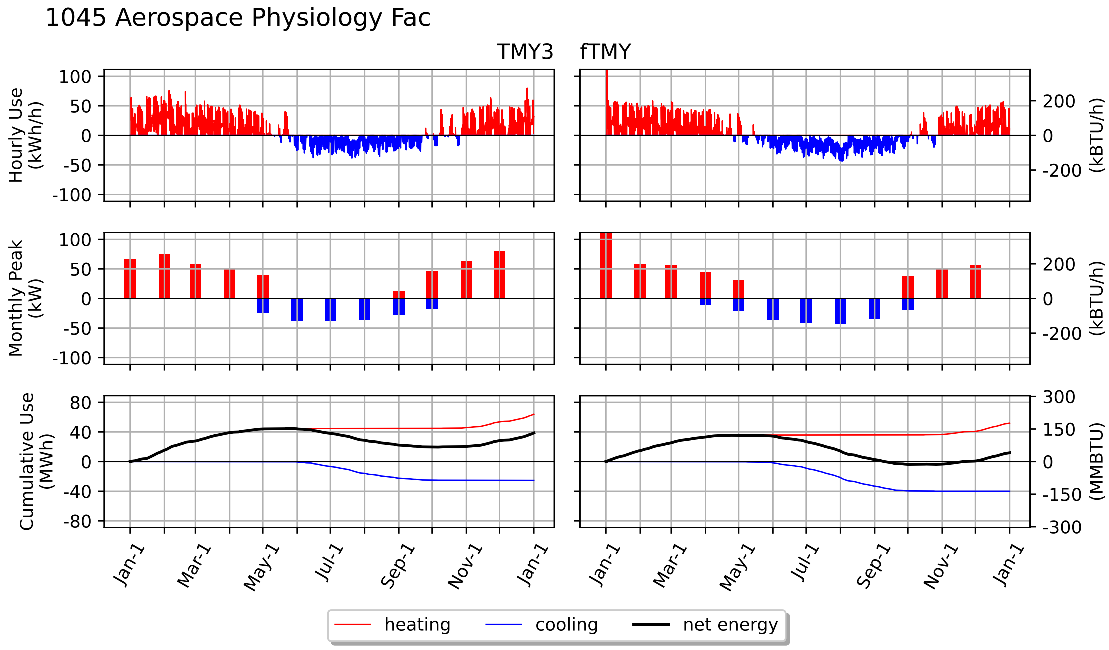

Figure C.1. Hourly energy consumption, monthly peak demand, and cumulative energy consumption of 1045 Aerospace Physiology Fac

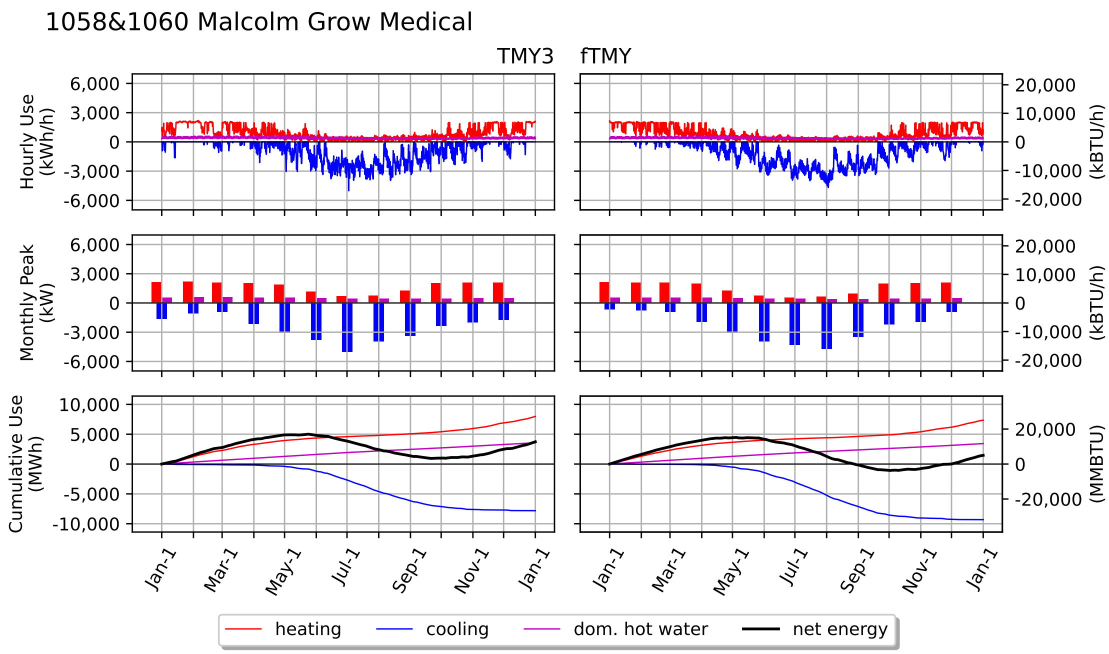

Figure C.2. Hourly energy consumption, monthly peak demand, and cumulative energy consumption of 1058&1060 Malcolm Grow Medical

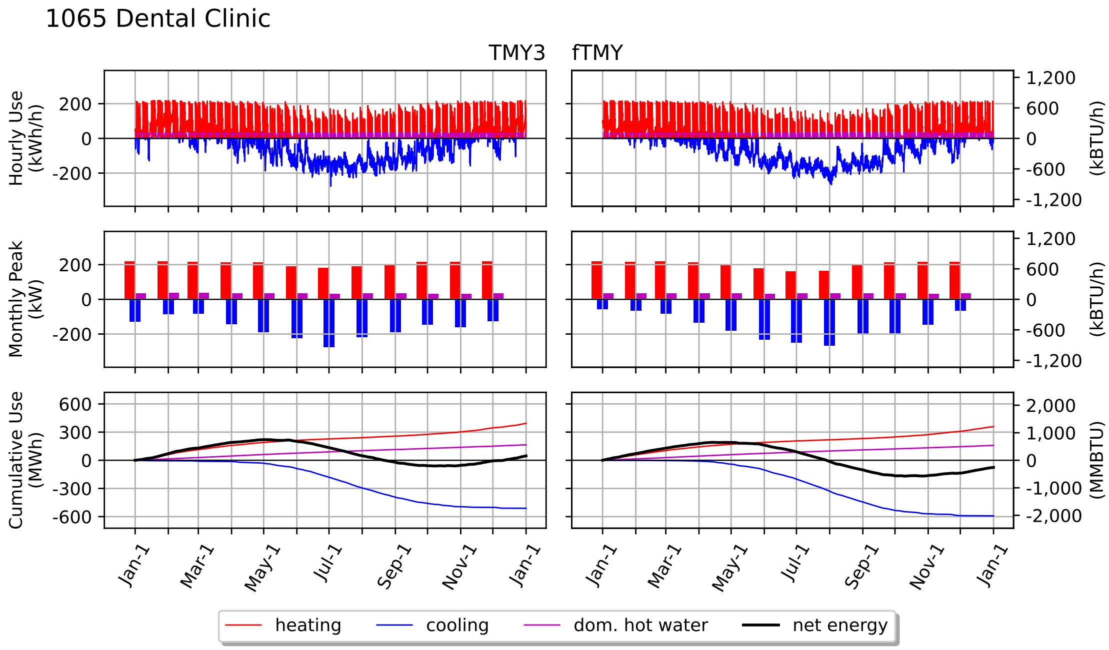

Figure C.3. Hourly energy consumption, monthly peak demand, and cumulative energy consumption of 1065 Dental Clinic

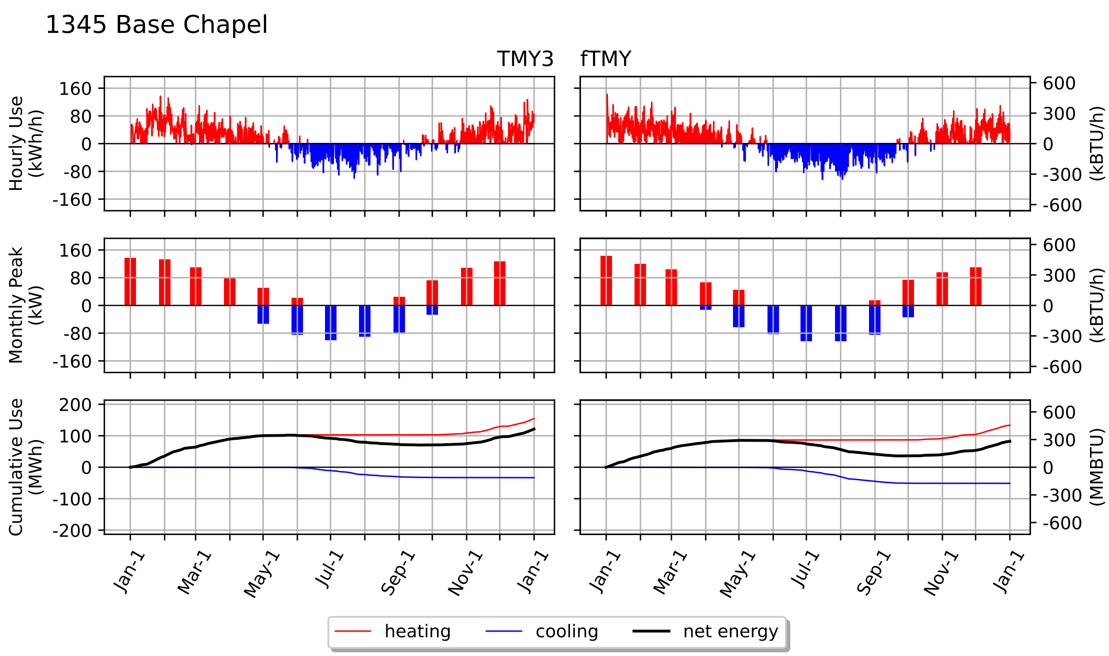

Figure C.4. Hourly energy consumption, monthly peak demand, and cumulative energy consumption of 1345 Base Chapel

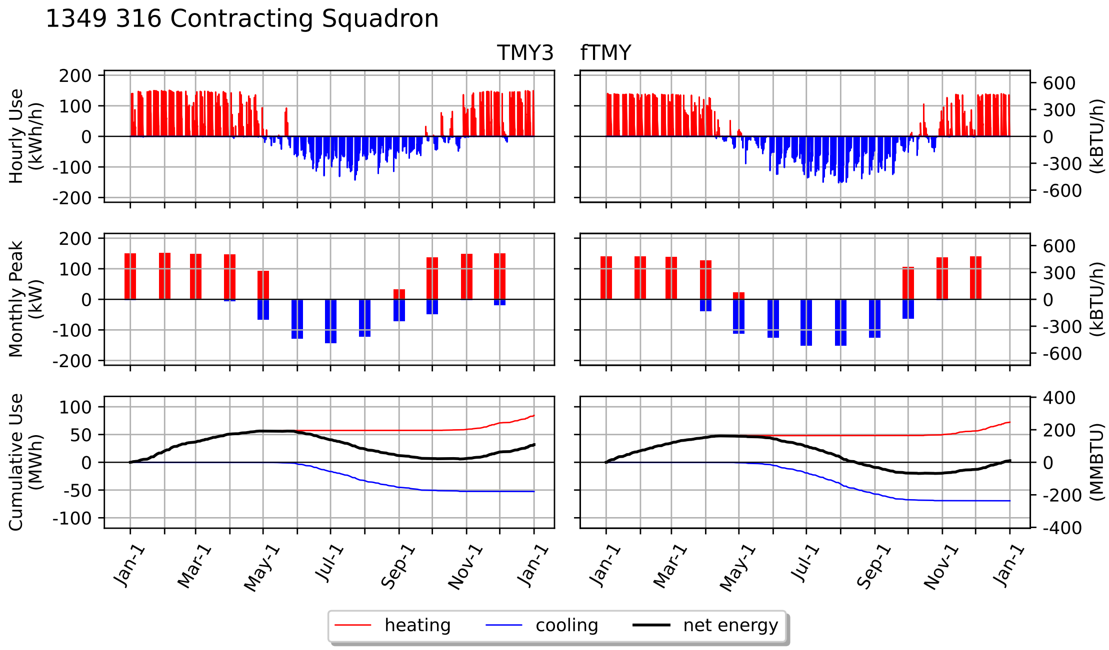

Figure C.5. Hourly energy consumption, monthly peak demand, and cumulative energy consumption of 1349 316 Contracting Squadron

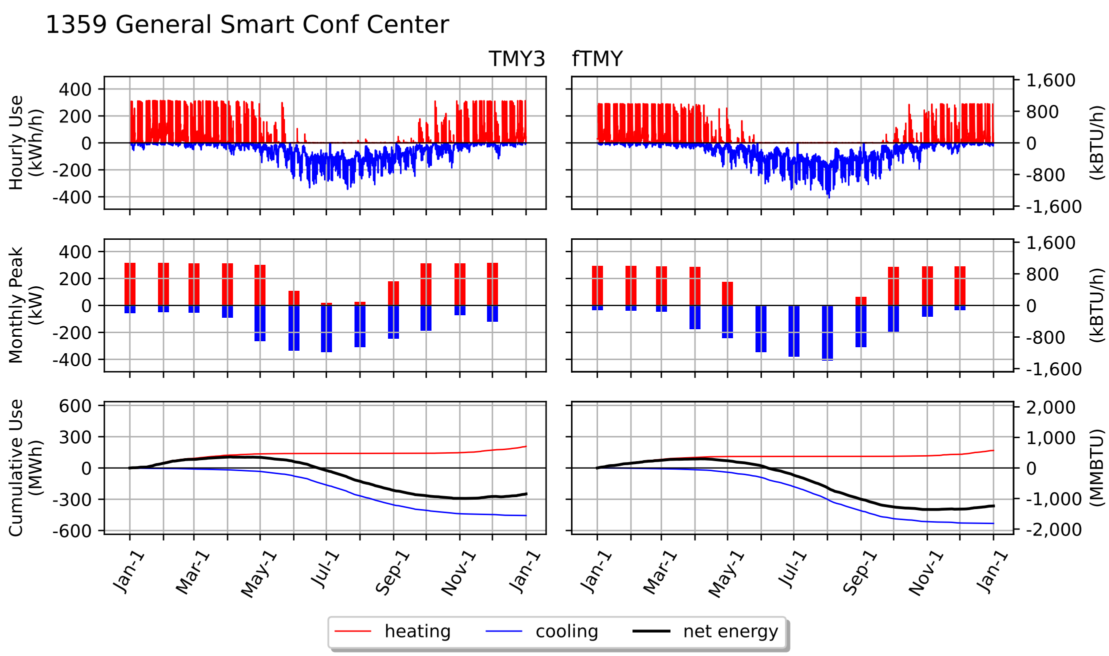

Figure C.6. Hourly energy consumption, monthly peak demand, and cumulative energy consumption of 1359 General Smart Conf Center

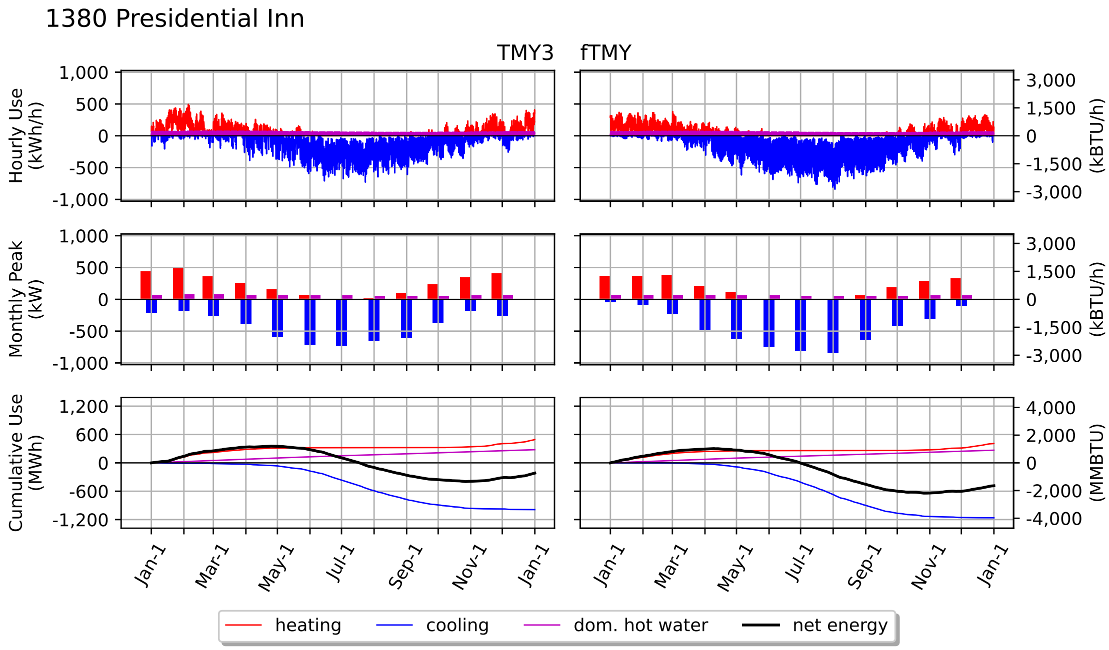

Figure C.7. Hourly energy consumption, monthly peak demand, and cumulative energy consumption of 1380 Presidential Inn

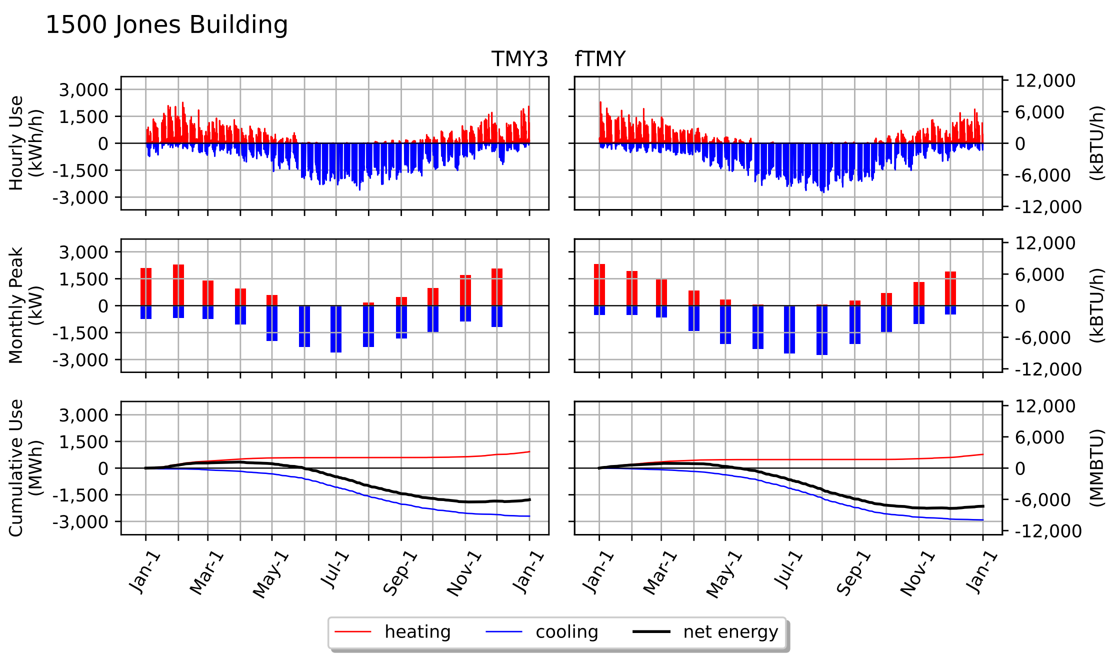

Figure C.8. Hourly energy consumption, monthly peak demand, and cumulative energy consumption of 1500 Jones Building

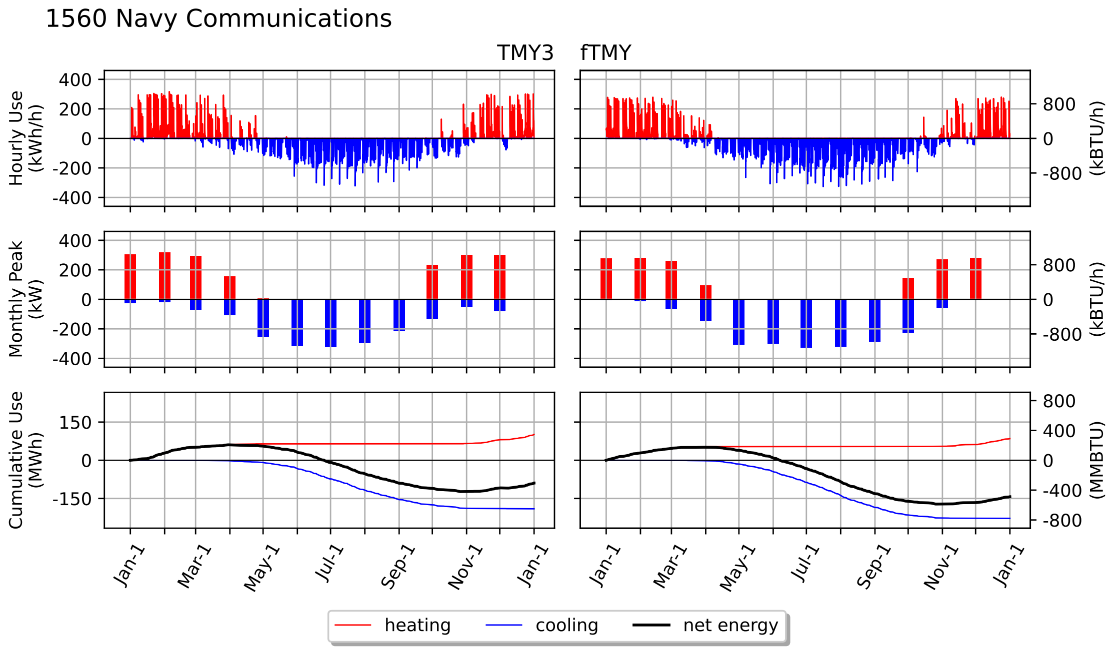

Figure C.9. Hourly energy consumption, monthly peak demand, and cumulative energy consumption of 1560 Navy Communications

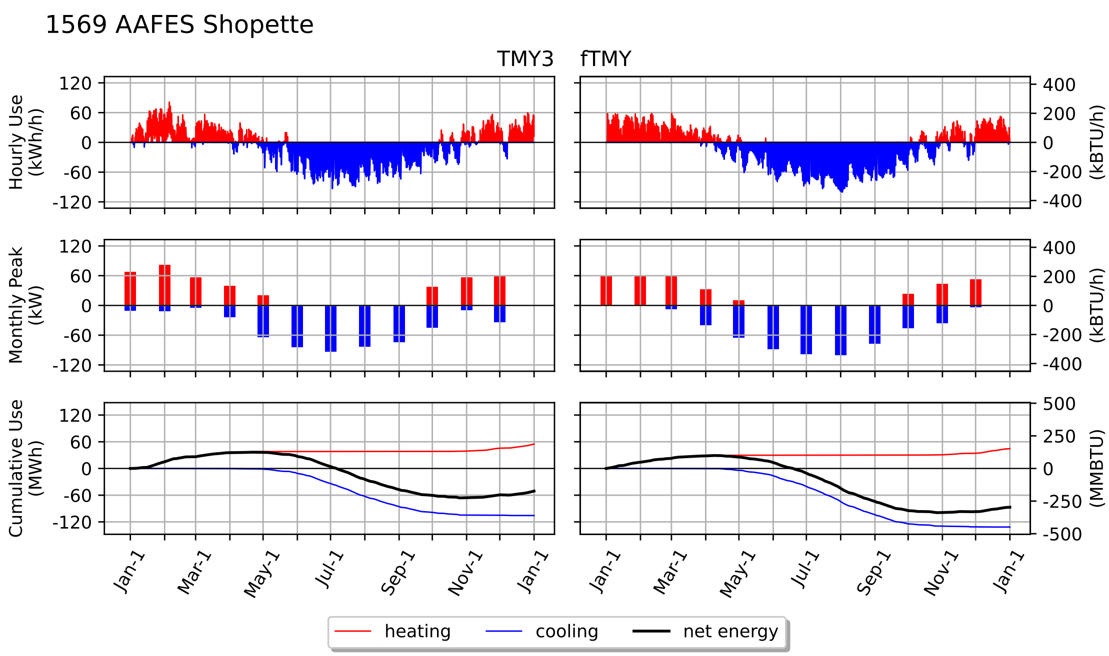

Figure C.10. Hourly energy consumption, monthly peak demand, and cumulative energy consumption of 1569 AAFES Shopette

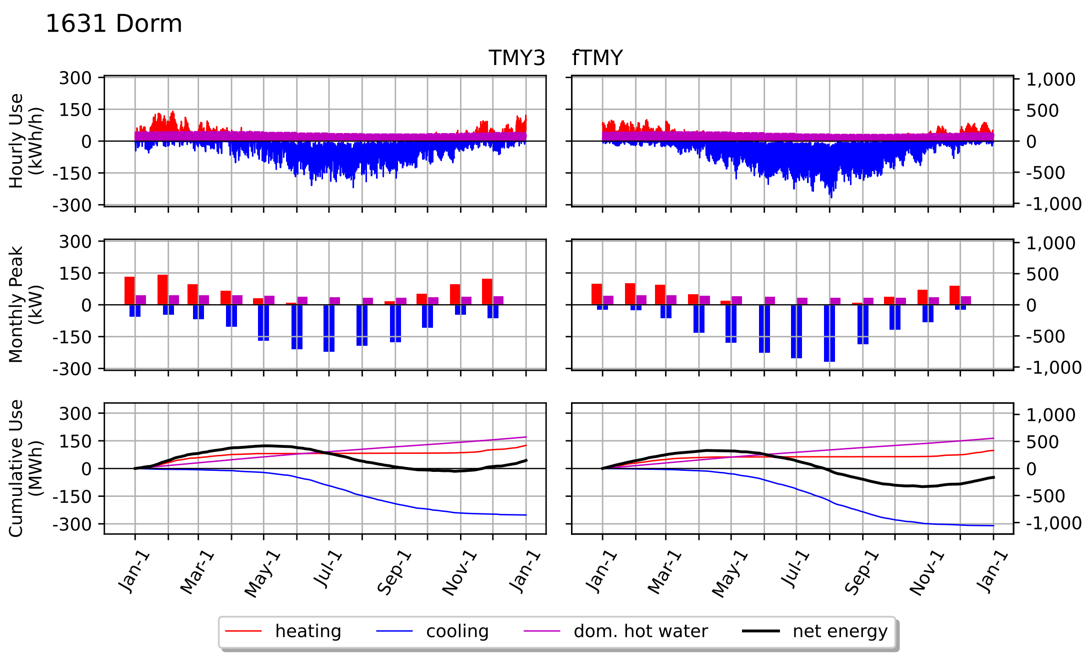

Figure C.11. Hourly energy consumption, monthly peak demand, and cumulative energy consumption of 1631 Dorm

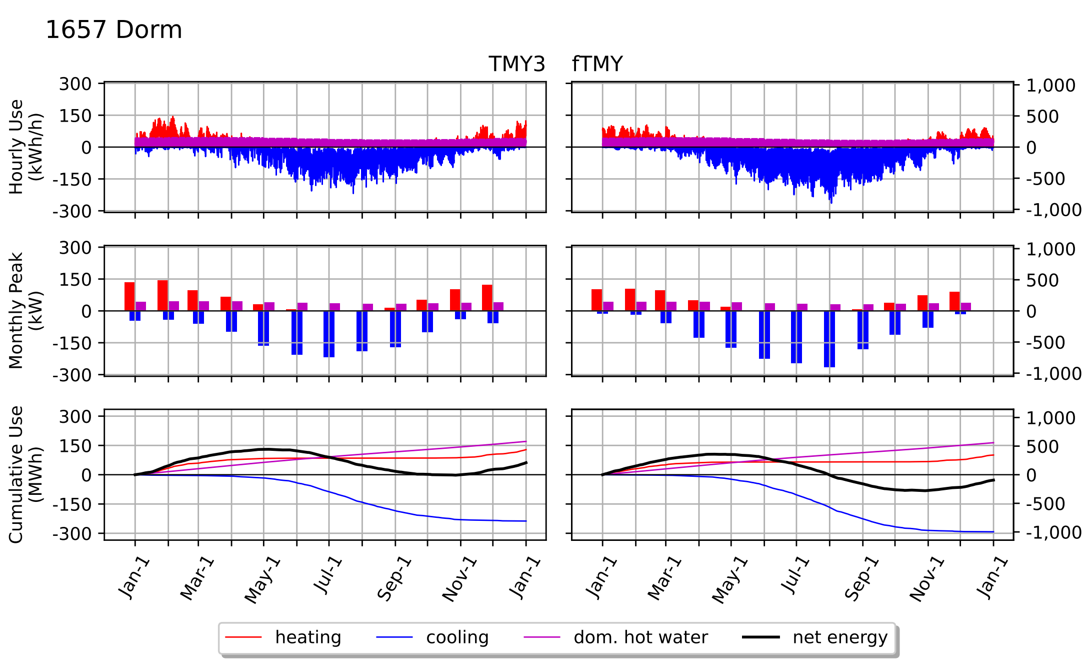

Figure C.12. Hourly energy consumption, monthly peak demand, and cumulative energy consumption of 1657 Dorm

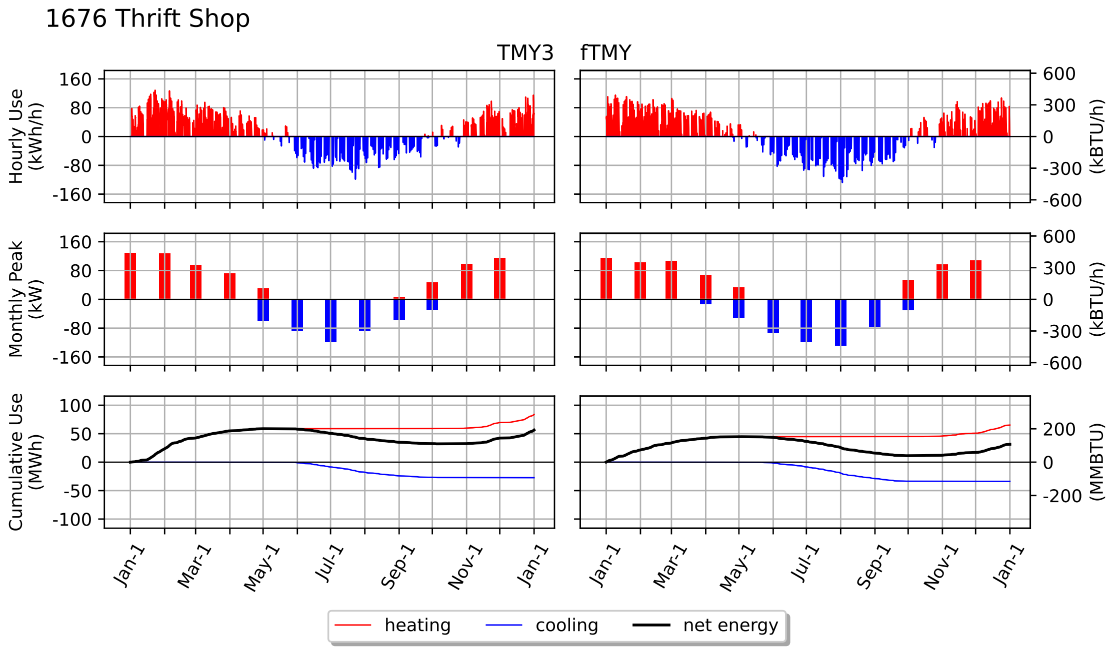

Figure C.13. Hourly energy consumption, monthly peak demand, and cumulative energy consumption of 1676 Thrift Shop

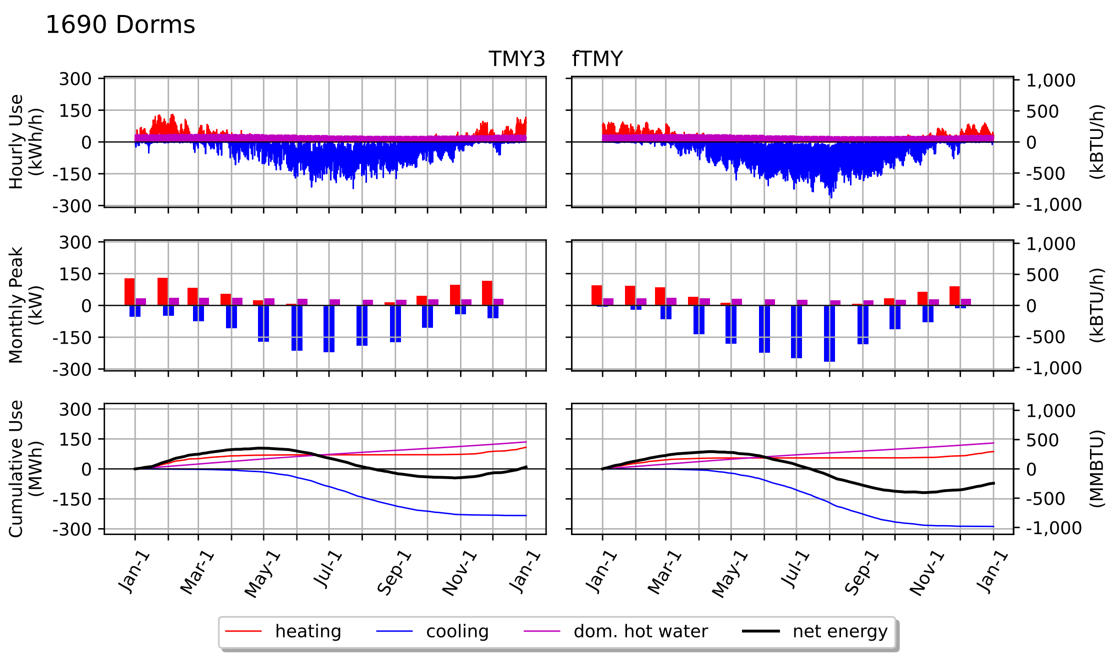

Figure C.14. Hourly energy consumption, monthly peak demand, and cumulative energy consumption of 1690 Dorms

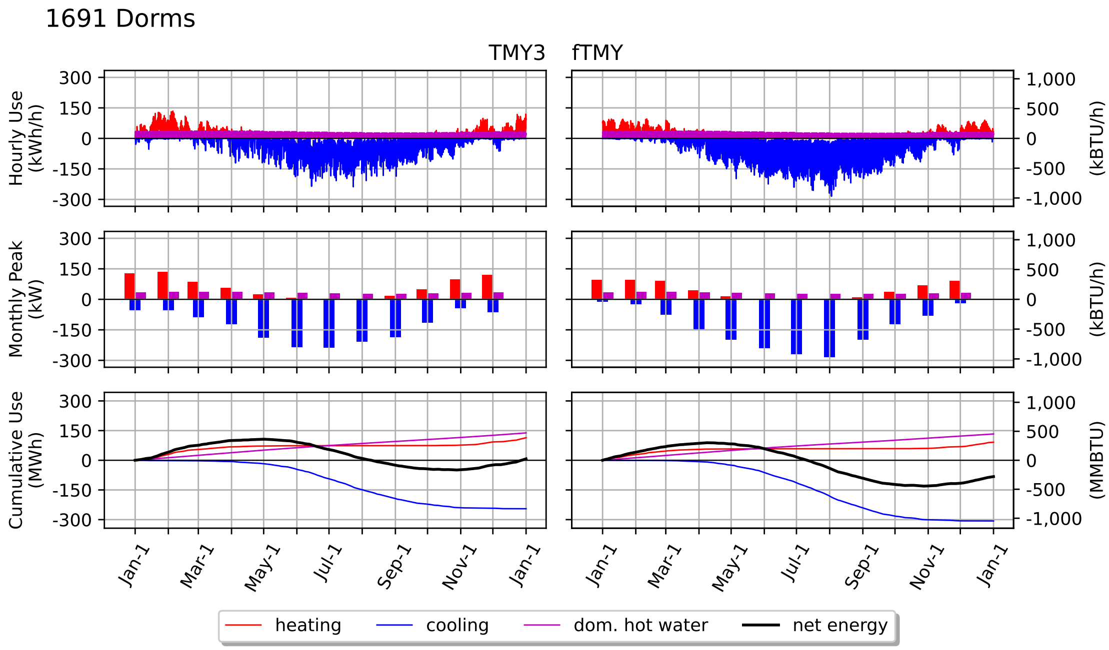

Figure C.15. Hourly energy consumption, monthly peak demand, and cumulative energy consumption of 1691 Dorms

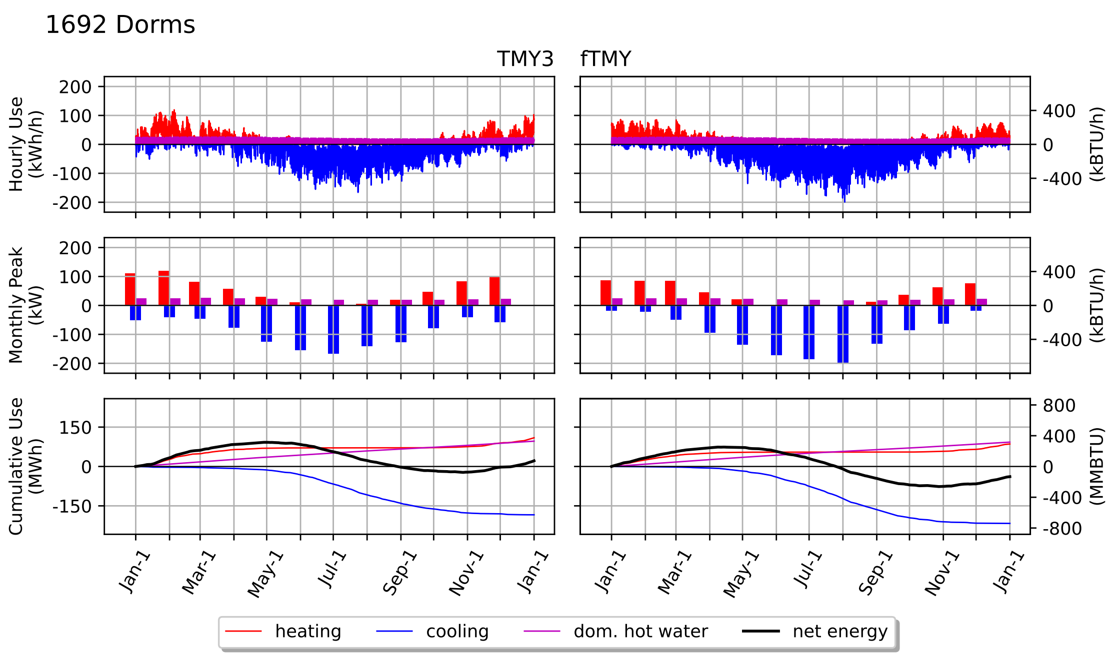

Figure C.16. Hourly energy consumption, monthly peak demand, and cumulative energy consumption of 1692 Dorms

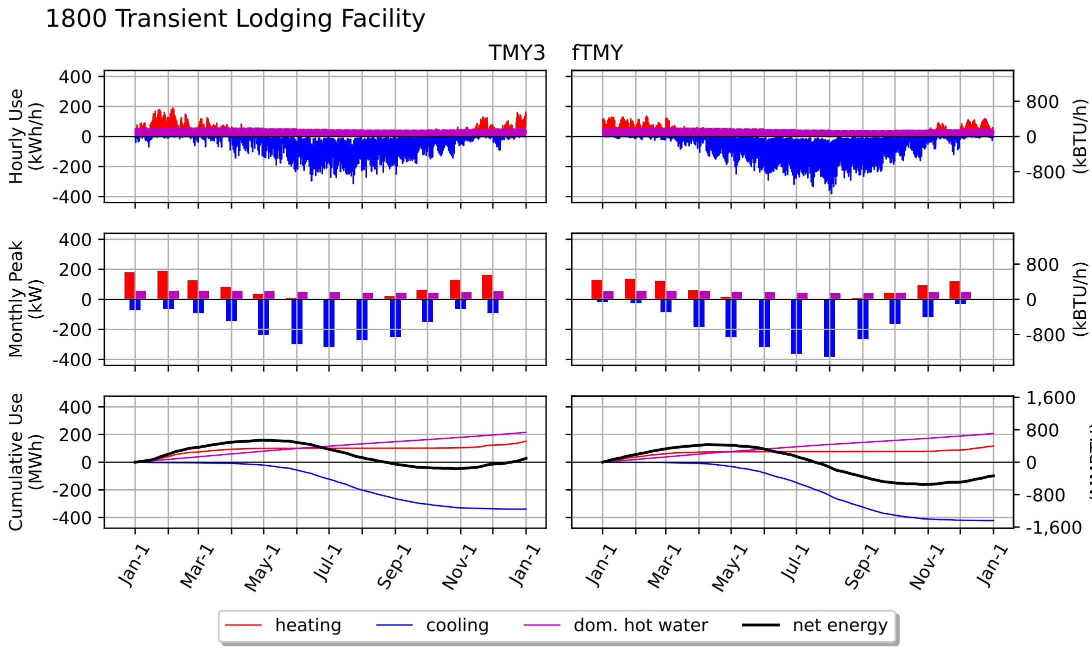

Figure C.17. Hourly energy consumption, monthly peak demand, and cumulative energy consumption of 1800 Transient Lodging Facility

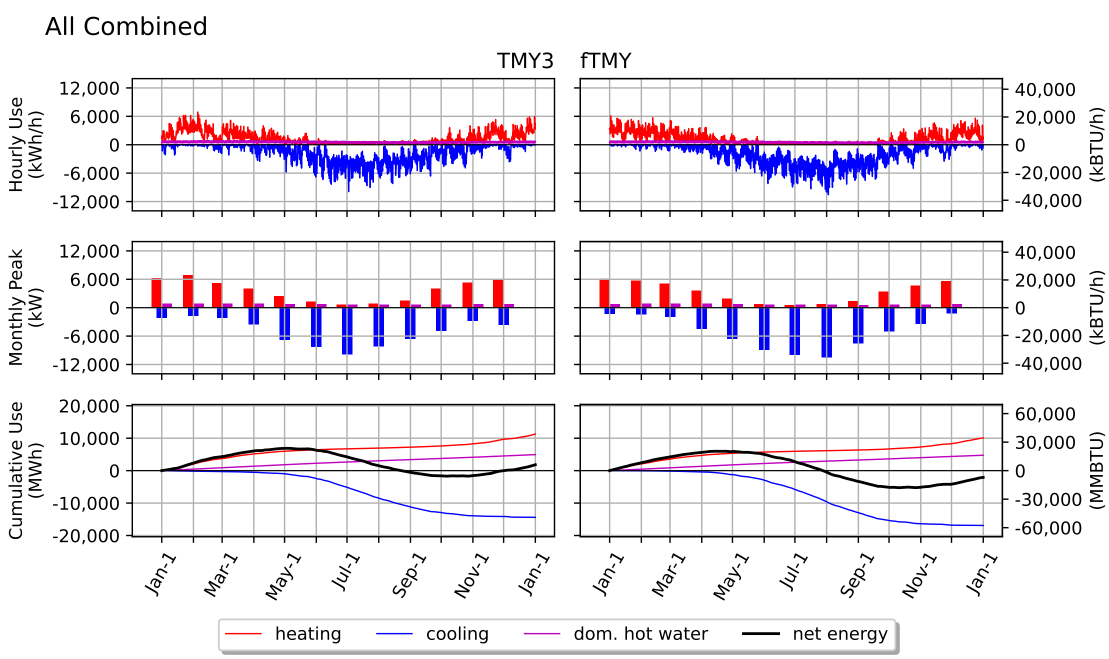

Figure C.18. Hourly energy consumption, monthly peak demand, and cumulative energy consumption of all in-scope buildings combined

APPENDIX D ECM Matrix

Strategy	1045	1058	1060	1065	1345	1349	1359	1380	1500	1569	1631	1657	1676	1690	1691	1692	1800
New Boiler Controls / Control Retrofits								X	X								
Heat Pump Chiller / Heater	X	X	X	X	X	X	X	X	X	X	X	X	X	X	X	X	X
Enhanced EMCS Sequences; Temp Setback Schedules		X															
Chiller Plant Optimization		X	X	X				X	X								X
Boiler Plant Optimization																	
Upgrade EMCS Network / Controllers / Front End	X	X			X	X		X	X	X	X	X	X	X	X	X	X
Add Analytics Package		X															
Add/Restore Air-Side Economizer		X	X						X								
Duct Sealing		X	X	X			X		X								
Coil Treatment				X			X	X		X			X				X
HVAC Replacement	X				X	X					X	X		X	X	X	
Add Heat Pump Chiller	X	X	X	X	X	X	X	X	X	X	X	X	X	X	X	X	X
Add Thermal Network Connection	X	X	X	X	X	X	X	X	X	X	X	X	X	X	X	X	X
Interior and exterior lighting retrofits and replacements	X	X	X		X	X		X	X		X	X	X	X	X	X	X
Intelligent lighting controls	X																
Insulation Installation	X										X	X		X	X	X	
Reflective window tinting	X	X	X	X			X	X	X		X	X		X	X	X	
Building Envelope Sealing	X				X	X	X	X		X	X	X	X	X	X	X	X

Table D.1. ECM matrix for in-scope buildings on the JBA site.

Building		sq-ft	ECM					
			Lighting		Envelope		Controls	
			$/sq-ft	$	$/sq-ft	$	$/sq-ft	$
1045	Aerospace Physiology Fac	8,230	1.21	$9,989	1.41	$11,607	2.23	$18,326
1058&1060	Malcom Grow Medical	248,896	2.75	$683,938	1.41	$351,011	2.23	$554,228
1065	Dental Clinic	28,120	2.75	$77,271	1.41	$39,657	2.23	$62,616
1345	Base Chapel	13,840	0.76	$10,512	1.41	$19,518	2.23	$30,818
1349	316 Contracting Squadron	18,415	1.21	$22,351	1.41	$25,970	2.23	$41,005
1359	General Smart Conf Center	45,747	0.00	$0	1.41	$64,516	2.23	$101,867
1380	Presidential Inn	143,000	1.85	$264,515	1.41	$201,669	2.23	$318,424
1500	Jones Building	330,000	1.91	$631,036	1.41	$465,389	2.23	$734,826
1560	Navy Communications	25,336	1.64	$41,493	1.41	$35,731	2.23	$56,417
1569	AAFES Shopette	10,792	1.91	$20,637	1.41	$15,220	2.23	$24,031
1631	Dorm	45,449	1.85	$84,070	1.41	$64,095	2.23	$101,203
1657	Dorm	46,000	1.85	$85,089	1.41	$64,872	2.23	$102,430
1676	Thrift Shop	15,395	1.91	$29,439	1.41	$21,711	2.23	$34,281
1690	Dorms	53,126	1.85	$98,270	1.41	$74,922	2.23	$118,298
1691	Dorms	50,532	1.85	$93,472	1.41	$71,264	2.23	$112,522
1692	Dorms	36,609	1.85	$67,718	1.41	$51,629	2.23	$81,519
1800	Transient Lodging Facility	69,799	1.85	$129,111	1.41	$98,436	2.23	$155,425
Category total				$2,348,910		$1,677,216		$2,648,235
Grand total								**$6,674,361**

Table D.2. ECM cost matrix for in-scope buildings on the JBA site.

APPENDIX E COPs for MILP

T_{eva} [a]	T_{con} [a]	$COP_{awhp,ini}$ [a]	COP_{Car} [b]	$\eta_{Car,awhp}$ [c]
−10	55	1.84	5.05	0.364
−7	52	2.04	5.51	0.370
2	42	3.29	7.88	0.418
7	36	4.55	10.66	0.427
12	30	5.88	16.84	0.349

(a) AWHP.

T_{eva} [a]	T_{con} [a]	$COP_{wwhp,ini}$ [a]	COP_{Car} [b]	$\eta_{Car,wwhp}$ [c]
10	55	3.69	7.29	0.506
10	52	3.9	7.74	0.504
10	42	4.87	9.85	0.494
10	36	5.64	11.89	0.474
10	30	6.39	15.16	0.422

(b) WWHP.

[a] Data extracted from Eschmann (2021) using average COPs of the table.
[b] See Eq. (19).
[c] See Eq. (18).

Table E.1. Data used to calculate the COP values for AWHP and WWHP for the MILP optimization.

Table E.1b shows the raw data of the COP values that were used to compute COP values for the MILP optimization.

APPENDIX F MILP Model Key Parameters

F.1 PARAMETERS PER HUB

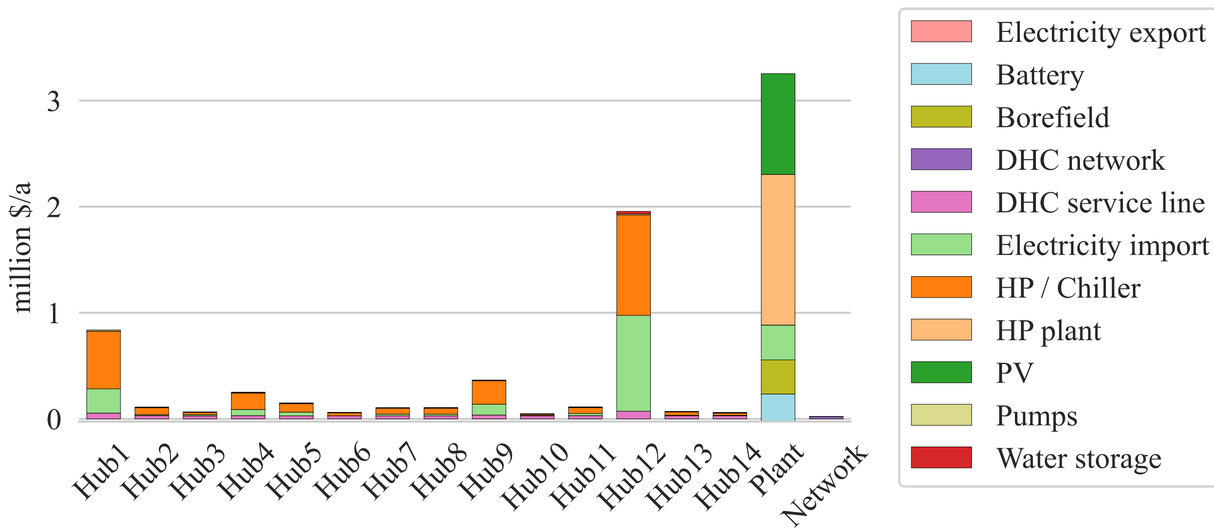

Figure F.1. ALCC for the different equipment and the different hubs.

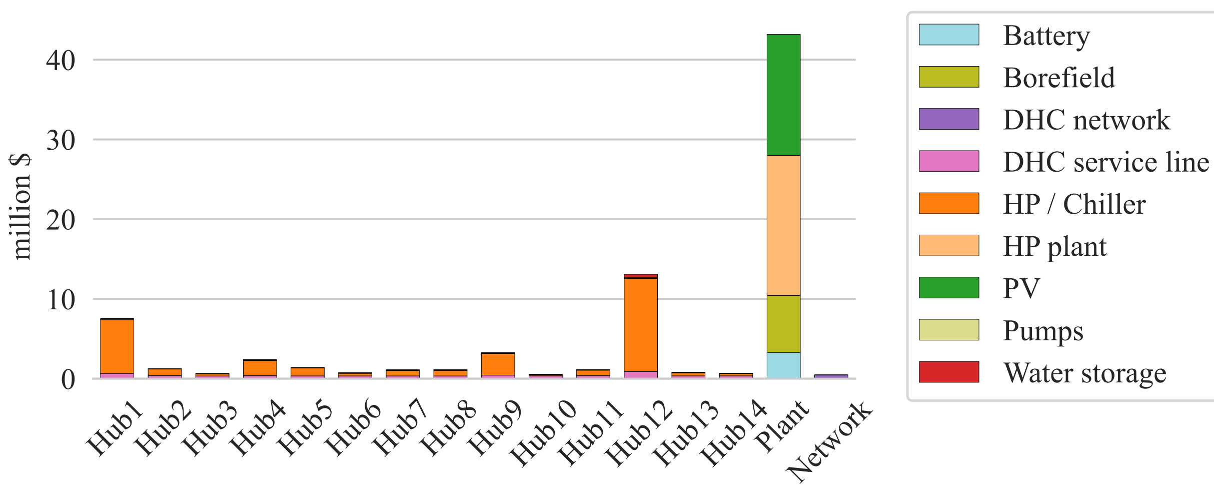

Figure F.2. Investment costs for the different equipment and the different hubs.

	Hub1	Hub2	Hub3	Hub4	Hub5	Hub6	Hub7	Hub8	Hub9	Hub10	Hub11	Hub12	Hub13	Hub14	Plant	Network
Battery															260,057	
Borefield															321,448	
DHC network																23,142
DHC service line	53,949	30,646	27,453	30,248	28,501	28,292	28,114	28,046	35,671	28,935	30,340	71,600	28,707	28,844		
Electricity export															−25,704	
Electricity import	228,447	8,280	12,193	57,990	35,076	1,062	16,039	15,794	102,159	3,447	20,879	903,471	5,122	4,438	327,930	
HP / Chiller	544,270	66,145	21,451	155,599	79,780	26,858	56,063	56,712	220,108	10,214	55,909	946,126	31,637	22,088		
HP plant															1,419,757	
PV															950,638	
Pumps	11,389	5,346	4,733	4,083	3,642	4,853	3,513	3,512	4,764	4,782	3,631	9,235	4,921	4,865		
Water storage				3,382	2,350	908	2,048	2,048	2,774	908	2,283	25,276				

Table F.1. ALCC in $/a for the different equipment and the different hubs.

	Hub1	Hub2	Hub3	Hub4	Hub5	Hub6	Hub7	Hub8	Hub9	Hub10	Hub11	Hub12	Hub13	Hub14	Plant	Network
Battery															3,300,617	
Borefield															7,125,000	
DHC network																461,764
DHC service line	667,576	379,220	339,709	374,297	352,680	350,087	347,891	347,050	441,400	358,051	375,437	885,988	355,229	356,919		
HP / Chiller	6,734,889	818,491	265,441	1,925,406	987,209	332,350	693,728	701,770	2,723,654	126,392	691,824	11,707,533	391,477	273,322		
HP plant															17,568,322	
PV															15,201,868	
Pumps	140,926	66,158	58,564	50,524	45,061	60,046	43,473	43,462	58,952	59,177	44,935	114,274	60,889	60,198		
Water storage				51,387	35,712	13,803	31,125	31,125	42,147	13,803	34,689	384,060				

Table F.2. Investment costs in $ for the different equipment and the different hubs.

	Hub1	Hub2	Hub3	Hub4	Hub5	Hub6	Hub7	Hub8	Hub9	Hub10	Hub11	Hub12	Hub13	Hub14	Plant
HP / Chiller (kW)	3,228	384	118	584	309	150	205	203	1,091	136	237	4,267	179	142	
HP plant (kW)															10,772
Battery (kWh)															4,360
Borefield (MWh)															4,750
Water storage (kWh)				1,139	664	0	525	525	859	0	633	11,220			

Table F.3. Capacities per equipment and per hub.

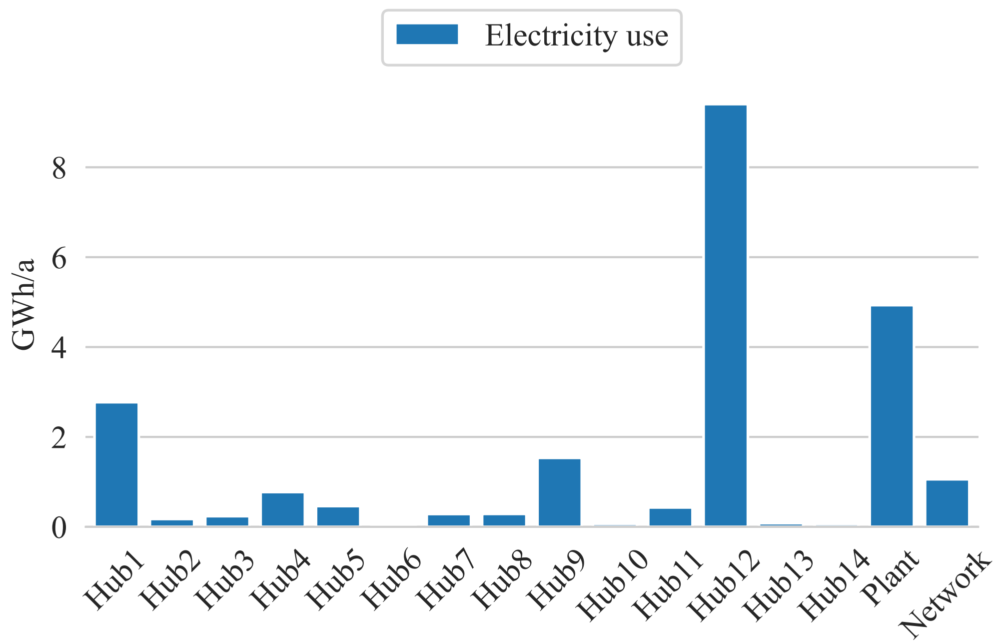

Figure F.3. Electricity consumption per hub.

APPENDIX G Modelica Model Key Parameters

	System capacity	SI unit		IP unit	
ETS 1	Heat recovery heat pump - heating	3,414	kW	11,650	kBTU/h
	Heat recovery heat pump - cooling	2,845	kW	809	ton
	District heat exchanger	3,091	kW	10,547	kBTU/h
	Connection pipe length (one way)	27	m	89	ft
ETS 2	Heat recovery heat pump - heating	5,616	kW	19,162	kBTU/h
	Heat recovery heat pump - cooling	4,680	kW	1,331	ton
	District heat exchanger	5,084	kW	17,349	kBTU/h
	Domestic hot water tank	403	m^3	106,374	gal
	Connection pipe length (one way)	226	m	741	ft
ETS 3	Heat recovery heat pump - heating	370	kW	1,264	kBTU/h
	Heat recovery heat pump - cooling	309	kW	88	ton
	District heat exchanger	335	kW	1,144	kBTU/h
	Domestic hot water tank	27	m^3	7,014	gal
	Connection pipe length (one way)	237	m	778	ft
ETS 4	Heat recovery heat pump - heating	1,303	kW	4,448	kBTU/h
	Heat recovery heat pump - cooling	1,086	kW	309	ton
	District heat exchanger	1,180	kW	4,027	kBTU/h
	Domestic hot water tank	93	m^3	24,690	gal
	Connection pipe length (one way)	48	m	157	ft
ETS 5	Heat recovery heat pump - heating	2,367	kW	8,076	kBTU/h
	Heat recovery heat pump - cooling	1,972	kW	561	ton
	District heat exchanger	2,143	kW	7,312	kBTU/h
	Domestic hot water tank	170	m^3	44,832	gal
	Connection pipe length (one way)	31	m	102	ft
Central plant	Heat pump - heating	4,268	kW	14,564	kBTU/h
	Heat pump - cooling	8,074	kW	2,296	ton
	Dry cooler - air side	13,514,761	m3/h	7,954,496	cfm
	Dry cooler - glycol side	1,349	kg/s	19,201	gpm
	Borefield perimeter zone	661	MWh	2,256	MMBTU
	Borefield center zone	3,083	MWh	10,521	MMBTU
District network	Distribution pump flow rate	685	kg/s	10,853	gpm
	Distribution pump pressure rise	479	kPa	70	psi
	District pipe length	3,460	m	11,352	ft
	District pipe diameter	505	mm	20	in

Table G.1. System capacities used in the Modelica model. Note that the capacities shown are for the whole sub-system, not for an individual component. For example, an installation will have multiple parallel heat pumps rather than a single large one.

APPENDIX H Parameter Comparison Between MILP and Modelica

Guideline values	MILP platform				Modelica platform	
ETS heat pump total capacity [a]						
condenser (space heating)	6.2	MW	21,155	MMBTU/h	13.071	MW
condenser (DHW)	2.4	MW	8,189	MMBTU/h	13.071	MW
evaporator (cooling)	11.1	MW	3,156	ton	10.892	MW
ETS heat pump average COP						
overall	5.6				6.5	
heating	4.8				4.3	
cooling [b]	7.0				13.6	
simultaneous	N/A				4.5	
Central plant heat pump capacity						
cooling	10.8	MW	3,063	ton	8.074	MW
Central plant heat pump average COP						
heating	4.8				5.0	
cooling	4.7				5.0	
BTES capacity						
	4,750	MWh	16,208	MMBTU	3744.5	MWh

Table H.1. Comparison of guiding values between MILP and Modelica.

[a] The MILP considers the capacities of the three utility productions separately, while in Modelica it is modeled as one single piece of equipment with coupled heating and cooling capacities.

[b] The high ETS cooling COP is achieved by rejecting heat to the district at a temperature as low as 16°C (86°F)

APPENDIX I PV Surfaces

Building	Comments from JBA	Building footprint		PV surface		
		(ft^2)	(m^2)	(% of the building footprint)	(ft^2)	(m^2)
1045	Possibly; may need reinforced roof construction	14,843	1,379	80	11,875	1,106
1051	Possibly; may need reinforced roof construction	34,627	3,217	80	27,702	2,579
1058/1060	Yes, not the full area though	38,944	3,618	50	19,472	1,813
1065	Yes, just the main building; not the services area at the rear of the building	27,104	2,518	50	13,552	1,262
1345	Possibly; may need reinforced roof construction	21,539	2,001	80	17,231	1,604
1349	Possibly; may need reinforced roof construction	18,471	1,716	80	14,777	1,376
1359	Possibly; but may have requirements to keep part of the roof clear of obstructions	66,521	6,180	50	33,260	3,097
1380	Possibly; may need reinforced roof construction	80,676	7,495	80	64,540	6,009
1500	None; vegetated roof installed	225,881	20,985	0	0	0
1560	Possibly; may need reinforced roof construction and may require part of roof remain clear of obstructions	16,146	1,500	50	8,073	752
1569	Yes	19,827	1,842	80	15,862	1,477
1631	Yes	29,181	2,711	80	23,345	2,174
1657	Yes	29,450	2,736	80	23,560	2,194
1676	Possibly; may need reinforced roof construction	26,393	2,452	80	21,114	1,966
1690	Yes	28,524	2,650	80	22,819	2,125
1691	Yes	28,535	2,651	80	22,828	2,126
1692	Yes	20,817	1,934	80	16,654	1,551
1800	Yes	68,652	6,378	80	54,922	5,114

Table I.1. Potential PV surface area, which was used as an upper bound in the MILP optimization.

APPENDIX J   US Census Regions Divisions

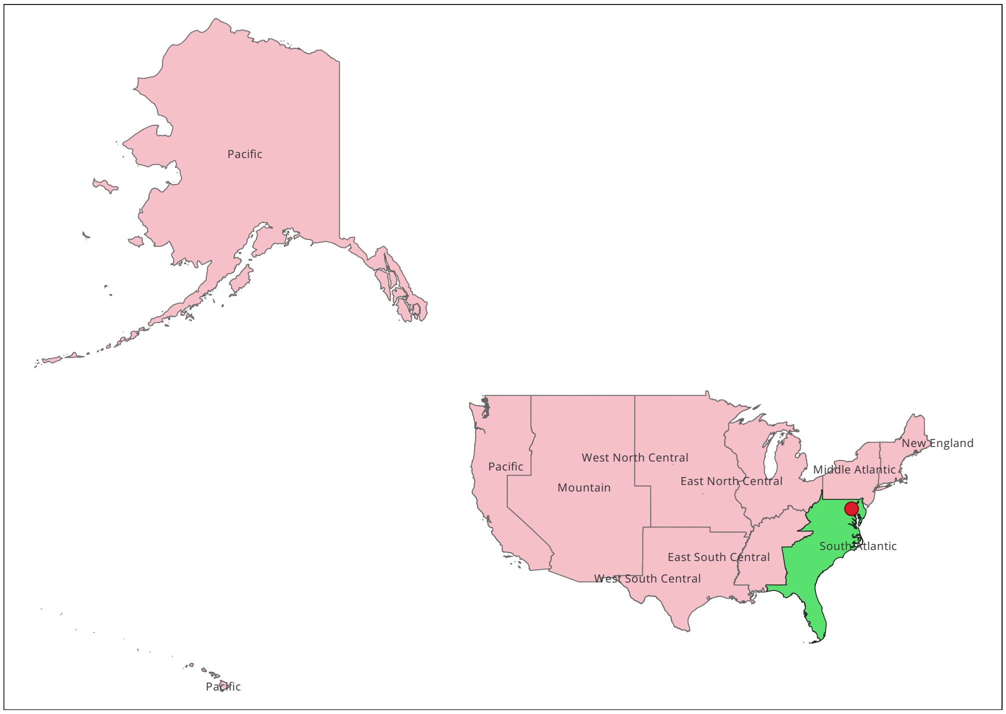

Figure J.1. US Census Regions Divisions (EIA, 2020)

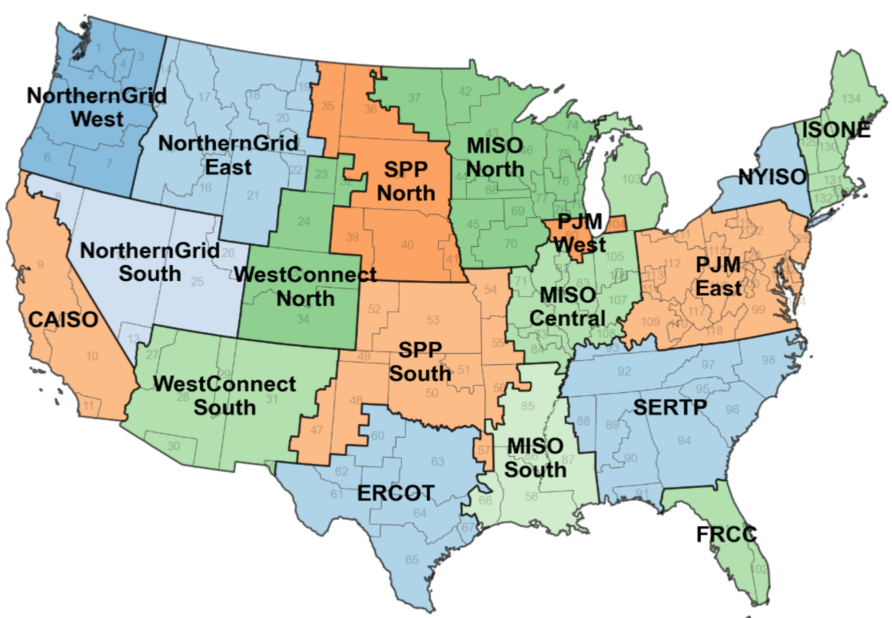

Figure J.2. Cambium's generation and assessment regions (Gagnon et al., 2024) 137

APPENDIX K Modelica Model for Zoned Borefield Operation

K.1 INTRODUCTION

The team implemented in the Modelica Buildings Library (Wetter, Zuo, et al., 2014) a new borefield model and conducted a comparative model validation against FEFLOW (DHI-WASY, 2010).[1]

The model allows individual boreholes to be grouped together and operated independently of other groups of the borefield. This allows for example to heat in fall the center of the borefield to store energy for winter while operating the perimeter to serve heating and cooling loads, or to operate a borefield with a hot center and a warm perimeter to reduce heat losses. This section documents a comparative model validation that was conducted by simulating two groups of boreholes. The simulations were done in Modelica and in the FEFLOW software, and the water outlet temperatures obtained with the two software was compared.

K.2 MODEL DESCRIPTION

The model can simulate any arbitrary configuration of vertical boreholes with equal lengths with both short and long-term accuracy with an aggregation method to speed up the calculations of the ground heat transfer.

The major features and configurations are as follows:

- User-defined borefield characteristics and geometry (borehole radius, pipe radius, shank spacing, etc.), including single U-tube, double U-tube in parallel and double U-tube in series configurations.
- User-defined vertical discretization of boreholes are supported.
- Borefields can consist of one or many boreholes. Each borehole can be positioned at an arbitrary position in the field using cartesian coordinates.
- The resolution and precision of the load aggregation method for the ground heat transfer can be adapted.
- The thermal response of the ground heat transfer is stored locally to avoid having to recalculate it for future simulations with the same borefield configuration.
- Pressure losses are calculated as a function of the mass flow rate.

The borefield models rely on the following key assumptions:

- The thermal properties of the soil (conductivity and diffusivity) are constant, homogenous and isotropic.
- The conductivity, capacitance and density of the grout and pipe material are constant, homogenous and isotropic.
- There is no heat extraction or injection prior to the simulation start.
- All of the boreholes in the borefield have uniform dimensions (including the pipe dimensions).
- Inside the boreholes, the non-advective heat transfer is only in the radial direction.

[1]The Modelica model implementation was conducted by Massimo Cimmino from Polytechnique Montreal and Michael Wetter from Berkeley Lab, and FEFLOW reference results were provided by Haiyan Zhou from RESPEC.

The borefield model is constructed in two main parts: the borehole(s) and the ground heat transfer. The former is modeled as a vertical discretization of borehole segments, where a uniform temperature increase or decrease (due to heat injection or extraction) is superimposed to the far-field ground temperature to obtain the borehole wall temperature. The thermal effects of the circulating fluid (including the convection resistance), of the pipes and of the filling material are all taken into consideration, which allows modeling short-term thermal effects in the borehole. The borehole segments do not take into account axial effects, thus only radial (horizontal) effects are considered within the borehole(s). The thermal behavior between the pipes and borehole wall are modeled as a resistance-capacitance network, with the grout capacitance being split in the number of pipes present in a borehole section. The second main part of the borefield models is the ground heat transfer. The heat transfer in the ground is modeled analytically as a superposition of convolution integrals between the heat flux at each of the borehole segments and the borefield's thermal response factor. The model uses a load aggregation technique to reduce the time required to calculate the borehole wall temperature changes resulting from heat injection or extraction.

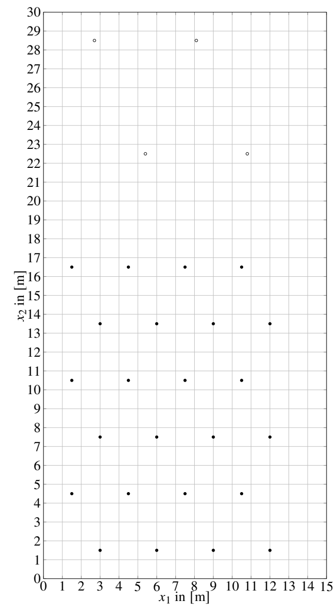

Figure K.1. Coordinates of the boreholes. The array of the bottom is labeled as 1 **in the results, and the array on the top is labeled as** 2. **Borehole sizes are not to scale.**

K.3 EXPERIMENT SETUP

The subsurface has a uniform initial temperature of 13.5 °C and there is no ground water flow. Figure K.1 shows the location of the boreholes. The top-four borefields, indicated with a non-filled circle, are operated as one array of parallel connected boreholes, and the other solid-filled circles indicate the other array of parallel connected boreholes. The boreholes are double U-pipes that start at a depth of 0.5 m below ground and the active depth of the boreholes is 85 m.

The inlet conditions are a water mass flow rate of $\dot{m} = 20\,\text{m}^3/\text{day}$ per borehole when operating. One of the experiments uses a step response in which the water mass flow rate is changed from 0 to $\dot{m}$ at $t = 0$, and the other experiment uses a pulse response in which the water flow rate is alternated between these values with 5 days on and then 5 days off.

The simulations were done using Dymola 2024x on Linux Ubuntu. A development version of the Modelica Buildings Library, commit 745315e was used.

For the detailed model specification, we refer to the models in the package `Buildings.Fluid.Geothermal.ZonedBorefields.Validation.FEFLOW.MassFlowRateStep100`, which is shown in Figure K.2, and to the other models in that package of the Modelica Buildings Library.

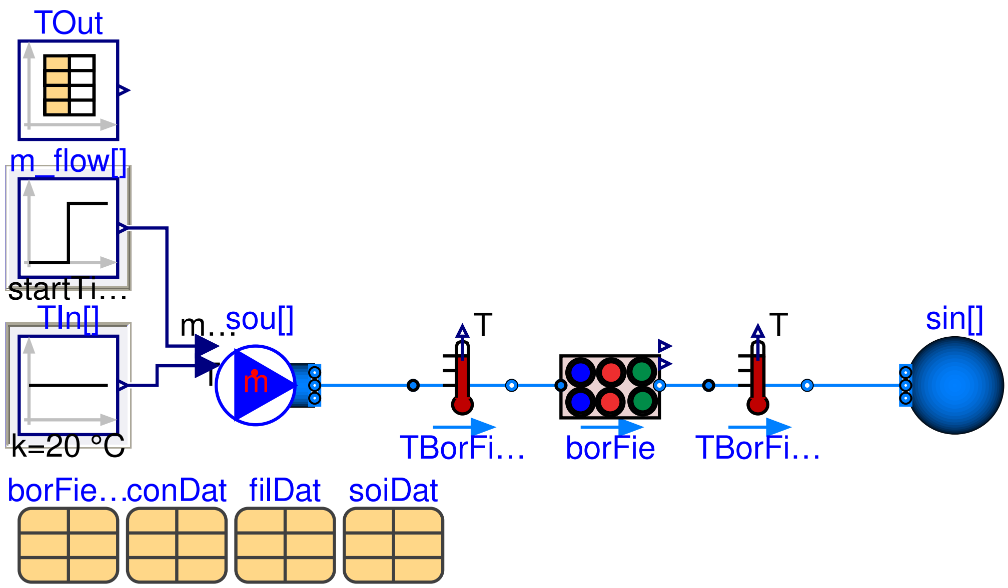

Figure K.2. Modelica model that was used in the validation of the step response.

K.4 RESULTS

Figure K.3 shows the leaving water temperature of the simulations, where the subscript *mod* is used for Modelica and *fef* for FEFLOW. The steps in the FEFLOW results are due to using piece-wise linear interpolation.

For all simulations, the leaving water temperatures between Modelica and FEFLOW show good agreement, with small deviations primarily in the early transients when the mass flow rate switches from zero to the design flow rate. The results after the step changes in mass flow rates show similar discrepancies as the comparison of FEFLOW's analytical and numerical solutions that is presented in the FEFLOW white paper (DHI-WASY, 2010). In the FEFLOW white paper, it is explained that the reason for this difference is due to the FEFLOW's analytical solution not being valid for such short-time dynamics. Note that the leaving water temperature comparison at times when the temperature drops is irrelevant, because in these time intervals, there is no water mass flow rate.

For the step response, the leaving water temperatures show good agreement. After 180 days, the temperature differences between Modelica and FEFLOW are 0.005 K for the larger section of the borefield and 0.015 K for the smaller borefield.

Therefore, the validation of the Modelica implementation is satisfactory.

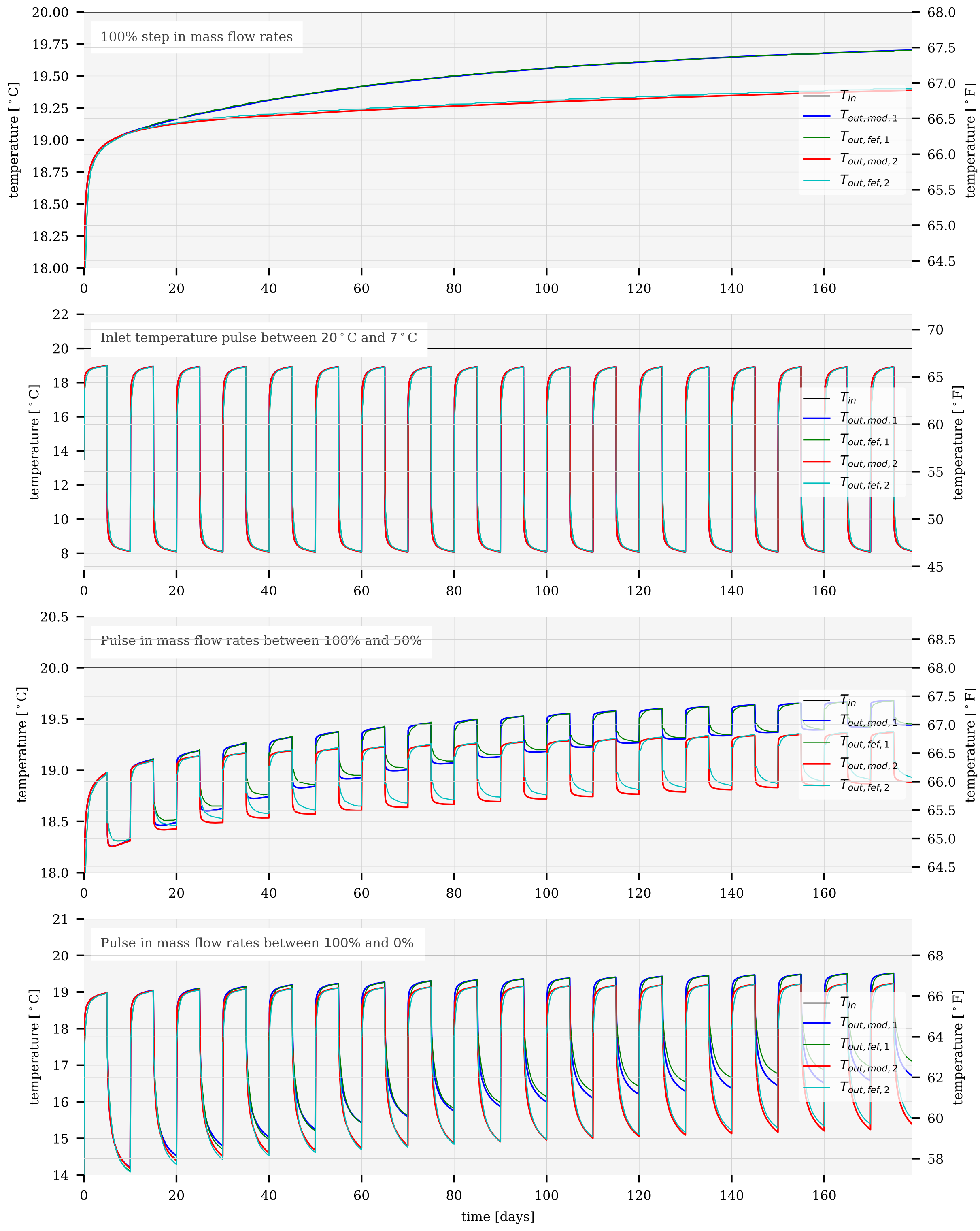

Figure K.3. Inlet and outlet water temperatures of the Modelica and FEFLOW simulation for the validation cases. The initial undisturbed soil temperature was 13.5 °C and the inlet water temperature was 20 °C, except for the second plot from the top which varied the inlet water temperature as described in the plot.